Technische Universität München

Fakultät für Chemie

Professur für Industrielle Biokatalyse

Development and evaluation of microalgae screening procedures and cultivation systems for biofuel applications

Johannes Schmidt

Vollständiger Abdruck der von der Fakultät für Chemie der Technischen Universität München zur Erlangung des akademischen Grades eines Doktors der Naturwissenschaften (Dr. rer. nat.) genehmigten Dissertation.

Vorsitzender:	Prof. Dr. Tom Nilges
Prüfer der Dissertation	1. Prof. Dr. Thomas Brück
	2. Prof. Dr. Dirk Weuster-Botz

Die Dissertation wurde am 04.12.17 bei der Technischen Universität München eingereicht und durch die Fakultät für Chemie am 24.06.18 angenommen.

Eidesstattliche Erklärung

Hiermit versichere ich die vorliegende Dissertation mit dem Titel „*Development and evaluation of microalgae screening procedures and cultivation systems for biofuel applications*“ selbstständig verfasst, sowie die Ausführungen und Gedanken, welche anderen Schriften sinngemäß oder wörtlich entnommen wurden, sowie weitere Quellen und Hilfsmittel kenntlich gemacht habe. Die vorliegende Arbeit wurde bisher weder in gleicher noch ähnlicher Form einer anderen Prüfungsbehörde vorgelegt oder anderweitig veröffentlicht.

Darmstadt, den 04.12.17 _____

Acknowledgements

I would like to thank my supervisor Prof. Dr. Thomas Brück for his excellent support throughout my PhD studies, the liberty he gave me to pursue new scientific approaches and his constant availability for critical discussion of ideas and strategies. By working under his supervision, I've learnt so many things which I will benefit from in my future professional life.

Furthermore, I would like to thank Dr. Daniel Garbe, who led my colleague and me with great foresight and guidance through this organizationally and scientifically demanding project. Speaking of whom, I particularly thank Matthias Glemser for numerous fruitful discussions on scientific issues and technical obstacles, great conference visits and of course the beverage supply during long sampling sessions. I also thank the project partners of the Institute of Biochemical Engineering Christina Pfaffinger, Andreas Apel and Timm Severin for the excellent collaboration, the close scientific exchange and the cheerful AFK-PhD-meetings.

Also, many of the members of the Industrial Biocatalysis group contributed in one way or another to the completion of this work:
I thank Monika and Norbert for their tremendous scientific input and their constant effort in improving the quality of the group as a whole.
Even in the most dire of times, I could always count on the constructive scientific feedback of my office neighbor Felix and its visionary variations of the modern Greek cuisine.
Special thanks also to Tom, for a lot of help with the lab robot and all technical issues in the lab in general and especially for frequently taking over the unrewarding task of organizing events for the group outside of the lab.

I also thank Martina Haack for her help with the analytics and her eventual can-do attitude towards new procedures.
A big "thank you" goes to the members of the office on the first floor for letting me participate in their internal Monday meeting and the weekly evaluation of failed experiments.

I also thank all the other current and former members of the group, which made my time in Garching truly memorable: Mahmoud, Wojtech, Dania, Kathi, Veronika, Sam, Gülnaz, Freddy, Steven, Bettina, Christian, Patrick, Sateesh, Marion, Jan, Max, Dirk, Wolle, Pariya and Tobias.

Of course, I also would like thank all of my students – some which became colleagues – for their contribution to the completion of this work, the exchange of ideas in the daily lab work and the things I've learnt by working with them. Dear Dirk, Sebastian, Pablo, Andrei, Rodrigo, Benjamin, Nanthini, Claudia and Julian: thanks to all of you.

Apart from the people in the lab I would like to thank my family for their support during the time of my PhD studies and beyond.

Above all, however, I would like to thank Christina, both for the scientific discussions on the topic and her patience and overwhelming support.

Content

Summary

This work was focused on three bottlenecks which currently hinder the large-scale application of microalgae as bio-based platform for chemical building blocks.

The first obstacle identified is the low number of currently exploited microalgae strains, despite a huge variability of described and cultured strains [1, 2]. In order to retrieve the enormous potential hidden in the versatile biodiversity of the organism group, a targeted isolation and screening process of environmental strains was conducted. Thereby a thorough identification of suitable habitats proved to facilitate the finding of strains with desired traits. In the course of this work, Southeast Australia was identified as a favorable area for the isolation of strains which can endure broad salinity, temperature and light intensity ranges. All of these properties are preferable for strains, which are cultivated in an open cultivation system. On a field trip to the identified area, samples were taken from eleven sites and subjected to an integrated enrichment and selection process. From this procedure, three strains from the genus *Dunaliella* could be identified, showing robust and fast growth and considerable lipid productivity values. The identified strains are promising starting points for further optimizations and implementation in large-scale cultivation systems.

As the second bottleneck, the lack of small-scale cultivations systems for phototrophic organisms was identified. Whereas microplates and low volume bioreactors are frequently used in screening of heterotrophs, only small advances were made in the screening of microalgae. Therefore, a manual screening set-up was established, based on purchasable components. Subsequently, an automatable microplate screening system for microalgae was developed and constructed by Additive Manufacturing. With this system a continuous gas transfer to the samples could be realized. Furthermore, by integrating the system into a laboratory robot system, a continuous growth monitoring could be implemented which resulted in more valid growth curves. Also, a cultivation chamber for the temperature regulation of the box was constructed and integrated in the robot

environment. For the whole set-up a proof-of-concept trial could be conducted, showing a principal applicability to microalgae screening. Finally, the automated system was evaluated in comparison to the manually operated system.

The third aspect of this work was focused on the pond management of a large-scale cultivation system. These systems are prone to the invasion of other algae strains, algae grazers or various parasites. In order to avoid a potential cultivation crash, robust strains need to be selected for such an application, which are able to withstand harsh, selective criteria like high pH or high salinity. A sudden change of these chemical conditions is, among others, used as a pond management strategy, which should reduce the number of unwanted co-organisms [3]. Within this study, a halotolerant strain was subjected to steep increases in pH and in NaCl concentration in a laboratory photobioreactor. It could be shown, that the strain can tolerate a short incubation under these harsh conditions. Thus, it was amenable for the application of pond management strategies in an open cultivation system. The effect of the implemented procedures was analyzed by Next Generation Sequencing (NGS). The genera *Halomonas*, *Psychroflexus* and *Stappia* could be detected as the most abundant bacterial groups in both the photobioreactors and open cultivation systems. Both shifts in the two systems led to a relative enrichment of the *Halomonas* group which was previously identified as favoring algal growth. Further evaluation of pond management strategies could lead to measures to decrease specific bacterial consortia which stabilize biomass production in open cultivation systems.

Zusammenfassung

Im Rahmen dieser Arbeit wurden drei Flaschenhälse, die momentan gravierend die Anwendung von Mikroalgen als Produktionsplattform für chemische Grundbausteine verhindern, bearbeitet.

Als erste Hürde wurde die geringe Zahl von Mikroalgenstämmen identifiziert, die heute produktionstechnisch relevant verwendet werden [1, 2]. Um das gewaltige Potential, das in der hohen Biodiversität dieser Organismengruppe verborgen liegt zugänglich zu machen, wurde ein zielgerichteter Isolations- und Musterungsprozess von Umweltstämmen aufgesetzt. Durch die Identifikation von geeigneten Mikroalgenhabitaten, konnte die Isolation von Stämmen mit günstigen Eigenschaften erleichtert werden. Im Zuge dieser Arbeit wurde Süostaustralien als geeignetes Gebiet für die Isolation von Stämmen identifiziert, die eine hohe Toleranz gegenüber stark schwankenden Salinitäts-, Temperatur- und Lichtintensitätswerten zeigen. Diese Eigenschaften sind für einen Stamm, der in einem offenen System kultiviert werden soll, essentiell. Auf einer Forschungsreise konnten Proben aus elf Gewässern genommen werden, die unter Laborbedingungen einem integrierten Anreicherungs- und Selektionsprozess unterworfen wurden. Am Ende dieses Prozesses konnten drei Stämme aus der Gattung *Dunaliella* identifiziert werden, die robustes und schnelles Wachstum sowie eine moderate Lipidproduktivität zeigten. Die Stämme sind damit vielversprechende Ansatzpunkte für weitergehende Optimierungen und die anschließende Implementierung in einer Massenkultivierung.

Als zweiten Flaschenhals wurde der Mangel von Kultivierungssystemen im mL-Maßstab für phototrophe Organismen identifiziert. Während Mikrotiterplatten und Bioreaktoren mit niedrigen Volumina weitläufig für das Screening von heterotrophen Mikroorganismen im Gebrauch sind, wurden nur wenige Studien für phototrophe Organismen in diesem Bereich durchgeführt. Daher wurde zunächst ein auf manuell messbaren Mikroplatten basiertes Musterungssystem etabliert. Im Nachgang wurde ein automatisiertes

Mikroplattensystem entwickelt und über Generatives Fertigungsverfahren konstruiert. Mit diesem System konnte ein kontinuierlicher Gastransfer in das Innere der Platte während des Prozesses gewährleistet werden. Darüber hinaus konnte durch Integration des Komponenten in ein Laborrobotersystem eine automatisierte Wachstumsüberwachung über regelmäßige Absorptionsmessungen erreicht werden. Zudem wurde eine temperierbare Kammer entworfen, in der die Mikroplatte durch den Laborroboter positioniert werden konnte. So konnte eine gleichbleibende Kultivierungstemperatur gewährleistet werden. Für das gesamte System konnte die prinzipielle Durchführbarkeit gezeigt werden.

Der dritte Teil dieser Arbeit untersuchte Möglichkeiten die Biomasseausbeute in offenen Systemen zu erhöhen. Offene Massenkultivierungssysteme sind anfällig für die Einbringung anderer Algenstämme, Grazern oder verschiedener Parasiten. Um ein mögliches Absterben der Algenkultur zu verhindern, müssen robuste Stämme für solche Anwendungen gefunden werden, die selektive Bedingungen wie einen hohen Salzgehalt oder hohen pH tolerieren. Eine plötzliche Änderung zu diesen harschen chemischen Bedingungen ist eine Möglichkeit die Konzentration unerwünschter Nebenpopulationen zu senken [3]. In dieser Arbeit wurde ein halophiler Mikroalgenstamm zunächst unter Laborbedingungen einer starken Erhöhung des pH-Wertes und des Salzgehaltes unterzogen. Es konnte gezeigt werden, dass der Stamm diese Bedingungen toleriert und erneut Wachstum zeigt. Diese Versuche wurden dann unter realistischen Klimabedingungen und in einem offenen Kultivierungssystem wiederholt. Der Effekt der Änderung der chemischen Bedingungen auf die bakteriellen Populationen wurde über Next Generation Sequencing (NGS) untersucht. Die Genera *Halomonas*, *Psychroflexus* und *Stappia* konnten als Hauptgruppen festgestellt wurden. Nach den Änderungen der Kultivierungsbedingungen zeigte sich jeweils für *Halomonas* eine relative Anreicherung unter den Bakterienpopulationen. Diese Gattung zeigte bereits Wachstum fördernde Eigenschaften für Algen und deren Anreicherung durch Änderung der Kultivierungsparameter könnte damit zu einer stabileren Biomasseausbeute beitragen.

List of related articles

The following review article was published during this thesis:

1. Glemser, M., Heining, M., Schmidt, J. et al. Appl Microbiol Biotechnol (2016) 100: 1077. https://doi.org/10.1007/s00253-015-7144-6

List of Abbreviations and Symbols

μ_{max}	maximum specific growth rate
C12-TAG	glyceryl tridodecanoate
C19-TAG	glyceryl trinonadecanoate
CDW	cell dry weight
CO_2	carbon dioxide
DHA	docosahexaenoic acid
DI	deionized water
DT	direct transesterification
EPA	eicosapentaenoic acid
EPDM	ethylene propylene diene monomer
FA	fatty acid
FAME	fatty acid methyl ester
FID	flame ionization detector
FLL	female Luer Lock
GC	gas chromatography
H_2	hydrogen
HCl	hydrochloric acid
HDPE	high density polyethylene
ISTD	internal standard
MLL	male Luer Lock
MTP	micro titer plate
MW	molecular weight
N_2	nitrogen
NP	National Park
NR	Nile Red
OD	optical density
PC	polycarbonate

PPFD	photosynthetic photon flux density
PTFE	polytetrafluorethylen
RPM	revolutions per minute
RSD	relative standard deviation

1. Introduction

1.1. General Introduction

It is estimated that at the end of the century world's population will reach approximately 11 billion [4]. Concomitantly, the demand for natural resources like food, water and space as well as chemical commodities like fuels and pharmaceuticals will increase. However, the current living standard of the so-called Western World cannot be transferred to the anticipated number of humans. Therefore, mankind is urged to developed new principles for the production, consumption and recycling of the goods, which are essential to the survival of the species. A cheap and widely applicable measure for avoiding a shortage of natural resources is abstinence of their consumption. Where ever this is not feasible, sustainable processes in the production and consumption of natural goods must be implemented. Various industry sectors, for instance, depend solely on the supply of fossil fuels for the production of chemical building blocks and value-added compounds. A change to a bio-based source for their substrates would lead to reduced carbon dioxide emissions, thus a decelerated climatic change and a diminished dependence on natural fossil fuel deposits, which require increasingly complex extraction techniques.

In the exploration of sustainable alternatives for current oil sources, microalgae have shown great potential. They not only produce lipids, from which bio-diesel and bio-kerosene can be produced, but also high-value products like docosahexaenoic acid (DHA) and eicosapentaenoic acid (EPA) [5]. This makes microalgae amenable to a bio-refinery concept, where multiple products from a single source are used in an industrial process, leading to an enhanced value-added chain. Furthermore, microalgae use CO_2 as a substrate, which results in a CO_2-neutral process and show higher oil yields per area compared to other biomass sources [6]. They can also be cultivated on arid lands and avoid thus a food-vs-fuel debate, that hindered the rise of second generation biofuels. Given this potential, microalgae research might contribute to the transition from a fossil fuel based industry towards a sustainable one.

1.2. Microalgae

1.2.1. Algae diversity and ecology

An alga is defined as an oxygen producing photosynthetic organism that lacks sterile tissue around its sexual reproductive structure(s) [7]. Species which form at least in one of their life stages a multicellular thallus are designated as macroalgae and the strictly unicellular forms as microalgae [8, 9]. The term is commonly applied out of convenience, as algae are spread among four of the five major eukaryotic groups and hence do not represent a monophyletic group [2]. The reason for this wide distribution is the complex evolution of plastids in the different lineages, during which the cell organelles were taken up, shifted, lost and/or replaced at different points of their evolutionary development [10]. Although there is consensus that algae show a great variety, estimations on the current total number of algae and especially the predictions of yet undiscovered algae vary greatly among phycologists [11–13]. Additionally, these estimates do not differ between macro- and microalgae. Guiry attributes the broad range of species to the uncertainty of what an algae species actually is, as molecular taxonomy tools can contradict the classical identification based on morphology and the ability to reproduce sexually [2]. At the same time, he gives a conservative estimation on the current algae specifies, which amounted to approximately 42,000 at the time of the work.

Due to their metabolism, this variety of strains plays an essential role in the geochemical cycle now and has been for the last 2.2 billion years [14]. They function altogether as the main primary producer of organic compounds by the light-dependent reduction of inorganic carbon with oxygen as a by-product of the process [15]. Although the phytoplankton biomass only amounts to approximately 1-2 % of the total global plant carbon, they annually fix about 40 % of the total carbon [16]. In doing so, they have taken up a broad range of habitats and ecological niches. Prokaryotic representatives of algae e.g. can thrive in temperatures of around 70 °C in the hot springs of Yellowstone National Park, whereas in the Antarctica and Arctic so-called Snow Algae were identified, which survive annual mean temperatures of -18 °C [17–19]. Furthermore, some

species also manage to accommodate harsh chemical niches like acidophilic lakes or mine-impacted environments, i.e. lakes with a pH of around 2, by an mechanism which prevents H^+-ions from entering the cell [20, 21]. On the other end of the pH-scale, alkaliphile cyanobacteria grow well at an average pH of 10 [22, 23]. A tolerance to high concentrations of salt, allows eukaryotic algae like the commonly known species *Dunaliella salina* to strive in water bodies with a salinity near the saturation point [24]. With increasing salt concentrations, the intracellular glycerol content is increased by the cell in order to maintain the osmotic balance to the environment [25].

1.2.2. Photosynthesis

1.2.2.1. Phototrophic growth in microalgae

Although many algae species are able to take up organic compounds and metabolize them heterotrophically [26–30], the oxygenic photosynthesis is their main energy source for the synthesis of organic matter. In this process, the energy of absorbed light is converted into a chemical gradient which delivers the energy for the synthesis of complex organic compounds. The process can be divided into two main processes: Light is absorbed by the cells via antenna complexes which transfer the energy of the light to an electron transport chain, to generate reduction equivalents and ATP. These components are then used in the light-independent Calvin-Benson-cycle to fix CO_2 in order to synthesize complex organic molecules. The overall chemical equation for this process is [31]:

$$12\,H_2O + 6\,CO_2 \xrightarrow{\text{Light}} C_6H_{12}O_6 + 6\,H_2O + 6\,O_2 \qquad (1)$$

1.2.2.2. Light harvesting

The first step in photosynthesis is the absorbance of incident light by the cell. The spectra of wavelengths of the electromagnetic radiation which drives photosynthesis ranges from

400 nm to 700 nm and is referred to as photosynthetic active radiation (PAR). The measurement of the light intensity from this wavelength realm is the Photosynthetic photon flux density (PPFD), which describes the amount of incident photons per unit of area and time. It is favored over the irradiance energy expressed in W/m^2, as the amount of photons is stoichiometrically connected to the amount of CO_2 fixed per cell [32–34].
The incident photons are absorbed by the light harvesting complex (LHC) of the photosystem II (PSII). PSII is located in the thylakoid membranes of the chloroplast. It consists of the reaction center which is embedded in the membrane and the LHC, which is attached to the reaction center and protrudes from the membrane. The latter consists of various amounts of chlorophylls as well as, depending on the algae group, different carotenoids like β-carotene, fucoxanthin or zeaxanthin.

The function of the chlorophylls within the LHC is mainly the absorption of photons and the transport of the resulting excitation state to the reaction center of PSII. Due to their double bonds and loosely bound valence electrons, these molecules are lifted to electronically excited states upon absorption of a photon. The state to which they are lifted depends on the energy content of the absorbed photon. From the excited state, the chlorophyll molecule reverts to the ground state by the release of energy. This can be conducted by emission of heat and/or fluorescence or the energy can be transferred to an adjacent molecule [35]. The close proximity of the chlorophyll and carotenoid molecules within the LHC allows for a transfer of the excitation state from molecule to molecule by resonance energy transfer [36, 37]. The excitation state is eventually transported from the outer regions of the LHC to the reaction center, where the energy collected by pigments of the LHC is funneled to the P680 chlorophyll *a* pair. The name of this complex is derived from "P" like "pigment" and 680, which is the maximum absorbance wavelength [38]. The complex has sufficient reduction potential to oxidize water to molecular oxygen [39]. With the energy collected from LHC, P680 conducts a

charge separation, generating an electron to be transferred to the electron transport chain [38].

The carotenoids in the LHC have also two other functions beside the transport of the excitation state. They also absorb light and due to their differing absorbance maxima compared to chlorophyll *a*, they increase the range of sunlight which can be used for photosynthesis. Secondly, they act as protectants against high light intensities, chlorophyll triplet states and reactive oxygen species [40, 41].

Varying the composition and the amount of pigments in the LHC is a wide-spread adaptation mechanism to different light quantities and qualities in algae [42, 43].

1.2.2.3. Linear electron transport chain

In the electron transport chain, the absorbed energy of the light is converted to chemical energy by a sequence of redox reactions leading to NADPH as final product. In parallel, chemical energy is produced by the phosphorylation of ADP, driven by the proton gradient established in the process. The first step in the process is the charge separation by the P680 chlorophyll *a* dimer. The electron is transferred to pheophytin and from there to a plastoquinone at the Q_A site (see Figure 1). Both pheophytin and plastoquinone are attached to the reaction center. In contrast to that is the next electron acceptor, a plastoquinone at site Q_B, movable. With a second electron from Q_A, the plastoquinone at Q_B is converted to plastoquinol (PQH_2) and released into the membrane. The electron gap of the $P680^+$ is filled by electrons from a tyrosine moiety (Y_z) of the D1-protein of the reaction center, whose electron gap is in turn filled by electrons produced by the water-splitting complex. This is a cluster of four manganese atoms which is also attached to PSII and splits water from the thylakoid lumen in a four step mechanism into protons, electrons and oxygen [44]. The produced protons accumulate in the lumen of the thylakoids, lowering the pH and at the same time establishing a proton gradient [14]. The mobile electron carrier plastoquinol transports the electrons to the Cytochrome b_6f Complex, a transmembrane component of the photosynthetic apparatus. Here, the

electrons are transferred via the Rieske-protein (FeS) to the mobile plastocyanine which then binds to Photosystem I (PSI). Two protons from the oxidation of PQH_2 are released and also transferred to the thylakoid lumen. PQH_2 is thus again oxidized to plastoquinone and attaches to PSII for an uptake of electrons from P680 and protons from the chloroplast stroma.

The electrons of plastocyanine fill the light-induced electron gap of PSI. As the absorbance maximum of the primary chlorophyll dimer in the reaction center of PSI is

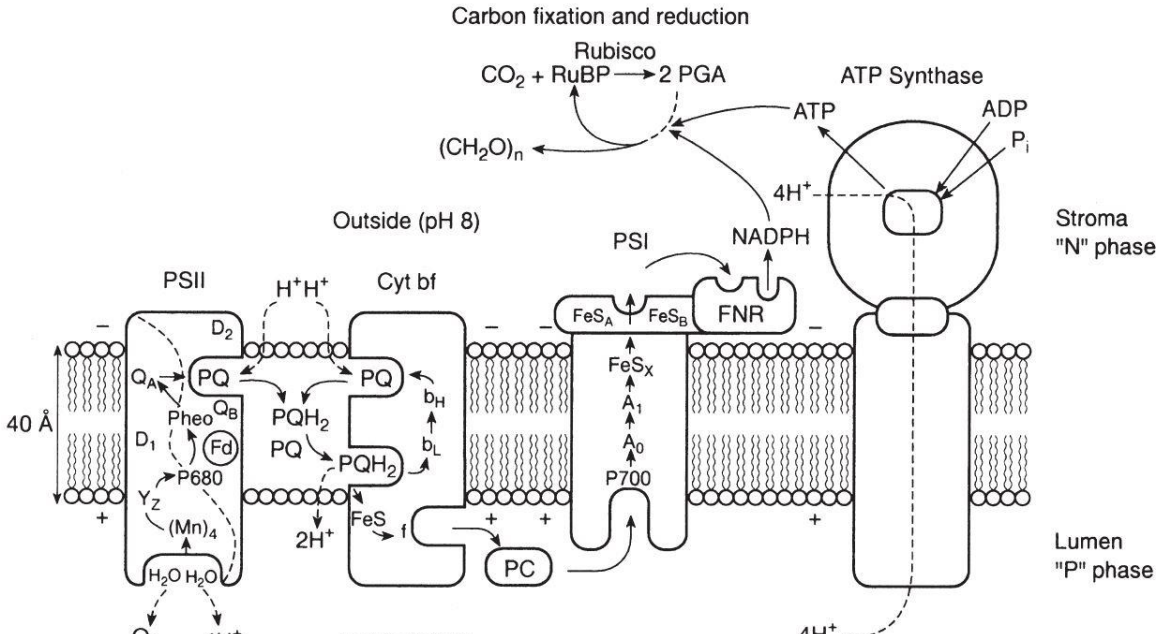

Figure 1: Schematic cross section through a photosynthetic (i.e., thylakoid) membrane showing the orientation and some of the major components of the photosynthetic apparatus. The complete membrane forms a closed vesicle. The electron-transport chain is indicated by solid arrows; proton transport is indicated with dashed lines. Electrons extracted from water in photosystem II (PSII) are sequentially transferred to the cytochrome b_6/f complex (cyt bf), and thence through either plastocyanin (PC) or another cytochrome (cytochrome c_{553}, also called c_6) to photosystem I (PSI), where they are used to reduce NADP to NADPH. Abbreviations: Y_z, a tyrosine that is the immediate electron donor to the PSII chlorophyll P_{680}; P_{680} and P_{700}, the reaction center chlorophyll a molecules of PSII and PSI, respectively; Pheo, a phaeophyton a molecule; Q_A, a bound plastoquinone; PQ, free (i.e., mobile) plastoquinone; PQH_2, free plastoquinol (reduced form of plastoquinone); b_L and b_H, low and high potential for of cytochrome b_6; FeS, iron–sulfur components in the cytochrome b_6/f complexes and on the reducing side of PSI; f, cytochrome *f*; PC, plastocyanin; A_0, the immediate electron acceptor from P_{700} (a chlorophyll a molecule); A_1, phylloquinone; Fd, ferredoxin; FNR, ferredoxin/NADP oxidoreductase; NADPH, reduced nicotinamide adenine dinucleotide phosphate; ADP, adenosine diphosphate; ATP, adenosine triphosphate; P_i, inorganic phosphate; +/−, polarity of electrical potential difference across the membrane established in the light; RuBP, ribulose-1,5-bisphosphate; Rubisco, ribulose-1,5-bisphosphate carboxylase/oxygenase; PGA, 3-phosphoglycerate; $(CH_2O)_n$, generalized carbohydrate. The stoichiometry of protons, electrons, O_2, ATP, NADPH, and CO_2 is not indicated. Modified from Whitmarsh and Govindjee 1995. Reprint with permission of publisher [1].

at 700 nm, the molecule is also referred to as P700. The charge separation at that cluster results in an electron transfer via A_0, A_1 and an iron-sulfur-complex to ferredoxin/$NADP^+$ oxidoreductase, which reduces $NADP^+$ to NADPH in the chloroplast stroma. The established proton gradient from the thylakoid lumen to the chloroplast stroma is used by the transmembrane ATP synthase for the phosphorylation of ADP to ATP. NADPH and ATP are then available for the subsequent light-independent carbon fixation in the chloroplast stroma.

1.2.2.4. Light-independent reaction of photosynthesis (Calvin-Benson-Cycle)

The light-independent reactions of photosynthesis can be divided into three phases [35]. In the carboxylation phase (i), CO_2 is bound to D-ribulose-1,5-bisphosphate to produce 3-phospho-D-glycerate (3-PGA). This reaction is catalyzed by Ribulose-1,5-bisphosphate carboxylase/oxygenase (RuBisCO) with Mg^{2+} as cofactor. The enzyme consists of eight large subunits with molecular weight of 51 to 58 kDa and eight identical small subunits of 12 to 18 kDa. Beside the carboxylation of ribulose-1,5-bisphosphate, the enzyme possesses also an oxygenation function, with a ratio of oxygenation to carboxylation reaction from 1:4 to 1:2 at 25 °C [45]. This process decreases the efficiency of the overall photosynthesis, as the product of the side reaction, 2-phosphoglycerate, cannot be used in the subsequent Calvin-Benson-cycle. However, it can be recycled in an ATP and NADPH-driven process called photorespiration, during which O_2 is consumed and CO_2 is produced. The reactions of the recycling process stretch from the chloroplast over the peroxisome to the mitochondrion, with the final step being the synthesis of again 3-PGA in the chloroplast. In the subsequent reduction phase (ii), 3-PGA is catalyzed by the energy of one ATP to 1,3-bisphosphoglycerate, which in turn is reduced to D-glyceraldehyde-3-phosphate (GAP) by NADPH. A triose phosphate isomerase establishes an equilibrium between GAP and dihydroxyacetone phosphate which together are referred to as triose phosphates. From 3 moles of fixed CO_2, six moles of triose phosphate

are synthesized. Only one mole of those is used by the cell metabolism for the synthesis of C6-sugars. The remaining 5 moles are used in the third phase (iii) in a series of reactions for the regeneration of D-Ribulose-1,5-bisphosphat as starting material of the cycle [45]. The sum of net reaction for the synthesis of one hexose is the following [37]:

$$6\,CO_2 + 18\,ATP + 12\,NADPH + 12\,H_2O \longrightarrow C_6H_{12}O_6 + 18\,ADP + 18\,P_i + 12\,NADP^+ + 6\,H^+ \quad (2)$$

1.2.3. Lipids from microalgae

Algae are capable of synthesizing a variety of lipids like waxes, sterols, and fatty acids and their derivatives. They can be divided into polar and non-polar compounds, each class with different functions in the cell. The main representatives of polar lipids are phosphoglycerides and glycosylglycerides. They consist of a glycerol backbone, which is esterified to two fatty acids. Depending on the lipid group, either a phosphate or a glycosyl group is attached to the third OH-group. The polar lipids constitute the main components of cellular membranes and maintain their functionality. The principal non-polar lipids in algae are the triglycerides (TAG). They comprise a third fatty acid instead of the hydrophilic group esterified to the glycerol backbone. They mainly act as storage compounds in the cell and represent the main substrate for the biofuel application of the microalgae [46].

In this section, the lipid synthesis pathways for the aforementioned groups is outlined. Especially TAGs are of interest for the application of microalgae in biofuel production. A common measure to increase the lipid content of cells is the cultivation under adverse conditions. Therefore, the biological background of this stress response is detailed and several strategies increasing the lipid productivity of a strain and the overall process are laid out in this chapter. Although microalgae both consist of prokaryotic and eukaryotic representatives, generally only eukaryotic algae show an increase in lipid productivity

upon cultivation under adverse conditions and therefore only this subgroup is part of this introduction section [47].

1.2.3.1. Biosynthesis of triglycerides in algae

The knowledge of lipid synthesis pathway for higher plants is based on the extensive research in the model organism *Arabidopsis thaliana* [48]. Until recently, the lipid synthesis pathway in microalgae thought to be very similar, but with increasing interest in microalgae for biofuel applications, however, algae lipid metabolism was examined in more detail and considerate differences to the synthesis in plants were found [47, 49]. This includes the use of different acyl groups as well as an altered role of the plastids in the assembly of TAGs. The deviations found mainly stem from a reconstruction of the glycerolipid metabolism in *Chlamydomonas reinhardtii* based on genomic and expressed sequence tags (EST) data [50]. The genome of *C. reinhardtii* is one of the few microalgal genomes sequenced, but only minor insights from this genome to the lipid accumulation process in oleaginous algae are expected, as these species accumulate starch instead of lipids during nutrient limitation [51]. Another constraint in the summary of the lipid accumulation process is the huge phylogenetic variability of microalgae. The differences found in *C. reinhardtii* might differ significantly from the pathway e.g. in a diatom. These limitations have to be considered when the lipid synthesis of oleaginous microalgae is outlined.

The initial compound of fatty acid synthesis is acetyl-Coenzyme A (acetyl-CoA) which is produced over several stages from the triose phosphate of the Calvin-Benson cycle of photosynthesis. In the subsequent committing step of the pathway, acetyl-CoA is bound to malonyl-CoA by the acetyl-CoA carboxylase (ACC) [52]. The product is linked to the acyl-carrier protein (ACP) and introduced as malonyl-ACP to the fatty acid synthesis. The process is conducted by the fatty acid synthase complex (FAS), in which sequentially additional acetyl groups are attached to the initial malonyl-ACP C16:0-ACP or C18:0-ACP as final products. The fatty acids are then released from ACP, hydrolyzed by the

fatty acyl-ACP thioesterase (FAT) to free fatty acids and then released into the cytosol. There, they are converted to acyl-CoA by the addition of a CoA. Subsequently, they are transported to the endoplasmic reticulum (ER) and in the membrane of the organelles the acyl groups of two acyl-CoAs are transferred onto a triose phosphate to yield diacylglycerol (DAG). From this compound either membrane lipids can be synthesized by the addition of a glycosyl or phosphate group or TAGs, which are produced by the addition of a third acyl-group catalyzed by the diacylglycerol acyltransferase (DGAT) [53]. The TAGs of the ER are released into lipid bodies, cell structures of 1-8 µm size [54, 54]. They consist of accumulated TAGs and pigment molecules, surrounded by a monolayer of polar lipids embedding various proteins [55].

1.2.3.2. Biotechnological approaches to increase TAG content in microalgae

The specific amount of intracellular TAGs in microalgae can be increased by application of various chemical and physical factors and by genetic engineering means. The most effective chemical stimuli of TAG accumulation in most algae group is a limitation to nitrogen [47, 56–58]. For diatoms, also silicon limitation increases the TAG levels [59, 60], whereas a phosphorous limitation has diverging results on microalgae [61, 62]. Likewise, increased salinity has an ambiguous effect on lipid content of different strains and it remains unclear whether the observed increases are species-specific or salt concentration dependent [40, 63, 64]. The addition of different modulators of the lipid synthesis to various microalgae strains resulted in a 1.84-fold increase in Nile Red fluorescence which indicates an increase in lipid content [65].

Regarding physical factors, the increase of temperature results in an increase of lipid content in some algae [66, 67], likewise the cultivation with elevated light intensities [68, 69].

Growing interest in biofuel application of microalgae has led to increasing approaches to genetically manipulate microalgae. Although the molecular toolbox is not as well equipped as for heterotrophic microorganisms, some advances could be made [44]. In

Phaeodactylum tricornutum, for instance, an overexpression of the FAT led to an twofold increase in total lipid content [70], whereas the overexpression of DGAT resulted in the same species in an 1.35-fold increase of neutral lipids. Enhancing the lipid content could also be achieved by a genetically engineered interruption of competing lipid degrading metabolisms. Knocking down the starch synthesis in *Scenedesmus obliquus* and *C. reinhardtii* led to a significant increase in lipid content [71, 72] and the knockdown of a multifunctional lipase/phospholipase/acyltransferase increased the lipid content of *Thalassiosira pseudonana* without effecting its growth [73].

1.2.3.3. Lipid productivity in microalgae cultivation processes

Increasing the lipid content in microalgae is favorable in biofuel application, as it increases the operation efficiency of the process by reducing the downstream processing costs [74]. A microalgae strain showing a high lipid content at a given time point in the cultivation is, however, not automatically a suitable candidate for biofuel application [75]. As this characteristic of a certain strain does not contain a time variable in its calculation, no information on the interval in which the strain accumulated the declared amount of lipids is given. Due to this shortage of information, lipid productivity is instead a more suitable screening parameter to select algae strains for biofuel production [75, 76]. Between two data points during a batch cultivation it is calculated according to [77] by:

$$P_L = \frac{C_2 \times CDW_2 - C_1 \times CDW_1}{t_2 - t_1} \tag{3}$$

with

P_L	volumetric lipid productivity	$g/(L \cdot d)$
C_2	lipid content at second time point	g/g_{CDW}
CDW_2	cell dry weight concentration at second point	g/L
C_1	Lipid content at first time point	g/g_{CDW}
CDW_1	cell dry weight concentration at first point	g/L

Throughout a batch cultivation, lipid content and CDW concentration change constantly due to decreasing nutrient concentrations and increasing light attenuation [78]. Therefore, the value for P_L is different for every pair of data points used for the calculation. Reported values for total lipid productivity for *Nannochloropsis oculata*, for instance, ranged from 0.009 g/(L · d) to 0.324 g/(L · d) [77, 79, 80]. For this reason, care has to be taken with the comparison of different strains and cultivation systems, as samples taken at different time points could lead to diverging lipid productivity values. This factor contributes additionally to the uncertainty in lipid productivity evaluation, as different light and nitrogen regimes result in diverging values for a given strain. A possible solution to this issue would be the evaluation of lipid productivity through a continuous cultivation. Once the steady state of the cultivation is reached, the lipid productivity stays constant and can thus readily be determined. By choosing this strategy, the more sophisticated set-up can be compensated for by the reduced downtime and improved control over TAG productivity [81]. This is even more valid for large scale cultivation facilities aiming on biofuel production.

1.2.3.4. Biofuel from microalgae

Various types of biofuel can be produced from microalgae [46]. They share a common production process in which algae are first cultivated in open mass reactor systems (see Figure 2). After the cultivation (i), the microalgae are harvested either in a one- or two-stage process (ii). Subsequently, the biomass paste is dried in order to enable the

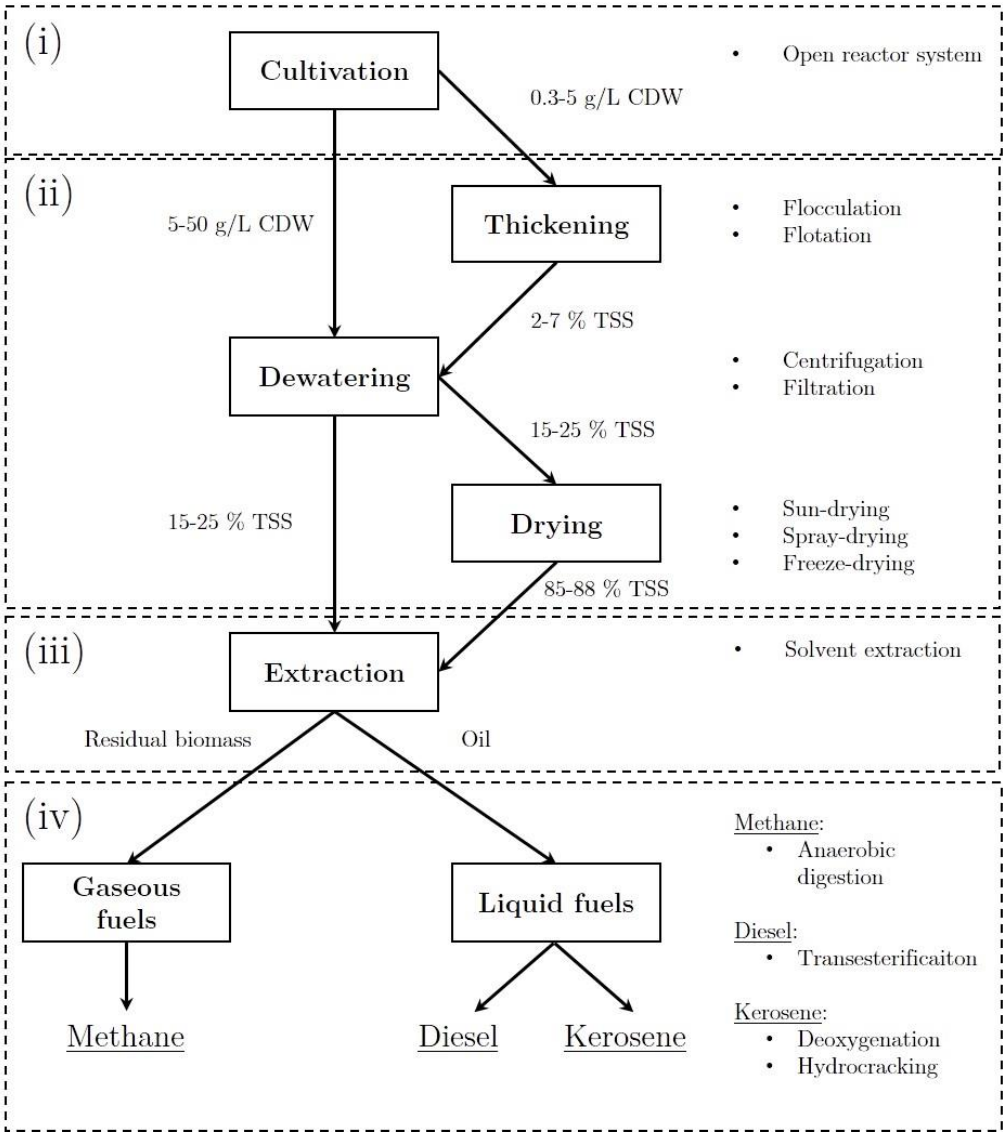

Figure 2: Generalized process overview of microalgae-based biofuel production. Modified scheme based on data from [93, 94, 102].

extraction (iii) of lipids, which are subsequently converted (iv) to liquid fuels like diesel or kerosene. After the extraction process the residual biomass can be used for the production of gaseous fuel.

Current approaches seeking an economical production of biofuel by algae are mainly envisaged for large, open reactor systems. These systems are reported to be economically favorable over closed photobioreactors [82–84]. They are operated non-sterilely and the culture is exposed to fluctuating environmental conditions. Various types of open cultivation systems have been developed: The most basic ones are shallow, non-mixed basins where growth parameters are not controlled at all [85]. CDW productivities in

these systems are consequently very low. More sophisticated are raceway systems which are mixed in most cases by a paddle-wheel [86]. The pH is controlled by the pulsed addition of CO_2 which also avoids a limitation of the carbon source during cultivation. Raceway ponds are commonly operated with a suspension depth of 100-300 mm, yielding CDW productivities of up to 24.5 g/($m^2 \cdot d$) [67]. Cascade systems show in contrast to that light path lengths of only 5-6 mm [87, 88]. Due to the smaller light-limited zone in the algae suspension, CDW concentrations and productivities of up to 50 g/L and 25 g/($m^2 \cdot d$) could be achieved [87]. Despite the comparatively high CDW productivities some major limitations for the economically efficient operation of open pond system remain [89]: Potential contamination by predators or competing microorganisms can lead to a significant decline in the cell concentration of the culture [90, 91]. Also, as suitable sites for an open reactor system are presumably located in tropical and subtropical climates, the elevated evaporation there steadily increases the salt concentration of the medium. Therefore, fresh water for the maintenance of the salt concentration needs to be added constantly and for economic reasons, the water source has to be in close proximity to the algae facility [83, 92].

Depending on the achieved final CDW concentration of the cultivation either a single-stage or two-stage harvest procedure is conducted [93]. For low CDW concentrations between 0.3 and 5 g/L, the algae suspension is thickened to a slurry of 20-70 g/L which corresponds to 2-7 % of total suspended solids (TSS), a general evaluation factor for dewatering processes [94]. These pretreatments enhance the effectivity of the subsequent procedures, as a smaller share of liquid has to be removed. Depending on strain, cell size and cell density, various methods can be applied [95]: By flocculation, the algae cells are aggregated to larger particles, which facilitates subsequent process steps like filtration or centrifugation. Aggregation is achieved by the addition of multivalent metal salts, cationic polymers or the increase of pH [96, 97]. Factors influencing this process are cell concentration, net charge of the cell surface, concentration of the flocculant as well as pH and ionic strength of the culture medium [98]. Favorable with this technique is the

low energy input as only slow mixing of the suspension is necessary. However, some of the applied flocculants are expensive and might infer with subsequent extraction steps [94]. Harvesting by flotation is based on the introduction of small gas bubbles to the medium, which attach to solid particles and transport them to the liquid surface [99]. From there the particles can be skimmed to a separate container. Various methods exist for the generation of bubbles, resulting in a different energy input per unit of volume. Ndikubwimana et. al evaluated various methods, whereas dispersed air flotation proved to have the lowest energy input (0.003 kWh/m^3) at a considerably high flotation efficiency of 76.7 % of total suspended solids in relation to the initial concentration [99, 100].

The thickening procedures result in an algae slurry which can be dewatered further [95]: Centrifugation, for instance, is a rapid and effective yielding broths with final suspended solids of up to 22 % w/v [101]. However, energy consumption of this process is comparatively high (8 kWh/m^3), limiting this method to high value products. Energetically more favorable is filtration of the harvested biomass, with energy consumption values ranging from 0.1-5.9 kWh/m^3 [102]. A major difficulty of this technique is the clogging of the filter membrane which increases the operational costs of the process [103]. Both, centrifugation and filtration can be used to dewater biomass of 2-7 % TSS in a single concentration step to the aforementioned TSS content of approximately 20 % TSS [93, 97].

Depending on the final product and the extraction procedure, the biomass needs to be dried after the dewatering process to a TSS content of 85-88 % [93, 104]. Possible methods are spray-drying, freeze-drying and sun-drying [97]. The first two procedures show a high energy consumption and are thus not economically viable on a large scale [93]. Sun-drying requires large surfaces and exhibits risk of material loss [105].

The extraction of lipids from the dried algal biomass is conducted with solvents like hexane, ethanol, chloroform and diethyl ether [97, 106]. Many of those are toxic, restricting their use in large-scale facilities. A possible solution to this problem is the

extraction by supercritical CO_2, which represents a non-toxic, non-flammable and non-polluting solvent [107–109].

The extracted lipids can be converted by transesterification of TAGs to biodiesel [110]. Although mostly dried biomass is used for this step, in some studies extraction methods from wet biomass of around 20 % TSS were developed which renders drying obsolete [111, 112]. Regardless of the initial water content of the biomass, the extracted triglycerides are converted into fatty acid methyl esters (FAMEs) by transesterification. The reaction is catalyzed either by acid or base and an excess of methanol pushes the equilibrium towards the product side. Previously, the process was separated into an extraction and esterification step, but recent studies showed the applicability of both in an integrated procedure [113, 114].

Whereas biodiesel is composed of FAMEs generated via transesterification, kerosene is a mixture of straight chain alkanes, cyclic alkanes and aromatics [115, 116]. These compounds can be derived from microalgal triglycerides by deoxygenation with H_2 and subsequent hydrocracking and hydroisomerization [117, 118]. The residual biomass after the extraction process can be digested anaerobically in order to increase the revenue of the whole biofuel process [119]. After hydrolysis, fermentation and methanogenesis of the biomass, a mixture of mainly methane, CO_2 and trace amount of other gases is produced [120].

1.2.3.5. Challenges in the commercialization of biofuel from microalgae

Despite the tremendous research effort on microalgae for biofuel applications, no process chain could so far be established and operated on a long term, which yields an economically viable biofuel in significant amounts. Several life cycle assessment (LCA) studies prospected the theoretical algal biofuel price based on published values for e.g. photon conversion efficiency, lipid productivity, and harvest cost. The general conclusion from these works is, that a "fuel-only" usage of the produced biomass is not economically plausible, neither for biodiesel [121–124], nor for aviation fuels as final product [125].

However, various research needs at different stages of the process have been identified in order to achieve cost competitiveness in the medium turn. At the cultivation level, identification of strains optimized regarding not only to lipid productivity but also to broad temperature tolerances, high pH values, high salinity and ease of harvesting is necessary [126, 127]. Especially the long-term maintenance of large-scale cultivation proved to be challenging. Frequently, parasites like fungi or amoeba invade the open reactor system and lead to a crash of the culture [3]. This can lead to a tremendous decline in biomass productivity of the open reactor system. Analytics of the mechanisms behind cultivation crashes experienced increasing interest in the face of biofuel applications [91, 128, 129]. Based on those findings, physical [3], chemical [90] or biological methods [130, 131] for open cultivations were studied in order to diminish the parasite concentration. As long-term stability is essential for stable biofuel production, tremendous research for each individual production strain is required in order to prevent frequent product losses. Depending on the development of GMO regulations, also further basic research on the metabolic networks during photosynthesis and lipid accumulation should be conducted, in order to incorporate the findings into improved processes with tailor-made strains [47, 132].

At downstream processing, research should be focused on less energy intensive harvesting techniques, which renders a huge potential for optimization [124]. Probably the most widely accepted requirement for cost competitive algal biofuel is the commercialization of other products like proteins, pigments, and sugars from the biomass [127, 133, 134]. In this approach, however, primarily the extraction techniques have to be adapted in order avoid e.g. denaturation of the protein fraction [135]. This modification of procedures previously tailored to maximum extraction efficiency of a single compound will probably lead to a reduced yield for all cell components. This loss has to be made up for by the additional use and commercialization of the additionally extracted cell products.

1.3. Small scale screenings of microalgae

A major drawback in the establishment of large scale microalgae production processes, is the identification of robust and productive strains as outlined in section 1.2.3.5.. Given the tremendous species variety, environmental habitats are a major source for new lead strains [82, 136]. In a process called bioprospecting, algae strains are isolated from the environment, screened for their ability to produce a certain compound in the laboratory and optimized for the production in large scale facilities [40]. Various strategies have been applied in order to facilitate and fasten the screening process. A summary of the applied procedures is given in section 1.3.4.

After the sampling of strains from the environment, the challenge of selecting the most appropriate strains under laboratory conditions arises. A high number of strains needs to be cultivated under homogenous and robust conditions in order to obtain meaningful results from this primary screening. A reasonable implementation of this task is only possible by reducing the culture volume and thus increasing the throughput. Small scale cultivations systems, however, have been developed so far mainly for heterotrophs [137–140]. The design considerations for phototrophic small-scale cultivations differ significantly. One aspect among others is e.g. that the light needs to penetrate the culture homogenously [141]. Microplates proved to be favorable in larger heterotrophic cellular growth screenings [142]. Only with the recent advent of microalgae research for biofuel applications, also research in parallel microplate cultivation systems for phototrophs was advanced. A summary of the current approaches is given in section 1.3.5.

1.3.4. Bioprospecting of microalgae

Screenings for new algae strains from the environment can be divided into univariate and multivariate approaches [40]. Univariates screening aim for a single trait in the tested strains. This can be tolerance to high CO_2-concentration [143], hyper-lipid-producing strains [144] or astaxanthin producing strains [136]. The chances of finding a new and/or suitable strain can be increased by limiting the sampling to favorable habitats. For

instance, strains, which are intended for outdoor mass cultivation, should screened for in extremophile habitats as they already inhibit the selective physiological properties [145]. However, the suitability of a given strain in large scale cultivations most often depends on more than one physiological trait. As outlined in section 1.2.3.5, e.g. lipid productivity is not the sole key factor in the selection of an isolated strain for a biofuel application. Easy harvesting, tolerance to a selective environment, dominance over invading strains and low nutrient requirements should also be taken into consideration. In order to include more than one factor in the screening, multivariate approaches were designed. Thereby, a given number of strains is enriched and/or screened at the same time for multiple factors like tolerance to a given cell size, heterotrophic growth, tolerance to high temperature, high CO_2-concentrations and high salinity [146]. Compared to the univariate approach, fewer strains have to be handled and maintained in the process and strains with more defined properties can be obtained from the procedure.

1.3.5. Small scale screening systems for phototrophic microorganisms

With the progress of microalgal biotechnology in recent years, considerate effort was put into the identification of new strains from the environment or the screening of known strains for benevolent traits. The screening was often conducted in cultivation systems once developed for heterotrophs and which were modified according to cultivation requirements. Those include sufficient light penetration of the algae suspension, uniform light distribution to each cultivation and high CO_2 transfer rates into the medium. Despite the increasing effort in algae screening, only rare attempts have been made to miniaturize the cultivation and selection process. Previously, microplates have been frequently used for freshwater algal toxicity tests [147]. As currently more and more strains from saline habitats are screened, it turned out that the incubation is in general longer. Therefore, measures in order to limit evaporation were tested. For instance, Han et. al flushed a microplate with different CO_2-concentrations and wrapped them in a combination of scotch tape and parafilm [148]. The overall homogeneity of algae growth

in microplates were tested by Pacheco et. al, obtaining CV of 9.4-12.9 % throughout a plate [149]. The effect of light on the growth rate of algae was studied by van Wagenen et. al [150]. They could show that the datasets of light intensity dependent growth rate obtained in microplates were comparable to those measured in a photobioreactor. Other studies focused on the evaluation of lipid productivity of microalgae in microplates. Due to the small volumes, this was mostly done by indirect determination via Nile Red (NR) fluorescence. For instance, Franz et. al studied the effect of bioactive compound on the growth and NR fluorescence of four microalgae strains [65].

All of the aforementioned studies were based on manual absorbance measurements. In order to increase the throughput and to generate more data points for a more valid growth curve, automated measurements need to be implemented. One of the few screenings conducted within an automated laboratory framework was published by Radzun et. al. [151]. They constructed a cultivation chamber with three shaking platforms, to each of those six 96-well-plates were mounted. The whole set-up was illuminated from above and below and CO_2 was released into the chamber in order to avoid limitation. Absorbance measurements were undertaken every 3 h. A total of 1512 wells could be examined simultaneously for media optimization approaches. Tillich et. al used a smaller throughput with a 96-deep-well plate, positioned in an enclosed cultivation chamber [152]. The chamber is flushed with a CO_2/air-mixture and a laboratory robot removes a small amount of cell culture for absorbance measurements. The plates were continuously shaken and humidity was regulated in the box. Apart from absorbance, MALDI-TOF-MS and chlorophyll concentration could be measured during the process. Morschett et. al modified the BioLector® system microplate (m2p-labs GmbH, Baesweiler, Germany) reader with a LED-based illumination unit [153]. The previously established system provides controlled temperature, atmosphere, humidity setup as well as controls shaking frequency to the proprietary 48-well plate. In a proof-of-principle cultivation the differences in scattered light measurements, as an indirect method to measure cell proliferation, showed differences of ± 5.2 % between the wells.

2. Material & Methods

2.1. Isolation and screening procedure of microalgae strains from environmental samples

2.1.6. Sampling procedure

The samples were taken in July 2014 in southeastern Australia. Within seven days 45 samples from 11 sites could be obtained. At each site, the following three samples were collected:

1. An untreated sample of the water column on the surface of the water body: In order to obtain that sample, a 50 mL tube was held under water and, when filled completely, closed.
2. A sample of the same location as sample 1 but filtered through a 30 µm mesh: For this sample a piece of mesh was wrapped around the opening of a 50 mL tube and water was filtered inside the tube until it was completely full.
3. A sample of the sediment of the water body: For this, a 50 mL tube was pushed through the bottom of the water body so that at least one fourth of the volume of the tube was filled with solid particles like stones and soil. The tube was then closed immediately under water in order to include as much water from sediment area as possible.

Beside those regular samples, varying samples were taken depending to the on-site conditions. These additional samples included organic material scrapped off rocks or mussels and plant material floating on the surface of the water body. All of the 50 mL tubes were closed with the lid and wrapped with parafilm.

The temperature, pH, conductivity and GPS values of the sampling sites were measured with a daily calibrated multiparameter probe (Aquameter AM 200 with AQUAPROBE™-1000, Innovative Messtechnik Dr. Weiss, Tübingen, Germany).

After sampling the last site, all tubes were sent in one, internally not illuminated package to the laboratory in Garching bei München, Germany. The duration of transport was six

days. In the laboratory, the samples were held as they were in a climate cabinet at 19°C without being shaken (IPP750, Memmert, Schwabach, Germany). The samples were illuminated constantly by warm-white LED panels (LED Matrix, warmwhite 12 V; Lumitronix; Hechingen; Germany) attached to the top of every cabinet compartment, providing a PPFD of 10 µmol/(s · m^2). The PPFD mentioned here and throughout the whole study was measured with a LI-190SA Quantum sensor attached to the LI-250A light meter (both LICOR, Lincoln, Nebraska, USA). Deviations from this approach are specifically mentioned. The samples were stored in the climate cabinet until further treatment.

2.1.7. Enrichment of the isolated cultures

The isolated cultures in the 50 mL tubes were shaken thoroughly and then filtered through a 30 µm mesh into another tube. Every sample was cultivated in four different media (ASW, BG11, ASP-M, f/2) in two different concentrations (1-fold and 0.2-fold). All media were prepared with a final NaCl concentration of 50 g/L and the pH was set to 8. The chemical composition and the reference to the origin of the receipts are enlisted in Appendix 1. For this assay, one half of the media was prepared with doubled the nutrient and salt concentration. Then, 750 µL of this solution were mixed in a cavity of a 24-Well Cell Culture Plate (Eppendorf, Hamburg, Germany) with 750 µL of the environmental sample, resulting in a 1-fold concentrated media. For the 0.2-fold concentration, a double concentrated nutrient solution with the five-fold concentration of NaCl was prepared. 1350 µL of the environmental sample and 150 µL of this medium were mixed, resulting in a solution with 0.2-fold concentrated nutrients and single concentrated NaCl.

With 45 samples taken from the sites and distributed on eight different media variations, 360 samples were cultivated in total for that experiment. On each plate, three samples of *Picochlorum* sp. and two of *Dunaliella salina KU11* were also cultivated as positive controls. The starting culture for these samples was diluted to an OD_{750nm} of 0.1, measured

by the Agilent Spectrophotometer and then a volume of 1.5 mL of this suspension was transferred to the plate. Furthermore, as a negative control one well was filled only with H_2O.

The plates were cultivated in an Innova S44i incubation shaker (Eppendorf GmbH, Hamburg, Germany). The shaking frequency was set to 160 rpm with a shaking orbit of 25 mm. The CO_2-concentration inside the shaking chamber was held constantly at 1 %, with the remaining 99 % being ambient air. The shaker was provided with an LED-panel attached to the internal ceiling. The relative light intensity that was adjustable through the shaker software varying between 0-100 % corresponded to a linear range (R^2=99.87) of 0-100 µmol/(s · m²). For this study, a 24-steps light intensity and temperature gradient was implemented in the software to approximate the day-night cycle as established by Glemser [154]. In that work, the actual irradiance intensity and temperature values of the 15th, June, 2012 in Almería, Spain, were modeled and the resulting function was implemented in a photobioreactor regulation. In order to apply this gradient to the S44i LED-panel, 24 values with an hour distance between each of the data points were extracted from the function. The temperature and light PPFD steps are shown in Figure 9. During the cultivation, the absorbance at 750 nm and the fluorescence emission at 690 nm, excited by a light beam of 440 nm wavelength, were measured with a Perkin Elmer Microplate Reader as described in section 2.4.10.2 and 2.4.10.4 respectively. The selection of the most favorable strains was based on these two parameters, macroscopic observations and the equipment that was provided for this project. A description of the whole process is laid out in section 3.1.2.

From each of the remaining 15 strain cultures a volume of 5 mL was transferred to a 50 mL flask containing 35 mL of the respective media. The flasks were cultivated in an incubation shaker at 26°C and 120 rpm at an orbit of 51 mm (Innova 44, Eppendorf GmbH, Hamburg, Germany) and growth was measured via OD_{750} measurements. An illumination of 70 µmol/(s · m²) was provided by a photosynthesis light panel mounted

to the ceiling of the interior of the shaker. Under these conditions the flasks were propagated until further treatment.

2.1.8. Purification of propagated strains

In order to obtain axenic cultures two purification strategies were conducted: On the one hand, the strains identified by the selection procedure were subjected to an antibiotic treatment in liquid media followed by streaking out the cultures on solid media without antibiotics. A detailed description of the steps being undertaken is given in section 2.1.8.1. The other approach was an isolation of the photosynthetic active populations from the mixed culture by FACS. Based on the method specified in section 2.4.10.2 the most dominant red fluorescent populations were sorted from the heterogenous initial cultures and the purification success was monitored. The exact procedure is given in detail in section 2.1.8.2

2.1.8.1. Antibiotic treatment of mixed cultures

A volume of 1 mL of each culture was mixed with 5 mL of the respective media in a 15 mL tube. This was done in duplicates. An antibiotic solution (Table 1) was prepared and 0, 50, 250, and 500 µL of that mix were added to two of the eight tubes respectively. The closed tubes were cultivated in the Innova 44 incubation shaker at 160 rpm and 26°C in a rack tilted by 45° for 72 h. Total cell concentration and percentage of sorted population were monitored daily via a cell sorter. In the same interval, 10 µL of each tube was streaked out on solid agar to allow for a visible contamination test. The agar plates were kept in the dark at 28°C. A successful purification was declared after 72 h of no visible growth on the agar plates.

Table 1: Antibiotic composition for purification process.

Antibiotic	Final concentration (g/L)
Cefotaxim	0.5
Carbenicilin	0.5
Kanamycin	0.2
Amoxicilin	0.2

2.1.8.2. FACS of mixed cultures

For all of the 15 strains stemming from the microplate selection process a specific cell sorting protocol was created with the ProSort™ software (V1.3.) of the S3 Cell Sorter (Bio-Rad, Hercules, California, U.S.). Gates were set on the highest fluorescing population appearing with the FL2 filter. The cell concentration and the percentage of the events in the sort gate in relation to total events were recorded before sorting and 19 days after sorting. In parallel, a non-sorted culture was cultivated and analyzed at the same day as the sorted samples in order to determine the efficiency of the sorting process.

2.1.9. Screening for FA productivity

The purified strains were cultivated in 500 mL shaking flasks for the analysis of the lipid productivity. For each strain four flasks were prepared, two with a nitrate concentration as shown in Table 18 and two with a 0.2-fold concentration of that. Due to spatial limitations in the shaker the reference strain *Nannochloropsis salina* was only cultivated in two flasks with the standard and the lower concentration, respectively. With a starting OD_{750nm} of 0.05 in 200 mL of media the flasks were put in an Innova 44 incubation shaker at 26°C and 120 rpm. The illumination was provided from underneath by a custom-made LED shaking platform at an PPFD of 150 µmol/(s · m²). The flasks were closed with a rubber stopper, which had two tubes as inlets connected to luer connectors at the outside of the flask. A polyethersulfone filter (PES) and a PTFE-filter were attached to the connectors. A mixture of 1 % CO_2 and 99 % ambient air (v/v) at a flowrate of 1.8 L/h was gassed via the PES filter into the headspace of the flask. The whole set-up is

schematically depicted in Figure 3. Daily measurements of absorbance and fluorescence were undertaken by measuring 200 µL of each culture in triplicates in a 96-well microplate via the Perkin Elmer microplate reader according to sections 2.4.10.3 and 2.4.10.4. Within the exponential growth phase, determined by the R-module, 100 mL of the culture was removed and used for the analysis of the lipid content as described in 2.4.10.7. Furthermore, a volume of 1 mL was taken separately for the measurement of the nitrate concentration (see 2.4.10.8). These two samplings were repeated at the end of the cultivation. The culture was aborted after three days of stationary growth.

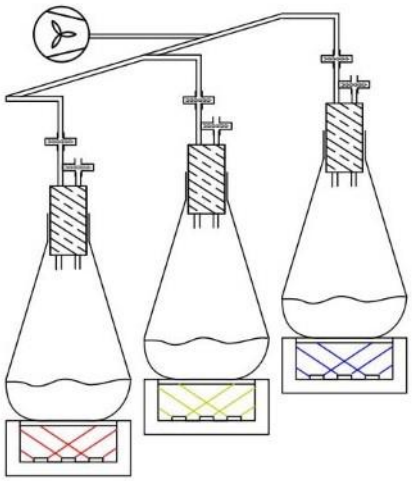

Figure 3: Schematic overview of cultivation set-up in the Innova 44 incubation shaker. Image by courtesy of Matthias Glemser [154].

2.1.9.1. Phylogenetic analyses

All strains which were isolated from the environment in the course of this work and *Picochlorum* sp. were identified by the analysis of the 18S-rRNA gene sequence.

For the extraction of genomic DNA (gDNA) a minimum of 3 mg dried biomass were used with the *innuPREP Plant DNA Kit* (Analytic Jena, Jena). A PCR was processed afterwards, using the gDNA as template together with different primers. The composition of the PCR sample is given in Table 2 and the applied PCR program in

Table 3.

Table 2: Composition of PCR-sample with 18S-primer. Primer and protocol were adapted from [155].

Component	Concentration	Unit	Amount	Unit
DI H_2O			41,5	µL
DreamTaq Green Buffer (Thermo)	10 x		5	µL
DreamTaq Polymerase (Thermo, #EP0703)	5	U/µL	0,5	µL
dNTP-Mix	10	µM	1	µL
EukA (fw primer)	10	µM	0,5	µL
EukB (rv primer)	10	µM	0,5	µL
DNA	50-100	ng/µL	1	µL

Table 3: Program for PCR with 18S-Primer. Protocol was adapted from [155].

Frequency	Step	Duration/s	Temperature/°C
1 x	Initial denaturation	130	94
	Denaturation	94	30
35 x	Annealing	45	59
	Elongation	130	72
1 x	Final Elongation	300	72
1 x	Storage	---	4

The PCR products were separated on a 1 % agarose gel stained with 4 µL of SERVA DNA stain. Appropriate bands were cut out of the gel and purified via a Kit (innuPREP DOUBLEpure, Analytic Jena, Jena, Germany). The purified PCR products were submitted as premixed samples to a DNA sequencing procedure.

For the identification of strains, sequences obtained from 18S rRNA genes were submitted to NCBI's blastn search [156]. Sequence alignments were performed with MUSCLE applying default settings [157]. The best model for calculating the phylogenetic tree was determined by an internal tool of MEGA software [158, 159]. In the same software, the tree was calculated under the following settings:

[Analysis Settings]

Analysis = Phylogeny Reconstruction

Statistical Method	=	Maximum Likelihood
Test of Phylogeny	=	Bootstrap method
No. of Bootstrap Replications	=	1000
Substitutions Type	=	Nucleotide
Rates among Sites	=	Has Invariant sites (I)
Gaps/Missing Data Treatment	=	Use all sites
Branch Swap Filter	=	None

[Analysis Statistics]

Sum of branch lengths	=	0.366
Model	=	Hasegawa-Kishino-Yano (1985) model (+I)
Num of params	=	14
Num of rates	=	1
AICc	=	7764.782
BIC	=	7857.575
LnL	=	-3868.354
Invar	=	0.528
Gamma	=	0.432
Ts/Tv	=	1.570

2.2. Development and assessment of microalgae screening platforms

2.2.1. Manual screening set-up (*es*MTP)

The manual screening set-up was denominated throughout this whole study as *es*MTP as it is based on a sterile and autoclavable membrane by the company *enzyscreen*, Heemstede, Netherlands. The set-up consisted of a laboratory shaker (HS 501 digital, IKA, Staufen, Germany) which was placed in a temperature-controlled incubator (AL01-07-100, Advantage-Lab, Schilde, Belgium). Three *es*MTP mounting devices were attached to the platform of the shaker. As LED units, the above-mentioned matrix LEDs by Lumitronix were used. The light intensity of each LED panel was regulated by constant current provided by an individual power supply (LABPS3005, Vellemann, Gavere, Belgium). The interior of the incubator was gassed with a mixture of 1 % of CO_2 and 99 % of air (v/v) at flow rate of 133 NL/h provided by a gas mixing station (MX4/1, DASGIP, Eppendorf, Germany). For OD_{750nm} measurements, the *es*MTP systems were removed from the halted shaker and the *enzyscreen* membrane was replaced in the laminar hood by a transparent PC lid. Then the OD was measured with one measurement per well in the Perkin Elmer Microplate Reader. After the measurement, the process was conducted backwards for the continuation of the cultivation.

2.2.1.1. Assessment of homogenous light distribution in *es*MTP

A lid of a Costar® plate was placed upside down in the *es*MTP-system which was placed on the first mounting device at a light intensity of 58 µmol/(s · m^2). A paper stencil with the outer dimensions of the lid was laid into the lid. The stencil possessed 12 openings with the exact position and diameter of the *am*MTP-wells. The optical sensor of the hand-held spectrometer (STS-VIS-RAD, Ocean Optics, Ostfildern, Germany) was placed onto the center of each of the openings and the light intensity was measured at an integration time of 1 s. After obtaining all the values from the first mounting device the

whole *es*MTP-system was transferred to the second one. First the current was set to obtain a PPFD value of 58 µmol/(s · m²) of the two center openings. Then the measuring process was conducted. For the third device the whole process was repeated. The statistical analysis was performed according to section 2.4.11.

2.2.1.2. Comparison of *es*MTP to other systems

P01 and P02 were cultivated and measurement as described in the previous paragraph. P03 could be measured directly in the microplate reader as the sealing tape was transparent and represented a sterile barrier.

2.2.2. Automatable screening set-up (*am*MTP)

The design of the *am*MTP was created with Autodesk Inventor Professional 2015 (Autodesk GmbH, Darmstadt, Germany) and manufactured by Airbus APworks GmbH (Taufkirchen, Germany). In Table 4 all of the parts for the assembly of the *am*MTP are listed. The simulation of the gas flow was conducted with Autodesk CFD 2016 (Autodesk GmbH, Darmstadt, Germany).

Table 4: Summary of parts used for *am*MTP system.

Part	Part No. (see Figure 26)	Material	Remarks	Company/ Workshop
Lid	1	Aluminum	Thickness: 2 mm	TU workshop chemistry department
Upper glass plate	2	Borofloat	85.5x63x1.75 mm	Micros optics, Schmiedefeld, Germany
Upper sealing	3	EPDM	104x85,6x2 mm. Type: RCT®-CHAP-1021-1-PL	Chemietechnik Reichelt, Heidelberg, Germany
Glass insert	4	Borofloat	Outer diameter: 18 ±0.16 mm Wall thickness: 1.2 ±0.05 mm	TU Munich Glassblowing
Sealing	5	Silicon	Thickness: 1 mm, ca. 60 Sh-A	Modulor GmbH, Berlin, Germany

Cover glass	6	Borofloat	Thickness: 0.13-0.16 mm, Diameter: 18 mm	Omnilab-Laborzentrum, Bremen Germany
*am*MTP corpus	7	AlSi10Mg		APworks, Taufkirchen, Germany
Lower sealing	8	EPDM	104x85,6x2 mm. Type: RCT®-CHAP-1021-1-PL	Chemietechnik Reichelt, Heidelberg, Germany
Steel washer	9	Steel	Diameter: 12 mm Thickness: 1 mm	Pradler Werkmarkt, Garching, Germany
Distance bush	10	Steel	Diameter: 9 mm, Length: 45.83 mm	Pradler Werkmarkt, Garching, Germany
FLL/M5-connector	11	Nickel plated brass		Wolfram Droh GmbH, Mainz, Germany
MLL/FLL-filter capsule	12	PTFE	Outer diameter: 15 mm, Filter size: 0.2 µm	Saint-Gobain – Filtration Technologies, Gaithersburg, MD, USA
MLL/M5-connector	13	Nickel plated brass		Wolfram Droh GmbH, Mainz, Germany
Lower glass plate	14	Borofloat	84.5x62x1.75 mm	Miros optics, Schmiedefeld, Germany
Lower plate	15	Aluminum	Thickness: 2 mm	TU workshop chemistry department
Screw	16	Steel	M3 – 8 mm	TU workshop chemistry department

The cover glass was glued with *GLASS Reparaturkleber* (UHU GmbH, Bühl/Baden, Germany) and for sealing the lid and the glass insert silicone was used.

The PLA printed acrylic plate positioning component, the *am*MTP (see (3) and (4), Figure 27) and the cultivation chamber (see Figure 31) were designed with Autodesk Inventor Professional 2015 (Autodesk GmbH, Darmstadt, Germany) and manufactured by Rapid Prototyping with the Creator HS printer (Leapfrog, Alphen aan den Rijn, The Netherlands).

2.2.2.1. Assessment of homogenous light distribution in *am*MTP

The spectrometer was centered on the lens of a LED and different currents were applied in order to obtain a linear curve between the values for current and the emitted PPFD.

Based on this curve the light intensity for cultivation was set. The statistical comparison between the LEDs and the plates were conducted as described in section 2.4.11.

2.3. Bacterial communities in open thin-layer cascade reactor system

2.3.3. Strain and media

In all experiments regarding the bacterial communities, *Dunaliella salina KU 11* was used in BG11 media at a pH of 8 and a NaCl concentration of 50 g/L.

2.3.4. Photobioreactor set-up

The shift experiments were first conducted in parallel Labfors 5 Lux stirred-tank photobioreactors (Infors, Bottmingen, Switzerland). The working volume of the reactors is 2.3 L. First the pH shifts were conducted in two parallel cultivations and then the salinity shifts, also in two parallel cultivations. In order to conduct the salinity shifts, bottles with either water or a 280 g/L NaCl solution were attached via a tube and a fitting to a free port in the lid of the reactor. Furthermore, bottles with 10 % phosphoric acid and 2 M NaOH were attached to control the pH value and induce the shift. PH was set to 8 and the regulation during the cultivation process was conducted by a programmed sequence within the integrated Iris 6 control software (see Appendix 3). Light intensity and temperature were regulated by another part of the sequence. The applied gradient simulated the climate scenario of Almería in Spain and was developed in the course of the work of Glemser [154]. As the integrated LED panels of the Labfors 5 reactor could not provide the light intensity measured in Almería at that day, the modeled curve was downscaled. The whole reactor was autoclaved and non-autoclavable media components were added afterwards by a heat-sterilized syringe through a heat-sterilized septum. Samples for OD and cell count concentrations were taken daily and samples for the metagenomic analyses of the bacterial populations were taken before, during and right after the shifts as well as two days after the shift and at the end of the cultivations.

2.3.5. Salinity and pH shifts in photobioreactors

Shifts of the chemical conditions of the culture were conducted at an OD_{750nm} of approximately 8. The pH-shifts were achieved by changing the settings to 5 or 11 respectively in the control sequence.

The shift to a salinity of 10 g/L NaCl was achieved by removing 1.84 L of the cultivation after 8 d. This was done sterilely via the sampling system and a sterile tube, fixated in a peristaltic pump. Then, the reactor was sterilely refilled with 1.84 L of autoclaved water and the respective dissolved nutrients for this amount of volume. Under these conditions the cultivation was continued for three hours. After this time, 0.34 L of culture was removed and the reactor was refilled with the same volume of the 280 g/L concentrated NaCl-solution and the nutrients for this volume.

The shift to a salinity of 150 g/L was conducted by removing 1 L of culture volume and refilling it with 1 L of the 280 g/L concentrated NaCl-solution and the respective nutrients. After three hours, 0.767 L of the culture volume were replaced by water and the respective amount of dissolved nutrients.

2.3.6. Open thin-layer cascade set-up

The reactor system was developed by the Institute of Biochemical Engineering of the Technical University of Munich (TUM). The system was set up in the TUM-algae Tec Center in Taufkirchen, Germany, and detailed specifications of the system were published by Apel et. al [87]. In the course of this work, two nearly identical reactors were used in parallel. The salt shift to 150 g/L was thereby in the reactor designated as FSG 2 and the temporal pH shift to 5 in the FSG 3 reactor. Both were operated with a total volume of 60 L. The pump frequency of FSG 2 was adjusted to 26 Hz and the frequency of FSG 3 to 17 Hz, resulting in a flow velocity of the culture of between 2.1 and 2.2. L/s. The reactors were initially filled with 60 L of 50 g/L concentrated NaCl solution in which the solid, pre-weighed nutrient salts were dissolved. The pre-culture originated from the

photobioreactor experiments and was added after the complete dissolution of the salts in the liquid.

2.3.7. Salinity and pH shifts in open thin-layer cascade

The salinity shift was achieved by adding 6 kg of NaCl to the reactor. This condition was maintained until the end of the cultivation. The pH shift to 5 was achieved by adding 32 mL of concentrated and 300 mL of 10 % HCl. After 3 h the pH was elevated by the addition of 160 mL of 1 M NaOH. The fine adjustment of the parameter was conducted by the automated CO_2-addition to the media.

2.3.8. Analysis of algae and side population by flow cytometry

The analysis of cell concentration during the experiments in the open thin-layer cascade system was conducted on the CytoFLEX cell counter (Beckman Coulter, Brea, California, USA). The measurement was conducted for 160.000 events in the sample, whereas the flow velocity was minimized in order to reduce the abort rate. Based on the event rate per volume provided by the device, the cell concentration could be directly calculated. For the analysis of samples, the software Kaluza (V.1.5a, Beckman Coulter, Brea, California, USA) was used. The selection of the algae gate was conducted by applying a respective gate in a plot of forward and side scatter values. Subsequently a threshold for the minimal red fluorescence of the selected samples was chosen in order to exclude non-fluorescent events of the same size (forward scatter) and granularity (side scatter).

2.3.9. Analysis of bacterial communities

The description of the analysis of bacterial communities is adapted from Bracharz et. al as the samples described in both works were treated in the same batch [160]:

The analysis of the bacterial communities in both reactor set-up was conducted at the Center for Biotechnology of the University of Bielefeld. First, rRNA gene amplicons were

sequenced as described by Maus et. al [161]. The primer set Pro341F (5′-CCTACGGGGNBGCASCAG-3′) and Pro805R (5′-GACTACNVGGGTATCTAATCC-3′) was used for the amplification of the 16-rRNA regions V3 and V4 of bacteria and archaea [162]. This primer pair also covers some algal chloroplast and some other eukaryotic mitochondrial genomes. Then, multiplex identifier (MID) and Illumina-specific sequencing adaptors were used for a two-step PCR approach. In the procedure PCR products of approximately 460 bp length were purified MPureXP® magnetic beads (Beckman Coulter GmbH, Brea, California, USA). The generated amplicons were quantitatively and qualitatively analyzed by the Agilent 2100 Bionanalyzer MPureXP® magnetic beads (Beckman Coulter GmbH, Brea, California, USA). For paired-end sequencing on the Illumina MiSeq system (Illumina, San Diego, California USA), the produced amplicons were pooled in equimolar amounts.

The quality control and the amplicon processing was performed in line with a previously described pipeline [163], which trimmed adapters and primers for all samples. For amplicon processing the FLASH pipeline [164], USEARCH 8.1 [165], UPARSE [166] and the RDP classifier [167] were used in a manner describe recently [161, 168, 169]. In the process, all sequences that were not merged by FLASH (default settings + -M 300) were filtered out. Additionally, sequences with more than one ambiguous bases and expected errors higher than 0.5 were discarded. The resulting data was processed and operational taxonomic units (OTUs) were clustered by USEARCH 8.1. These OTUs were taxonomically classified using the RDP classifier (V2.9) in 16S modus. Hits with a confidence value of 0.8 and higher were considered. The obtained raw sequences were mapped back onto the OTU sequences in order to get quantitative assignments.

2.4. General methods and materials

2.4.9.1. Strains

The strain *Picochlorum* sp. was isolated from an environmental sample, taken from the Salt Lake Pond on San Salvador, Bahamas (24°01'40.7"N 74°26'58.7"W). *Nannochloropsis salina* (now *Microlopsis salina*, 03.10.2017) was purchased from the Culture Collection of Algae at Göttingen University (SAG) where it is stored under the reference number SAG 40.85. *Dunaliella salina KU 11* was isolated from Salt Creek, South Australia, Australia, at S 36°09.6874' E 139°38.8328'.

2.4.9.2. Media

All media compositions are listed in Appendix 1. Nutrients were added from concentrated stock cultures to give the desired final concentration. PH was adjusted before autoclaving. Marked components (*) were sterile filtered and added sterilely to the media after the autoclaving.

2.4.10. Analytical methods

2.4.10.1. Determination of cell concentration

The cell concentration was determined via a cell sorter (S3, Bio-Rad, Hercules, California, U.S.) set up in a custom-made microbiological safety cabinet (ENVAIR Deutschland GmbH, Emmendingen, Germany). A measuring protocol had to established for every strain analyzed with the device. The first step in doing so was to run water in the device. Then the detection threshold determined by the FSC signal was lowered so that the event rate was stabilized below 10. This level of noise was considered as negligible. An aliquot of the sample was then analyzed to check for the distribution of the population and a gate in the FL2 histogram encompassing the desired population was created. Based on this histogram, cell debris was gated out of this population in another histogram set on the FSC channel by setting up a gate with an appropriate lower threshold. All of the events in the produced gate were regarded as "cells" of the desired population. The

protocol was then used in the subsequent measurements of three replicates of the sample containing 100 µL. The samples were each put in the sorter one after the other and measured until the notification "Bubble detected" showed up, meaning that the whole volume was taken up by the sample line and got measured. The cell concentration was calculated as follows:

$$Cell\ concentration = \frac{cell\ count}{V} \quad (4)$$

The acquisition of data files was done with the ProSort™ software (V1.3.). For the analysis of samples, the software Kaluza (V.1.5a, Beckman Coulter, Brea, California, USA) was used.

2.4.10.2. Cell sorting of photosynthetic active populations

The sorting of cells was done by applying an established protocol to a given sample. The desired population were chosen and sorted into 2 mL tubes. From there, the samples were pipetted into their designated cultivation vessels. The event rate during sorting was set to 1000.

2.4.10.3. Determination of optical density

Spectrophotometer (*Agilent 8453*, Waldbronn, Germany):

Here, a volume of 1 mL of medium was used to blank the device at the wavelengths 680 and 750 nm, respectively. If absorbance values over 0.5 occurred, the suspension was diluted to obtain values between 0.1 and 0.5 to ensure measurements in the linear range of absorbance.

Spectrophotometer (GENESYS, ThermoFisher Scientific, Waltham, Massachusetts, USA):

The analysis of OD_{750nm} during the experiments in the open thin-layer cascade system was conducted on the GENESYS spectrophotometer. The same procedure as for the Agilent device was applied here.

Microplate Reader (*EnSpire® Multimode Plate Reader*, Perkin Elmer, Waltham, MA 02451 USA):

Here, the absorbance of a certain volume of cell suspension was measured in an optical microplate. A blank well filled with media was measured before or in parallel to the measurement and was subtracted from the value. For every plate and volume used, a calibration curve between the microplate reader and the *Agilent* spectroradiometer was established to standardize every measurement to that device (see Appendix 2). With these values and the OD-to-CDW-coefficients (see 2.4.10.5) the CDW concentration was determined in the microplates.

Microplate Reader (FLUOstar Galaxy, BMG Technologies, Ortenberg, Germany):

This device was embedded in the automatic cultivation system described in 3.2.3.2. The longest wavelength that could be measured here is only 730 nm, a correlation factor between 730 nm and 750 nm was established to compare the values between the *EnSpire*® reader and the *FLUOstar* (see Appendix 2). With these corrected values the CDW concentration was determined likewise.

Comparison between measuring instruments and calculation of biomass concentration

The OD coefficients for the comparison of values of two different microplate readers were obtained by first measuring the same plate in both devices at 750 and 730 nm. Then those values were plotted on the x- and y-axis and a linear regression curve between the two data sets was calculated. The relation between values of the microplate readers and the Agilent spectrophotometer was evaluated by generating a serial dilution of a given cell suspension and subsequent measuring all samples with all three devices.

The measured absorbance values were converted to biomass concentration values by using the previously determined coefficient relating the measurements of the microplate reader to the OD values of the *Agilent* spectrophotometer. The transformed values were then converted to biomass concentration by a respective coefficient. All of the converting formulas for transforming the OD values between the different measuring devices as well as the formula for converting the OD values to biomass concentration of the analyzed strains are given in Appendix 2.

2.4.10.4. Determination of chlorophyll fluorescence

Fluorescence intensity was measured in a Microplate Reader (EnSpire® Multimode Plate Reader, Perkin Elmer, Waltham, MA 02451 USA). The sample was excited at 440 nm and the emission was measured at 690 nm, both from the top.

2.4.10.5. Determination of cell dry weight

First, 5 mL of the sample were centrifuged, the supernatant was discarded and the sample resuspended in DI water. These steps were repeated once and the 5 mL suspension then transferred to a moisture analyzer (Ohaus MB25, Parsippany, New Jersey, U.S.). At a temperature of 105°C the sample was dried on a pre-weighted aluminum dish. The device-specific setting stopped the drying process if a loss less than 1 mg within 60 s could be detected. The CDW concentration was determined as follows:

$$CDW\ conc. = \frac{(m_s - m_0)}{V} \quad (5)$$

m_s	mass of plate with sample after drying	g
m_0	mass of empty plate	g
V	volume of applied cell suspension	mL

For every strain a correlation coefficient between CDW concentration and the respective OD value was determined. In subsequent experiments, only this correlation coefficient was used to determine CDW concentration.

2.4.10.6. Determination of evaporation rate

As only masses could be determined reliably for the evaporation rate, but volumes are a more meaningful parameter in this manner, a density of 1 g/cm³ was assumed for the evaporated water in order to enhance the comparability with other studies.

*es*MTP

The whole microplate was measured at least four times during the cultivation and the evaporation per day was calculated according to the following formula:

$$Evaporation\ rate\ = \frac{\alpha}{N} \times (-1000)\ \mu L/(Well \cdot d) \quad (6)$$

m_{t0}	mass of plate on day 0	g
t	cultivation duration	d
α	slope of linear regression of mass differences and time points	
N	number of wells filled with liquid	

*am*MTP

The evaporation rate in the *am*MTP system was measured individually for each well. The rate was determined by subtracting the final mass at the end of the cultivation from the sum of the mass of the empty well and the applied initial culture volume. Assuming a density of 1 g/cm³ for the water, the evaporation rate in µL per well and day could be calculated based on:

$$Evaporation\ rate\ = \frac{(m_0 + m_v) - m_{t,final}}{t} \quad (7)$$

with

m_0	mass of empty well	g
m_v	mass of well and culture at the start of cultivation	g
$m_{t,final}$	mass of well and culture at the end of cultivation	g
t	cultivation duration	d

2.4.10.7. Determination of fatty acid content via Direct Transesterification

For the determination of the fatty acid content a suspension of cells was centrifuged down at maximum speed and the supernatant got discarded. Then, the pellet was resuspended in DI water and centrifuged again. The supernatant was discarded and the remaining pellet was frozen at -80 °C. After being completely frozen the tube was put in a freeze-dryer (Alpha 2-4, Martin Christ Gefriertrocknungsanlagen GmbH, Osterode, Germany) at 2 mbar and -74 °C. After 2 days the tube was taken out of the freeze-dryer and masses greater than 5 mg were weighed directly into a pressure-resistant glass tube with a PTFE-silicone membrane sealed cap (Laborfachhandel Ochs e.K., Bovenden / Lenglern). Masses below 5 mg were first transferred in a small aluminum bowl which was weighted blanked beforehand. The bowl with biomass was put with a tweezer on the scale (Mettler Toledo™ Excellence XS Microbalance, Mettler Toledo, Columbus, Ohio, US) and the biomass was transferred after measuring to a PTFE-silicone membrane sealed cap. The empty bowl was weighed again and the remaining value was subtracted from the sample.

The protocol for the Direct Transesterification (DT) of fatty acids was adapted from [114] and modified slightly. As exclusively freeze-dried biomass was used, the water scavenger in the protocol was omitted. Also, BF_3 in methanol was replaced by hydrochloric acid in methanol due to easier handling.

For the DT 0.2 mg of the internal standard C19-TAG (Sigma Aldrich, St. Louis, Missouri, US) respectively, dissolved in 500 µl GC-grade toluene (Sigma Aldrich, St. Louis, Missouri, US), was applied to the freeze-dried biomass. The sample was vortexed and 1 mL of a 0.5 M solution of sodium methoxide dissolved in methanol was added.

Then the sample was heated up to 80°C for 20 min while being shaken on a thermo-cycler (MHR 23, Ditabis AG, Pforzheim, Germany) at 800 rpm. After that, the tube was cooled down on ice for 5 min and subsequently 1 mL of a 0.5 M solution of HCl dissolved in methanol was added (Sigma Aldrich, St. Louis, Missouri, US). Again, the tube was shaken for 20 min at 80°C and afterwards cooled down on ice. In the next step 400 µl of DI water and hexane respectively were added. The sample was vortexed again and then centrifuged at 1000 rpm for 1 min. Thereof, 200 µl of the upper phase were transferred into a screw-thread vial for subsequent GC analysis.

The employed GC (Shimadzu 2025, Kyoto, Japan) was equipped with an auto sampler and a *ZB-Wax* column of 30 m length, an internal diameter of 0.32 mm and a film thickness of 0.25 µm (Phenomenex, Torrance, California, U.S.). The injector temperature was 245°C, the split ratio 1:10 and the injection 1 µl. Hydrogen was used as carrier gas with a flow rate of 30 mL/min and N_2 was used as makeup gas with a flow rate of 30 mL/min. Within a run, the column temperature was held for 1 min at 150°C and after that increased with 5 K/min for 18 min and then held again constant for 6 min at the final temperature of 240°C. This resulted in an overall time of 25 min per run.

A standard curve of internal standard (ISTD) was prepared to calculate the extraction and transesterification efficiency of the procedure and to calculate the fatty acid content of the sample. As first part of the calculation the maximum theoretical concentration of generated ISTD-FAME from the applied ISTD-TAG was determined,

$$ISTD_{FAME,max} = \frac{\left(\frac{MW_{TAG}}{m_{TAG}} \times 3\right) \times MW_{FAME}}{V_{UL}} \quad (8)$$

Where MW_{TAG} and m_{TAG} m_{TAG} is the molecular weight and the mass of the used ISTD-TAG, respectively. MW_{FAME} represents the molecular weight of the resulting FAMEs and V_{UL} the volume of the upper layer at the end of the DT procedure. The factor of 3 was added to account for the increase of amount of substance during the esterification of

trigylcerides to FAMEs. With the maximum theoretical FAME concentration and the actual ISTD-FAME the response factor was calculated:

$$RF = \frac{ISTD_{FAME,max}}{ISTD_{FAME}} \quad (9)$$

Based on this factor, the lipid content of the sample was calculated:

$$C = \frac{\left(\frac{Area_{total}}{Area_{ISTD}} \times c_{ISTD}\right) \times RF \times V_{UL}}{weighted\ bio\ mass} \quad (10)$$

$Area_{total}$ reflects the sum of all measured peaks in the sample minus those of the solvents and the area of the ISTD, which is coded with $Area_{ISTD}$. The concentration of the ISTD, calculated from the calibration curve, is nominated as c_{ISTD}. In order to obtain the produced fatty acids over time FA productivity was calculated as:

$$P_L = \frac{C_2 \times CDW_2 - C_1 \times CDW_1}{t_2 - t_1} \quad (11)$$

P_L	volumetric lipid productivity	$g/(L \cdot d)$
C_2	lipid content at second sampling point	g/g_{CDW}
CDW_2	cell dry weight concentration at second sampling point	g/L
C_1	lipid content at first sampling point	g/g_{CDW}
CDW_1	cell dry weight concentration at first sampling point	g/L

2.4.10.8. Determination of Nile Red fluorescence

For the measurement of Nile Red fluorescence an overall sample volume of 200 µL was used in a black 96-well plate with a clear bottom. First, sample was added to obtain a final OD_{750nm} in one well of 0.3. Then 20 µL of DMSO were added and both substances were topped to 150 µL with DI water. This mixture was shaken for 1 min at 800 rpm on

a shaker (Eppendorf ThermoMixer® C, Eppendorf, Hamburg, Germany) and then fluorescence and absorbance were measured in the Perkin Elmer microplate reader. For the fluorescence, the excitation wavelength was 530 nm and emission wavelength 560 nm and the absorbance was measured at 750 nm. Then 30 µL of a 10 µg/mL concentrated stock solution of Nile red was added, the plate was again shaken for 1 min in darkness and the fluorescence was measured after 10 min. All samples were analyzed in fivefold replicates. From the value at 10 min, a blank without cells and another blank without Nile Red were subtracted.

2.4.10.9. Determination of nitrate concentration

Nitrate concentration was determined spectrophotometrically in a 96-well-plate. 1 mL of the culture were centrifuged at maximum speed for 5 min. Based on the duration of the cultivation and the initial nitrate concentration in the media, a portion of the supernatant of the sample was diluted in order to obtain 500 µL of a solution with 30 mg/L of nitrate. This value was chosen, as it is in the center of the linear range (0-50 mg/L) of this assay. The volume was transferred to a plastic tube and 20 µL of 5 M NaOH and 10 mg of zinc powder were added. Then the sample was vortexed in a thermo-cycler for 5 min at 400 rpm and then centrifuged for 1 min at 15000 rpm. From this sample, four wells of a 96-well-plate were filled with 100 µL each and the absorbance at 535 nm was measured (Blank). Then 25 µL of glacial acetic acid were added and the plate was again put on the thermo-cycler for 5 min at 400 rpm. 5 µL of naphtlamine were added and the plate was shaken again. Then the color change was again measured in the Perkin Elmer microplate reader. On every plate, a standard curve of the sample media with nitrate concentrations of 0, 1, 5, 10, 20, 30, 40, 50 mg/L was measured. The quantification of the concentration was conducted by relating the OD_{535} of every sample to the calibration curve.

2.4.11. Statistical analysis

2.4.11.1. Test on Normality

Analysis of normal distribution of data as a pre-requirement for the ANOVA analysis (see section 2.4.11.2) was conducted within the software OriginPro 2016G (Northampton, MA, USA) by application of the Shapiro-Wilk-Test on a significance value of 0.05.

2.4.11.2. Analysis of variance (ANOVA)

ANOVA was conducted within the software OriginPro 2016G on a 0.05 significance value.

2.4.11.3. Intra- and interplate variability

For the intraplate variability, first the relative standard deviation (RSD) of all standards distributed over one plate were measured. Then the overall mean of the RSDs was calculated.

For the variability between plates, the standards were distributed on different plates. Then the values of each plate were grouped according to their positions and the RSD within each group was calculated. Finally, the overall mean of these groups was determined.

2.4.11.4. Z'-factor

The Z'-factor for the evaluation of a suitability of a high-throughput screening was calculated according to Zhang et. al [170].

3. Results & Discussion

3.1. Isolation and screening of microalgae strains from environmental samples

3.1.1. Establishing screening procedures to identify microalgae strains showing a high lipid productivity

The aim of this study was to screen for microalgae which are applicable as a source for biofuel production. The primary selection criterion was the growth rate of the cultures. In order to unify and fasten the determination of that value, an automated tool for selection of the maximum specific growth rate was developed in the software package R. The principle of the software tool is pointed out in 3.1.1.1.

The desired target compound for most biofuel applications from microalgae are fatty acids. In order to select for the best and fastest producer on a larger scale, the fatty acid (FA) productivity was selected as the second selection parameter in the screening process. FA productivity is determined by the biomass or CDW productivity of the strain and also by its lipid or FA content. Assays to determine the lipid content for also larger scale screenings should fulfill the following requirements: They should be (i) fast, (ii) reproducible, (iii) reliable, (iv) feasible for small culture volumes (max. 1mL) and (v) applicable to a wide range of algae, independent of their size, morphology and cell wall composition. In section 3.1.1.2 the considerations on the selection of Direct Transesterification as standard method are outlined and Nile Red is evaluated as a semi-quantitative alternative, as it is widely used in algal biotechnology.

3.1.1.1. Automated growth rate determination module

In primary screening experiments aiming to identify microalgal biomass producers the maximum growth rate is commonly used as the first indicator for rapid growing strains. This is particularly the case, when screening is conducted in small volumes in which a gravimetric determination of the biomass concentration is not feasible. In order to

facilitate and unify the calculations of the growth rate, a module in the software package "R" (Version 3.3.) was developed within this study.

It is based on the previously established package *growthrates* which uses a fix number of data points and a selectable threshold for the R^2 value [171]. Given these specifications, *growthrates* logarithmizes all OD or CDW values and iteratively calculates the maximum slope of the linear regression and the corresponding R^2-value throughout the cultivation. The principle of obtaining the data pairs is shown in Figure 4. For instance, if the length of the data range *h* is appointed as "4" then a calculation of the slopes between data point 1-4, 2-5, 3-6, etc. is undertaken. In addition to the slopes, the R^2-values of the corresponding data ranges are also calculated. From all of these data pairs of slope and R^2-values, the ones below the selected R^2-threshold are discarded. From the remaining data set the maximum slope of the regression curve between ln-transformed OD values

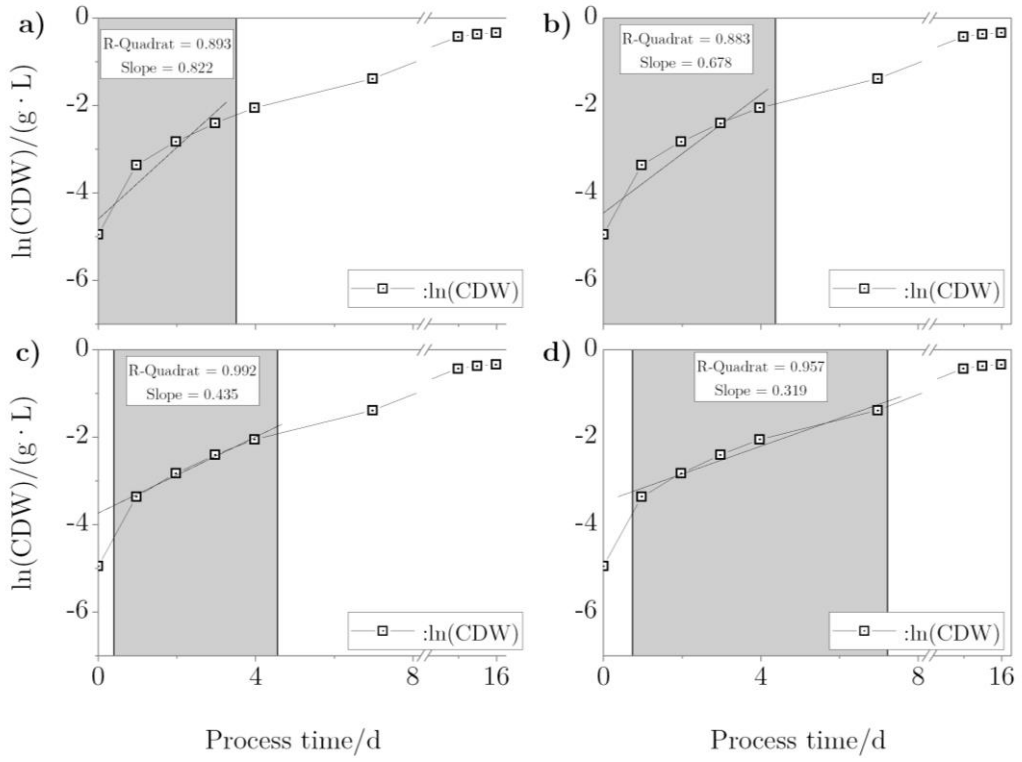

Figure 4: Principle for data generation of the R-module for four data pairs of R^2 and μ_{max}. Calculations are based on CDW data from plate 1 and well A02 of the homogeneity test in section 3.2.1.2. Different data ranges (h) and measuring time points (t_n) are shown: (a) data range h=4, t_1, (b) data range h=5, t_1, (c) data range h=4, t_2, (d) data range h=5, t_2.

and the normal time values is considered as the maximum specific growth rate for this strain within this cultivation given the R^2-threshold and the selected data range.

However, the tool established in this work not only gives a column with data pairs (μ_{max} and R^2) for a fix data range but also calculates the data pairs for all the data ranges possible (see Table 5).

Table 5: Exemplary determination of μ_{max}. Calculations are based on CDW data from plate 1 and well A01 of the homogeneity test in section 3.2.1.2. The number of measurement points is denominated as "h", the time points of measurement as "t_i". The analysis was conducted in the R-module with a R^2-threshold of 0.97 and a minimum of four measurement points. Marked in thick dashed and solid frames are the data pairs with a R^2-value above the threshold. Solid black frames mark the highest μ_{max} values of those values for *h*=4 and *h*=7. n=7.

Time points \data range	*h*=4		*h*=5		*h*=6		*h*=7		*h*=8		...	*h*=n	
	$\mu_{max/d^{-1}}$	R^2	$\mu_{max/d^{-1}}$	R^2	$\mu_{max/d^{-1}}$	R^2	$\mu_{max/d^{-1}}$	R^2	$\mu_{max/d^{-1}}$	R^2	...	$\mu_{max/d^{-1}}$	R^2
t_1	0.821	0.893	0.678	0.883	0.453	0.825	0.379	0.845	0.348	0.866	...	0.232	0.830
t_2	0.435	0.992	0.319	0.957	0.289	0.968	0.276	0.974	0.226	0.932	...		
t_3	0.278	0.973	0.261	0.985	0.081	0.967	0.204	0.941	0.185	0.932	...		
⋮	⋮	⋮	⋮	⋮	⋮	⋮	⋮	⋮	⋮	⋮	...	⋮	⋮
t_{n-5}	0.087	0.969	0.081	0.967							...		
t_{n-4}	0.068	0.989									...		

For instance, only the first column (*h*=4) in Table 5 would be the data base of the *growthrate* package.

The module developed in this study covers additionally the other columns (h=5...n). From these data pairs, all pairs with the R^2-values below the given threshold are not further considered. In Table 5 this accounts for the all the cells with grey frames. From the cells marked in thick black frames, the data pair with the highest value of *h* is

selected. In this case, it is the data pair for h=7 (R^2=0.974; μ_{max}=0.276 d^{-1}), which is marked with a solid frame. Although the data pair in the other marked frame shows a higher μ_{max} it is not considered due to its shorter data range. Thus, the module determines μ_{max} from the longest period (h) in which the cells grew exponentially with a R^2 of at least 0.97. Although in heterotrophic cultivations this value is often set to 0.99, in phototrophic cultivations this could lead to a too stringent selectivity which would exclude a large amount of well grown cultivations. The output of the calculation is listed in Table 6. The code of the module is shown in Appendix 5.

Table 6: Exemplary data output of R-module.

Well	Slope	R^2	# Points
Plate_01_A02	0.2756067	0.9736195	7

3.1.1.2. Evaluation of lipid quantification methods

Once the fastest biomass producers are identified, that lead group has to be screened for high lipid productivity among the strains. The procedure selected for those analysis needs to be fast, reliable and feasible with only a small culture volume. In the following section, the considerations on the selection of Direct Transesterification as standard method are outlined and Nile Red is evaluated as a semi-quantitative alternative.

Direct Transesterification

Several lipid extraction and analysis techniques are established and depending on the available culture volume, sample number, level of analysis detail, the state of the cultures after the procedure and analysis duration different techniques are favorable [172, 173]. After an extensive literature research, solvent based Direct Transesterification by Griffiths et. al [114] was selected as reference method and slightly modified (see section 2.4.10.7). Moreover, in this study the linear range of the method by Griffiths et. al could also be validated with lyophilized biomass (see Figure 5). This approach was concluded

to be closer to the actual procedure during a screening assay than applying wet biomass as it was done in the work of Griffiths et. al.

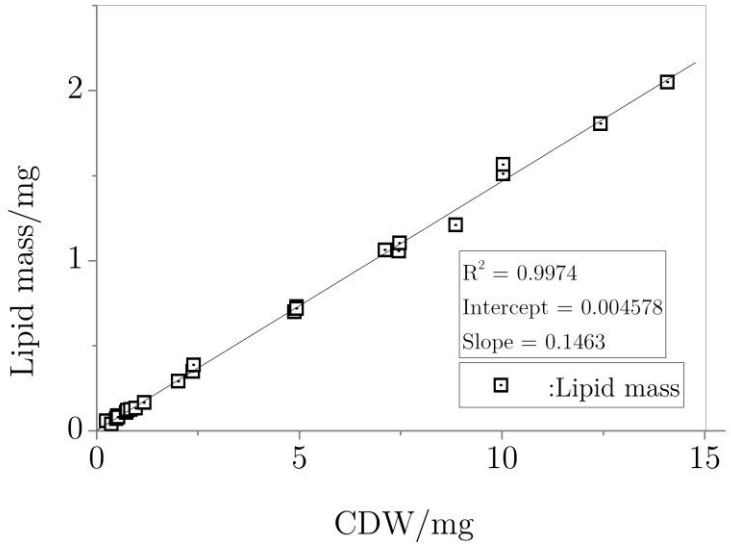

Figure 5: Linear range of DT method. Freeze-dried biomass of *Nannochloropsis salina* was weighted and the DT was conducted. Linear fit was calculated based on 24 data points. Lipid mass calculations were conducted based on C19-TAG as internal standard.

The method showed a linear response for the analysis of fatty acid amount from a minimum of 40.20 µg to 2.051 mg. The mean transesterification and extraction efficiency of the applied internal standard (C19-TAG) was 100.46 % ± 3.83 %.

Nile Red

The lipophilic compound 7-Diethylamino-3,4-benzophenoxazin-2-on, trivially known as Nile Red, is frequently used in microalgae biotechnology as an indirect indicator for accumulated lipids. Correlated to a direct quantification of lipids like solvent extraction combined with gravimetric determination, it potentially enables a fast quantification in small culture volumes. Dissolved in solvents like acetone or DMSO which increase the permeability of the algae, it enters the cell and binds mainly to phospholipids and triglycerides. Binding of those is detectable at specific emission wavelengths for the polar phospholipids and the non-polar triglycerides respectively. In this section, the

applicability of Nile Red for the rapid and semi-quantitative determination of intracellular triacylglycerides in a microplate format was evaluated. The first step in establishing a quantitative detection method is the proof of a linear correlation between the application of various amounts of the substrate, in this case the algae biomass, and the resulting signal which is here the fluorescence intensity. For that reason, it was initially attempted to determine the linear range of the fluorescence intensity for varying amounts of microalgae biomass. In a staining protocol derived from Chen et. al [174], the response of different cell concentrations was tested (see Figure 6). The linear sector of the emission spectrum spreads from 0.1 to 0.3 OD for *Picochlorum* sp. (see Figure 6). Therefore, the center of this range was used as target cell density in further experiments.

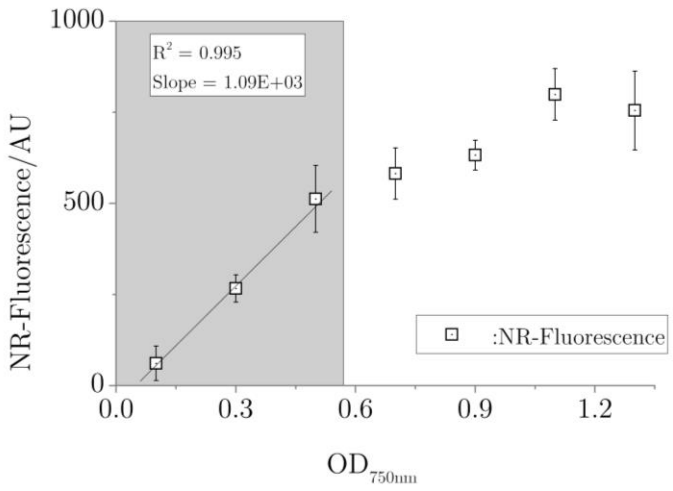

Figure 6: Effect of different cell concentrations on Nile Red fluorescence for *Picochlorum* sp.. N=5 for each OD level.

This optimized protocol was tested for different strains of different microalgal groups stemming from different cultures, e.g. non-shaken cultures, actively shaken pre-cultures for other experiments and cultures from the stationary growth phase. All of the cultures in NR assay were diluted to an OD of 0.3. In order to avoid pipetting errors which would lead to different algae concentrations in the wells, the OD_{750nm} was measured before the addition of the dye. With this OD value the obtained fluorescence values could be normalized. From the same cultures, lipid contents were determined via DT. The lipid

mass from the DT procedure and the NR fluorescence values were then plotted (see Figure 7). However, no linear response of the NR fluorescence to the corresponding lipid content could be obtained.

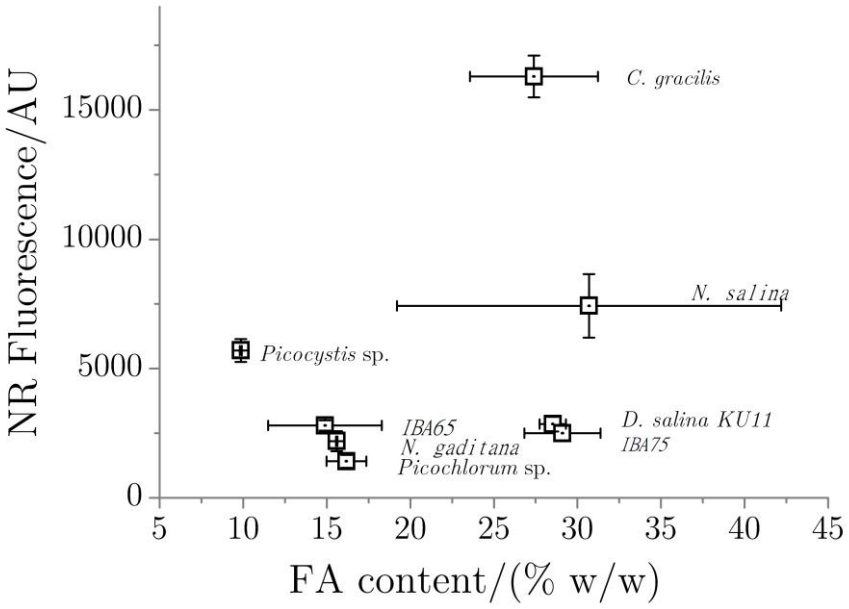

Figure 7: Relation of FA content to NR fluorescence analyzed by GC/FID. Cultures for NR assay were diluted to an OD_{750nm} and normalized to the measured value. N_{NR}= 5, $N_{GC/FID}$=2.

3.1.1.3. Discussion

An automated software tool for the determination of the growth rate of a culture could be established within this study and was applied as the standard method for the evaluation of growth performance of the strains. It represents a further development of the *growthrate* package in "R" as it enables a growth rate determination based on the entire exponential growth phase according to a defined R^2-threshold. Especially in measurement set-ups where a huge number of data points are generated, a fixed, short value for *h* could overestimate μ_{max} as it doesn't cover the whole exponential growth phase. Also, a small value of *h* is more prone to the effect of outliers. Likewise, a high value for *h* with only few measuring points available would result predominantly in R^2-values below the threshold as the range for the calculation of μ_{max} overlaps the actual exponential growth phase and includes thus data points from the lag- and stationary

phase into the calculation. In order to avoid manual adaption of *h* according to the number of measuring points and the cultivation duration for every cultivation run, the tool uses the R^2-value of ln-transformed OD values and the time. It is thus guaranteed that the values obtained, stem from the whole exponential growth phase during a cultivation under the criteria of a given R^2. However, it has to be considered that a high value, e.g. 0.999, for this parameter could lead to a very selective analysis when slow growing strains are evaluated or the number of measuring points is not sufficient. On the other side, a low value of e.g. 0.95 would not produce more false-positives values, as μ_{max} values calculated from higher R^2-threshold are supposedly higher and are therefore favored. The R^2-value in this study was adjusted to 0.97 due to the cultivation duration and growth performance of microalgae and should be overthought when used for other organism groups and set-ups.

Direct Transesterification was evaluated and identified as the standard method for the direct determination of the total fatty acid content of a sample. It fulfilled the requirements previously set up for the evaluation of a favorable lipid analyzing method. A preparation duration of 2 h for approximately 30 samples allows the handling of a larger set of samples. Except for the weighting step, the procedure is in principal also automatable. It could be successfully down-scaled from a standard required biomass of 5 mg to 239 µg. During the downscale of the assay, the balance which was used for weighing, proved to be the limiting parameter for the lower quantification level. Small bits of the freeze-dried biomass were easily electrostatically charged and therefore could have stuck to the spatula or the aluminum bowl. These minimal residues could have altered especially in the lower range of the assay the applied biomass, which would explain the non-linear response of the procedure below a mass of 239 µg. The response of the GC shows a linear range for much lower quantities. Therefore, a minimum applicable biomass of 0.239 mg was determined for the assay. That translates into a

minimal quantitatively detectable FA mass of 40.20 mg obtained from biomass with a lipid content of 11.29 % (w/w) at an efficiency of 100.46 ± 3.83 %.

It has in contrast to Nile Red a broad linear range and applicability throughout different classes of microalgae. Although NR is more easily automatable, it needs thorough optimizing steps when used for another strain. Therefore, Nile Red cannot be used for the fast screening of various, unknown strains in the same batch. These findings were also confirmed by other worker [175]. The dye remains thus a helpful tool for quick estimations on the neutral lipid development of one strain, given that the assay was optimized to this strain beforehand. Once certain findings in the lipid development persist, these have to be validated with a direct detection method like DT or gravimetric measures. Whether a sole detection by DT or the two-step validation with a preceding NR step is less time consuming remains a question of application, number of strains and number of samples and cannot be answered in general.

3.1.2. Isolation of microalgae from saline lakes in Southeast Australia

3.1.2.1. Identifying suitable sampling sites

Before undertaking the sampling field trip, three main favorable characteristics for a microalgae strain considered for an outdoor, open mass culture were determined: (i) Firstly, the strain should show a broad temperature tolerance in order to grow consistently in outdoor facilities. In those cultivation systems, a temperature regulation is economically not feasible and temperature changes over the course of a day should therefore be tolerated by the candidate strain. (ii) The second characteristic of the potential strain is a tolerance to high salt concentrations in the media. In such a hypersaline environment, growth of contaminants and predators is either completely avoided or diminished significantly. With mainly the microalgae proliferating in the reactor, a continuous biomass yield is guaranteed. (iii) The last physiological trait aimed for was a high FA productivity for the strain. Good performance of the strain for this parameter ensures a high product formation and therefore an economically improved

process. However, FA productivity has to be determined by definition over a certain amount of time [75], so it is not possible to obtain a value for this parameter during an individual sampling procedure particularly with a mixed culture as subject. Neither is an ecological niche known, where the rapid accumulation of lipids is known to be favorable and can be observed on a regular basis. In case such a habitat existed, sampling should have been concentrated on these sites. Due to these reasons, it was concluded to evaluate the FA productivity only for the isolated strains at the end of the screening process.

Based on the first two phenotypic traits mentioned above, a literature research was conducted in order to identify habitats which potentially favor strains with those characteristics. The research was restricted spatially due to project related dependencies merely to the Australian mainland and chronologically to July 2014. The spatial limitation required also a consideration of the current water levels in that geographical area, as many sites closer to the Red Centre of Australia bear the risk of being dried-out.

Based on these prerequisites a first limitation to the climate region was done. According to Figure 5 in De Deckker [176] the arid zone was excluded from further investigation due to the beforementioned low water levels or even dried-out water bodies. Further work of the same author [177] investigating the seasonal fauna of the Coorong Lagoon in South Australia suggested a water temperature range between 7 and 29°C (Table 1 in [177]) for this area. In the same study, also salinities up to the saturation point were observed for these sites (Fig. 6 in [177]). Furthermore, a more recent work of Schapira et. al [178] also showed promising salinity values. Thus, the Coorong Lagoon was chosen as the first sampling area.

In close proximity, Lake Eliza is located, which was, based on the data given in Burne et. al [179], considered as the second sampling area. Bayly et. al mention a salinity from below 100 ppt in winter to over 360 ppt and temperatures below 0°C and over 40°C [180].

In close distance to the prior water bodies and based on the works of Williams et. al [181] and Hammer [182], Lake Corongamite and its surrounding lakes were included to the sampling site selection. In those studies, salinities over 50 ppt and water temperatures between approximately 5 and 23°C were recorded.

Given the assembled data and their proximity these three areas in South Australia and Victoria were determined as sampling sites. A sample taken later during that sampling trip in Cape Tribulation National Park in Queensland, Australia, was additionally included into the screening.

3.1.2.2. Sampling

The sampling of the lakes was conducted from 11th to the 13th of July 2014 and the sampling in Cape Tribulation National Park at the 18th of July. The geographical locations of the sites are shown in Figure 8. The sites with their geographical positions are listed in Table 7 including the recorded physicochemical values at the respective site.

Figure 8: Sampling sites of microalgae in the Australian states of South Australia and Victoria (left) and Queensland (right).

Table 7: Summary of geographical location and physico-chemical values of chosen sampling sites. Missing data could not be generated due to issues with multiparameter probe (----*) or due to the absence of the device (----).

Sampling site	Temp. /°C	pH	Salinity /ppt	Latitude	Longitude
(1) Lake Colac	10.9	----*	----*	S 38°19.9009'	E 143°35.2498'
(2) Lake Beeac	----*	----*	----*	S 38°11.6019'	E 143°36.7986'
(3) Lake Cundare	13.1	8.72	3.02	S 38°10.7592'	E 143°36.9846'
(4) Lake Corangamite	13.2	----*	29.39	S 38°03.9409'	E 143°25.5823'
(5) Lake St. Claire	12.4	8.05	55.51	S 37°17.7659'	E 139°53.4604'
(6) Lake Eliza	10.8	8.44	24.55	S 37°16.7222'	E 139°51.8103'
(7) Little Dip Lake	11.8	8.19	29.24	S 37°15.6567'	E 139°49.2794'
(8) Coorong National Park I	8.5	8.5	19.69	S 36°30.7013'	E 139°49.5774'
(9) Salt Creek	10.8	8.26	49.79	S 36°09.6874'	E 139°38.8328'
(10) Coorong National Park II	12.9	8.37	23.95	S 35°47.7934'	E 139°19.0701'
(11) Cape Tribulation National Park	----	----	----	S 16°04.4552'	E 145°28.2401'

The measured temperature ranged from 8.5 to 13.1°C, the pH from 8.05 to 8.72 and the salinity from 3.02 to 55.51 ppt. This minimum value recorded at Lake Cundare differs significantly from the other values which lie between 19.69 and 55.51 ppt. As the sample in the Cape Tribulation National Park was taken without prior planning, no measurement of the water parameters could be done.

3.1.2.3. Discussion

The physicochemical properties of the identified water bodies published in the literature could be confirmed, whereas the values measured in this study were on the lower section of the published temperature and salinity ranges. This can be attributed to the different sampling time points within the calendar year. As the date of the field expedition was fixed to winter time, temperature and thus evaporation during that time of the year were lower compared to the summer months and the salinity therefore also below the published values. A relocation of the sample sites further to the center of the country would have led to increasing distances and thus fewer samplings and a higher threat of dried-out water bodies. Nevertheless, in two water bodies high salinities of approximately 1.4 times of the average ocean salinity of around 35 ppt in that region were found [183]. Whether

sampling during the colder season led to a dominance of cold adapted strains could not be proven as no second sampling during other seasons from the same lakes could be conducted. As phytoplankton can form cyst and spores in order to outwear unfavorable conditions [184, 185], it remains debatable to what extent also warm adapted strains were sampled, which in turn could outgrow the cold adapted strains once exposed to the warmer cultivation temperatures in the laboratory. As a quantitative comparison between the dominant algae groups over the course of a year was not within the scope of this study the sampling remains a one-point analysis with aim of enriching strains with the desired properties. This goal, although, could be achieve for many strains, considering the findings from the subsequent chapters. It was thus shown that a valid identification of sites and a thorough planning of the sampling constitutes a major step in the isolation of suitable strains from the environment.

3.1.3. Screening procedure of isolated strains regarding lipid productivity

3.1.3.1. Enrichment and multivariate screening of environmental samples

After sampling and sending the probes to our laboratory in in Germany they were subjected to a multivariate growth assay. The purpose of this experiment was on the one hand to propagate photosynthetic active populations in the obtained mixed cultures by cultivating the samples under enriched CO_2-atmosphere and in four different media and two concentrations of those. This should allow for growth of the maximum number of strains from the water samples. On the other hand, this assay was set up as a multivariate selection experiment, as already restricting conditions were applied to the cultures. It aimed at reducing the selected candidates from the screening to the most suitable for further mass cultivation processes. The applied selective conditions included (i) a temperature and light gradient (see Figure 9) in order to select for temperature tolerant strains under realistic light conditions, (ii) a salinity of 50 ppt set for each of the four

media to primarily obtain halotolerant strains and (iii) the filtering of all of the samples through a 40 µm mesh to avoid any growth of filamentous algae.

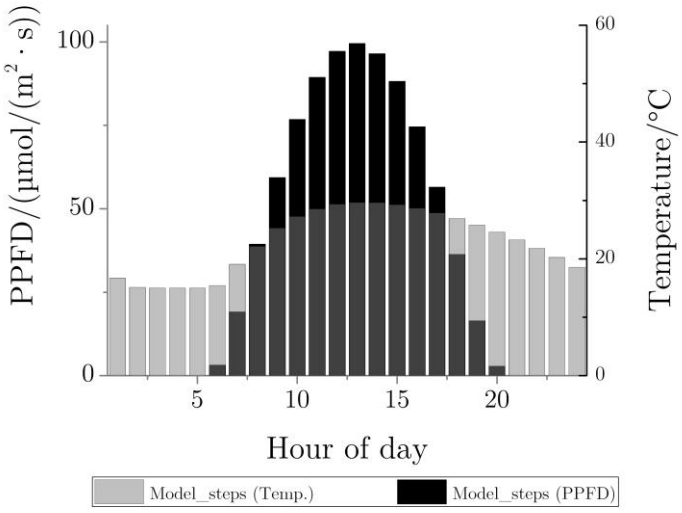

Figure 9: Temperature and PPFD gradient for the primary screening of environmental sample. Values stem from a regression to real climate data conducted in the work of Glemser [154].

From the eleven sites visited, 45 samples in total were cultured in four media with two concentrations resulting in a total sample number of 360. The samples were distributed on 20 24-Well-plates with additional two samples of the reference strains *Picochlorum* sp. and *Dunaliella salina KU11* in each plate. To identify the best growth performer in this pool the chlorophyll fluorescence intensity increase over time was nominated as Q_{FI} and calculated according to equation (12). This quotient was used as the primary selection parameter as it is known that the fluorescence of a microalgae culture is correlated to its growth in microplate assays [150, 186, 187]. In a mixed culture as present here, it correlates with the increase in pigment concentration which shows the growth of photosynthetic organisms. Furthermore, as only photosynthetic organisms are able to produce this signal a false-positive growth indication, where only heterotrophic organisms grow and scatter light during the absorbance measurement, is therefore avoided.

$$Q_{Fl} = \frac{Fl_{max} - Fl_{t0}}{t_{Fl,max}} \quad (12)$$

Q_{Fl}	Fluorescence increase over time	---
Fl_{max}	Max. fluorescence during cultivation	AU
Fl_{t0}	Fluorescence at t=0	AU
$t_{Fl,max}$	Time point when fluorescence was maximum	d

In addition to the fluorescence, the maximum absorbance increase (see equation (13)) at 750 nm was applied as the secondary selection parameter Q_{Abs}. This parameter indicates indirectly a gain in biomass concentration and is frequently used in microalgae biotechnology for the estimation of CDW concentration from OD measurements, showing a greater robustness to pigment alterations compared to OD_{680nm} [188]. By adding this parameter to the selection criterium a false-positive detection of strains with an increasing pigment concentration but at the same time stagnating cell concentration should be avoided.

$$Q_{Abs} = \frac{Abs_{max} - Abs_{t0}}{t_{Abs,max}} \quad (13)$$

Q_{Abs}	Increase of absorbance at 750 nm over time	---
Abs_{max}	Max. absorbance during cultivation	AU
Abs_{t0}	Absorbance at t=0	AU
$t_{Abs,max}$	Time point when absorbance was maximum	d

First, the Q_{Fl} and Q_{Abs} values for the reference cultures were calculated and used as a basis for the evaluation of the suitability of the assay. This was done by calculating the Z'-Factor for both measurement parameters (see section 2.4.11.3). The water samples

were used as a negative control in the calculation of the factor whose outcome is detailed in

Table 8. It can be seen that the Z'-value on this assay depends on the measurement parameter and on the reference strain used for calculation. Whereas the Z'-Factor values are above 0.5 for Q_{FL}, they are below this threshold for the Q_{Abs} values.

Table 8: Arithmetic mean, standard deviation and Z'-Factor of negative control, Q_{FL} and Q_{Abs}.

	Q_{FL}			Q_{Abs}		
	Mean	SD	Z'-Factor	Mean	SD	Z'-Factor
Neg. control (DI H_2O)	11.31	10.16	---	0.0050	0.0073	---
D. salina KU11	901.16	97.82	0.636	0.0941	0.0174	0.168
Picochlorum sp.	1883.63	284.89	0.527	0.0897	0.0132	0.274

Q_{FI} and Q_{Abs} were then calculated for all environmental samples individually and a ranked list for each parameter was created. Then the top 30 % strains of the Q_{FI} ranking list were chosen as within the hit selection limit and were then identified in the Q_{Abs} ranking list. Samples that also appeared in the top 30 % quantile of the Q_{Abs} list were further propagated, the remaining ones were transferred to the strain collection of the institute. A total of 43 cultures fulfilled these criteria and those samples are colored in black columns in the lower row of Figure 10. The evaluation of the Q_{FI} values of the reference parameter show an almost two times higher value for *D. salina KU11* compared to *Picochlorum* sp. with the Q_{Abs} values being similar. Compared to the environmental samples both values are in general higher for the reference strains. The enriched cultures show a broad distribution for both parameters.

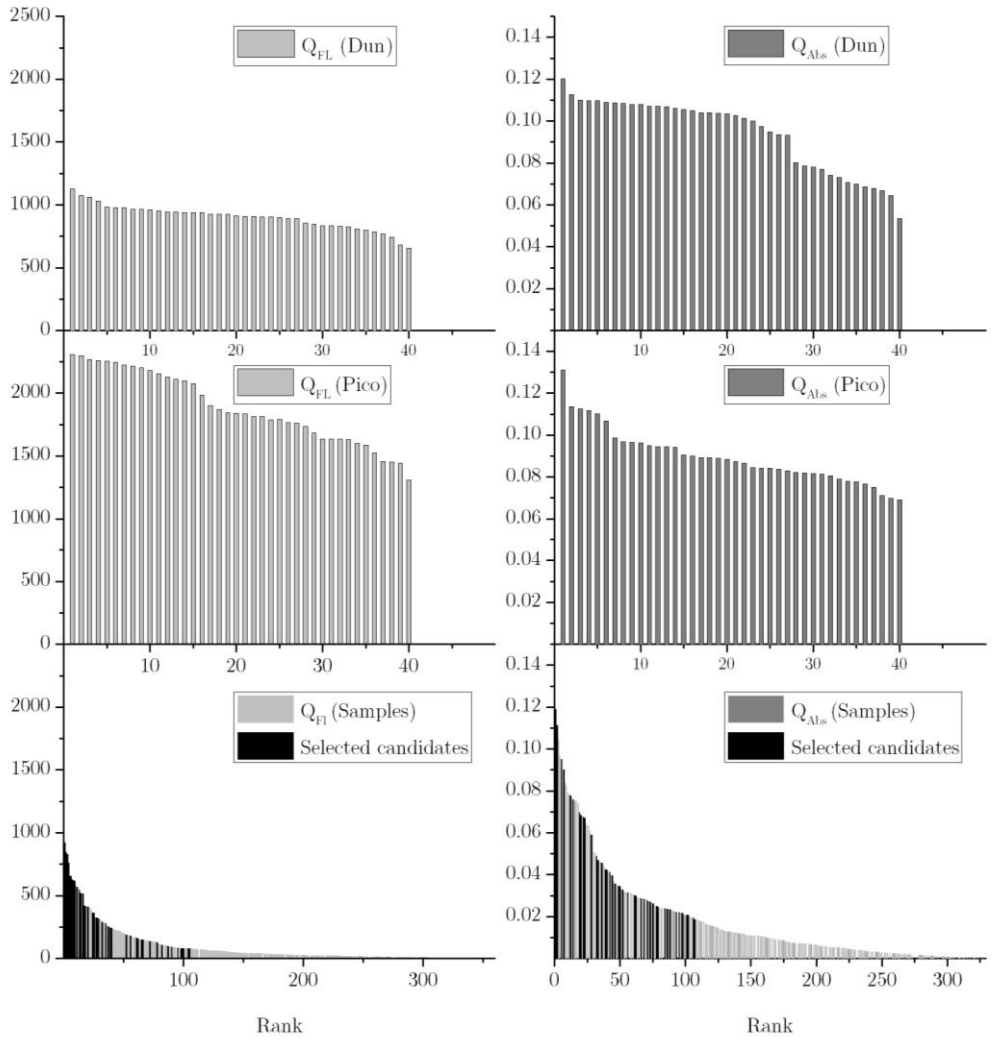

Figure 10: The ranked Q_{Fl} and Q_{Abs} values for the reference strains *D. salina KU11* (top left and top right) and *Picochlorum* sp. (middle left and middle right) and the environmental samples (bottom left and bottom right). Selected candidate strains are colored in the lower row in black.

From the 43 samples, 16 showed in spite of the previous filtering step a filamentous growth and were therefore not considered for further analysis. Additionally, 12 of the 0.2 times concentrated were samples taken out from this pool as the single concentrated sample version also fulfilled the selection criteria. The final summary of the 15 candidates subjected to the isolation process is shown in Figure 11.

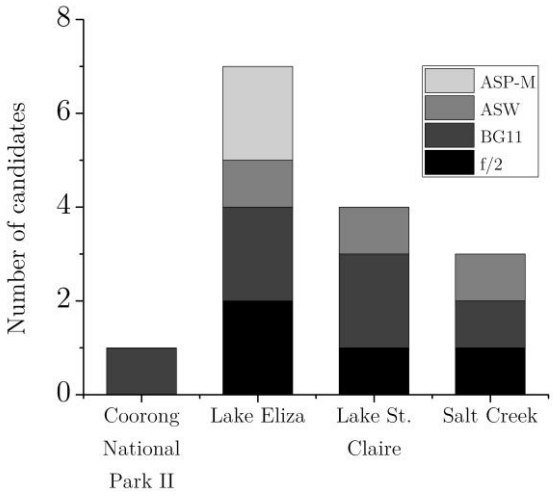

Figure 11: Summary of final selection of candidates depending on their origin and media.

3.1.3.2. Purification of selected candidates

The 15 candidates were subjected to two different isolation methods in order to obtain the maximum number of unialgal strains.

As a first step, the selected strains were transferred after the screening in MTPs to 50 mL flasks in order to generate biomass for further experiments. At the end of a 28 d cultivation time only 12 of those showed exponential growth for their absorbance values (see Figure 12), three of them were not regarded due to filamentous growth. Due to differences in the OD and fluorescence development over the course of the cultivation, not for all of strains a R^2-value could be obtained for both parameters. The remaining nine strains were then used for the FACS and antibiotic isolation approaches.

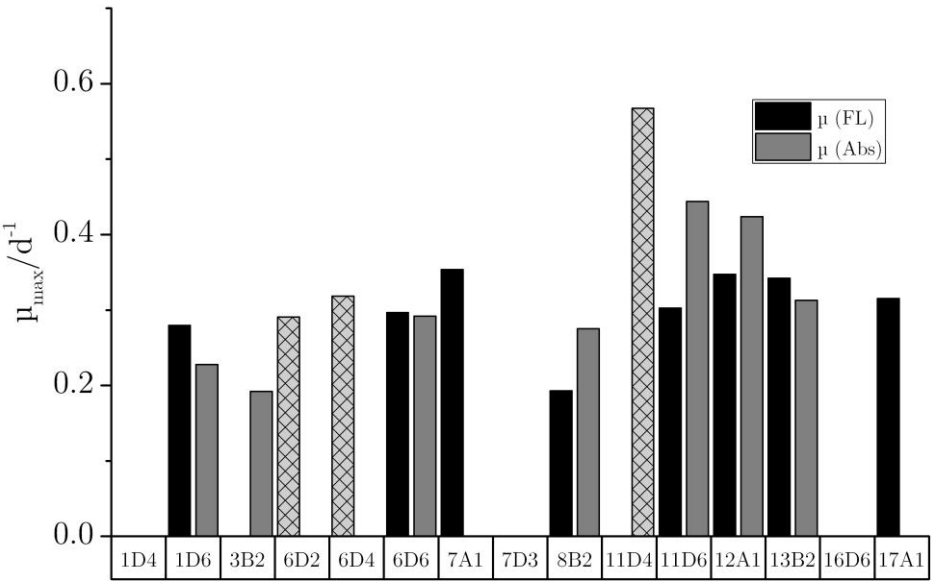

Figure 12: Summary of growth rate values after re-cultivation of favorite strains in 100 mL flasks. The values of μ_{max} are shown based on a calculation of fluorescence values (black) and absorbance values (dark-grey). Calculation of μ_{max} was done over four ln-transformed data points with a threshold value of R^2 of 0.97. Strains with a R^2-value below the threshold are not shown. Patterned data bars indicate a development of filamentous structures during the cultivation, which led to removal from screening. Sample number indicate with the first number the plate of the MTP-screening and with the letter and the second number the coordinate within the plate.

Cell sorting

The nine favorite strains were submitted to cell sorting in order to obtain purified cultures. For that reason, approximately 100,000 cells of each flask were sorted into 40 mL media in 100 mL flasks and the relative abundance of the desired population was measured after 19 d for the sorted and non-sorted cultures (see Figure 13). In this diagram, the differences in the percentage of the desired population, thus the algal population, is shown for the sorted and the unsorted population. In Figure 14,

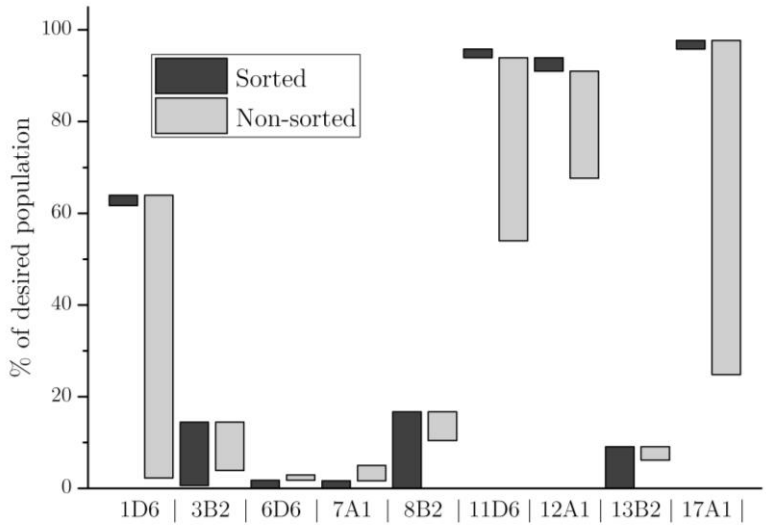

Figure 13: Summary of sort efficiencies after 19 d of cultivation. For each sample, the percentages of the desired population for sorted and non-sorted controls are shown in a column pair. Both bars show the same initial starting value, which represents the percentage of the desired population at t_0. The value after sorting is marked by the end of the bar other than the initial value. E.g. the algae population in sample 1D6 had a share of 63 % of the total sample at t_0, the sorted sample had a share of 61 % after 19 d and the non-sorted sample a share of 2,24 % respectively. N=1.

additionally the cell concentrations of the different cultures are shown. It can be seen that the percentages of desired populations after sorting showed in most cases the same or lower values after 19 d. The high abundance of the photosynthetic active population in sample 1D6, 11D6, 12A1 and 17A1 could be maintained, but not increased significantly. Lower abundances in the other samples could not be increased due to Cell Sorting. The cell sorting procedure resulted in elimination of active cell growth in 3B2, 6D6, 7A1, 8B2 and 13B2.

The measured cell concentrations show similar developments: At the end of the cultivation they dropped significantly for all the non-sorted populations with the exception of 11D6 and 12A1 (see Figure 14). The exceptions showed an approximately 3-fold increase in the cell concentration. For evaluation of the growth of the sorted population first the theoretical cell concentration right after sorting was determined. The sorter software provided a calculated volume per sorted cell of $3{,}06 \cdot 10^{-6}$ mL. With this value, the number of sorted cells and the total media volume of 40 mL the theoretical

cell concentration of each culture after sorting was calculated as 2400.36 ± 201.6 cells/mL.

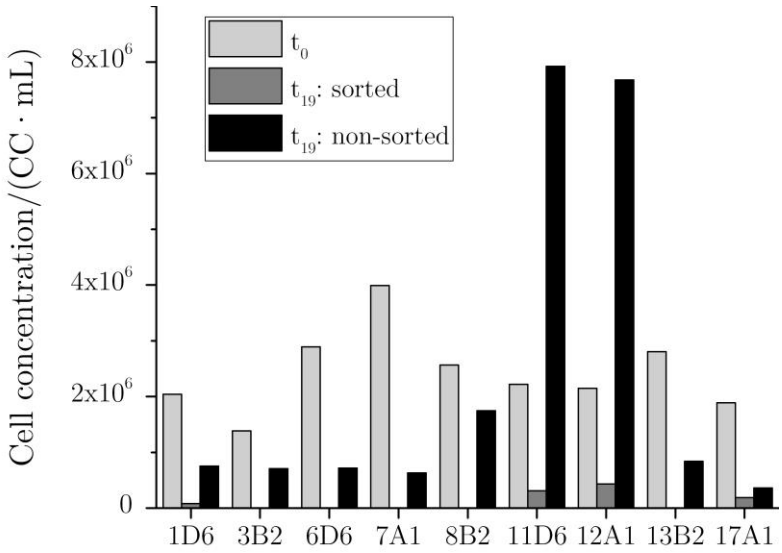

Figure 14: Cell concentrations in the sort population at the beginning of the cultivation and for the sorted and non-sorted cultures after 19 d.

This value was compared to the cell concentration after 19 d. At the end of the cultivation 1D6 (84610 CC/mL), 3B2 (4870 CC/mL), 11D6 (314330 CC/mL), 12A1 (432510 CC/mL) and 17A1 (190520 CC/mL) showed an increase over this initial cell concentration, thus only these strains showed growth after the Cell Sorting procedure.

Antibiotic treatment

The nine remaining samples were subjected to an antibiotic treatment (AB) in liquid cultures for several days and under different concentrations in order to evaluate the suitability of the procedure for establishing pure strains. Each day the percentage of the sorted population in the sample was evaluated and, as a second assessment, an aliquot of the sample was transferred to an agar plate for a visual observation of growth of contaminants. The development of the sorted population in the AB-treated samples is shown in Figure 15. For all cultures except 17A1, a change of the sorted population between -1 and 1 %/d occurred whereas no general correlation of these values to the

applied antibiotic concentrations could be observed. Only 17A1 showed an increase in purity from 9.76 to 21.08 %/d concomitantly with increasing antibiotic concentrations. Samples with negative values in Figure 15 showed a decrease in cell concentration after antibiotic treatment. Noteworthy is the fact that the untreated sample also showed an increase of the sorted population. The samples on the agar plates showed for 1D6, 3B2 and 17A1 no growth for both replicates after 3 d of cultivation in darkness. This was observed at the highest antibiotic concentration for the samples. Those bacteria-free strains were then subjected to the screening of FA productivity.

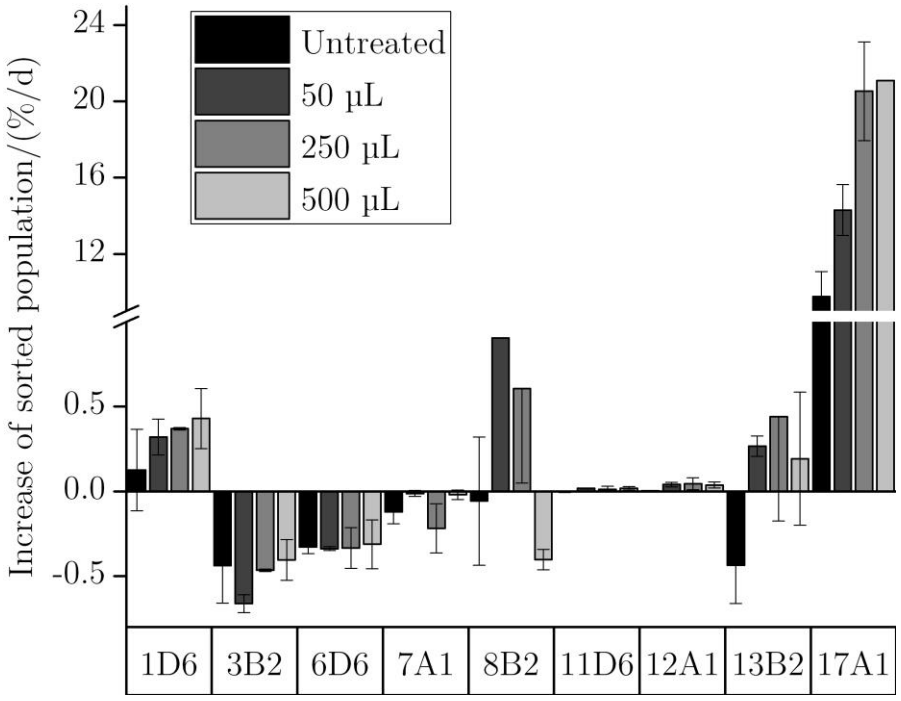

Figure 15: Effect of antibiotic treatment on the development of sorted population. N=2.

3.1.3.3. Screening on FA productivity

The three strains were cultivated in CO_2-flushed shaking flasks illuminated by LED panels from below. The whole set-up used was established during the course of this work

and is described in further detail in [154]. As FA productivity even differs with cultivation system, light conditions and time of sampling for a single strain, the values obtained for the 1D6, 3B2 and 17A1 obtained in this new set-up are not likely to be comparable to values derived from other systems. In order to avoid illegitimate comparisons of FA productivity values to those measured in systems showing e.g. a different gas transfer rate or light attenuation, *Nannochloropsis salina* was cultivated in the same run as a

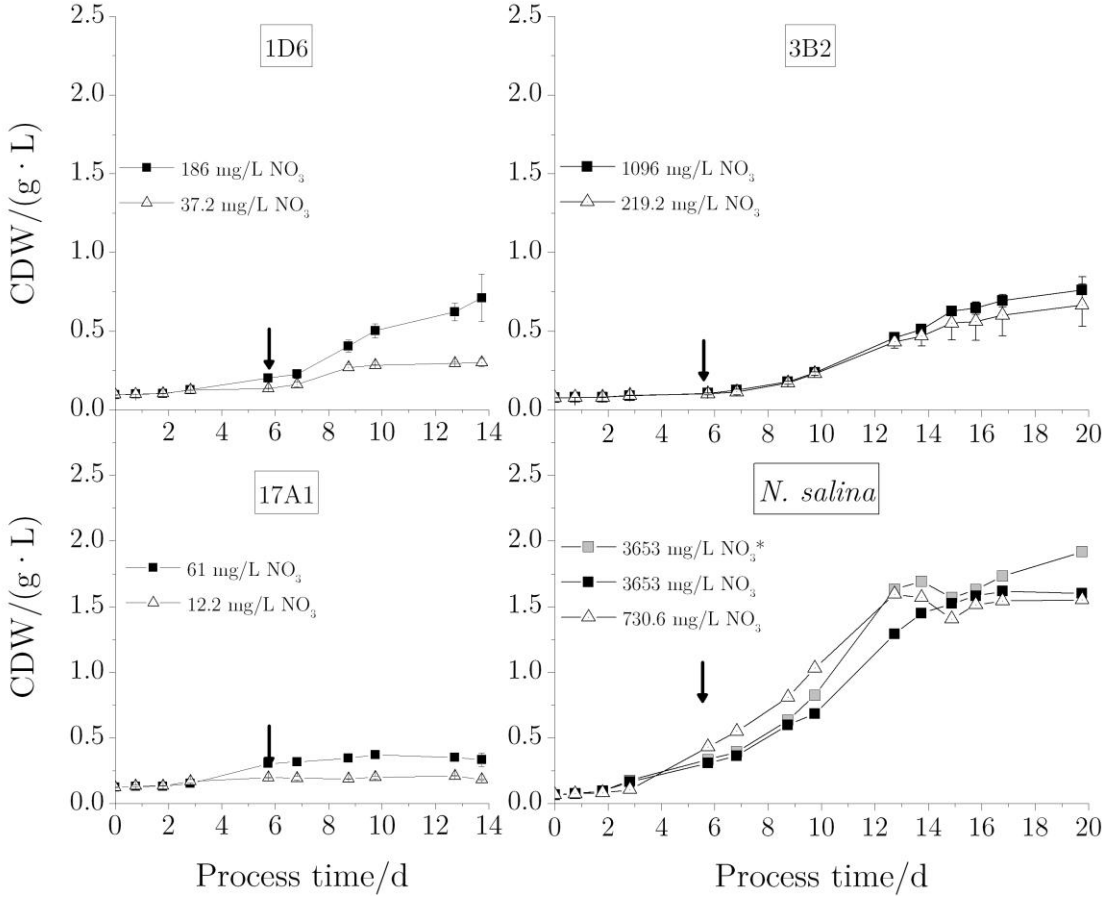

Figure 16: Development of CDW in the course of the experiment on FA productivity. Arrows indicate the first sample taken for lipid content determination. The second sample was taken at the end of each cultivation. Cultivation was ended after a minimum of three consecutive OD measuring points in the stationary growth phase. Strains were cultivated with 1-fold (high nitrate, HN) and 0.2-fold (low nitrate, LN) concentration of nitrate of the initial media. The PPFD of the third *N. salina* strain (high nitrate, HN*) was increased after 15 d in order to avoid a light limitation.

benchmark strain (see Figure 16). All of the cultures showed an increase in CDW over time with *N. salina* reaching the highest maximum biomass concentration. For the evaluation of FA productivity, the strains were cultivated under different nitrate concentrations. The strain 1D6 under lower nitrate showed a 2.36-fold reduction in the

final CDW concentration, resulting in a stationary phase of at least 3 d. That fulfilled the criteria to end the cultivation. Sample 17A1 showed after 9.75 d decreasing CDW concentrations and therefore the cultivation was also stopped after 13.7 d to avoid further biomass losses. Sample 3B2 didn't show a clear limitation after this process time and the cultivations were therefore continued for another 6 d. The nitrate replete cultures and the nitrate depleted samples of *N. salina* didn't show any significant differences in growth after 13.7 d, although, all three entered a stationary phase after this process time simultaneously. Their media showed nonetheless only traces of nitrate left (see Table 9). In order to rule out a light limitation at this point, the light intensity of sample HN* was doubled to a final PPFD of 300 µmol/(s · m^2). The measure led to an increase in CDW concentration of the sample compared to the unaltered sample but at the same time to a decrease in the lipid content in the sample. In Table 9 the nitrate concentration of media is shown in the exponential and stationary growth phase. Furthermore, the weighed, thus theoretical, and the measured initial concentration are listed in order to give an assessment of the goodness of the nitrate assay. According to Table 9 and taking into consideration the measured deviations of the test, only sample 3B2 cannot be considered as nitrate limited at the time of sampling.

The comparison of the specific maximum growth rate μ_{max} and the FA productivity shows that none of the strains could exceed the measured values of the benchmark strain. For the low nitrate cultures of strain 17A1 and *N. salina* show a higher lipid productivity than the nitrate rich cultures. All four strain contents in the exponential growth phase are similar for the low and the high nitrate concentration applied. Together with the FA contents shown in Table 9 it becomes clear that only 3B2 increased its content significantly over the course of the cultivation.

Table 9: Summary of nitrate concentration and FA content values during exponential and stationary growth phase during lipid productivity assay. Nitrate concentrations in exponential (arrows in Figure 16) and stationary phase (end of cultivation in Figure 16) were measured by a colorometric assay. Theoretical nitrate concentration of media alone and respective measured value at the beginning of the cultivation are compared and the deviation between theoretical and measured values are shown. HN (high nitrate) refers to the 1fold nitrate concentration, LN (low nitrate) to the 0.2-fold concentrated media.

		FA content		NO_3-concentration				
Sample	NO_3-Level	Exp. phase	Stat. phase	Exp. phase	Stat. phase	Theor. conc.	Measured conc.	Deviation
		%	%	mg/L	mg/L	mg/L	mg/L	%
1D6	HN	9,5	14,4	194,51	-0,67	186	250,52	34,69
	LN	10,3	11,6	37,55	-0,48			
3B2	HN	10,4	16,4	1885,14	466,37	1096	1152,83	5,19
	LN	10,1	14,0	252,22	78,75			
17A1	HN	8,3	9,4	26,54	6,19	61	84,97	39,30
	LN	8,3	11,6	6,57	30,25			
N. salina	HN	11,0	10,4	5247,40	-1,69	3653	5948,8	62,85
	HN*	10,8	7,4	5747,40	-1,35	3653	5948,8	62,85
	LN	10,5	12,7	915,02	30,67			

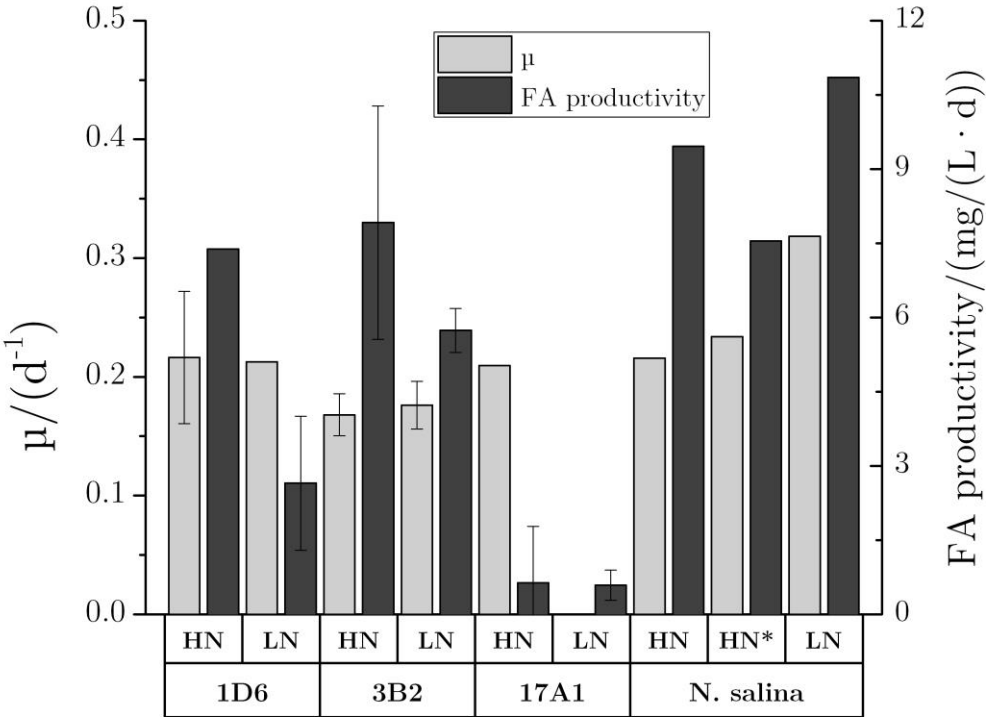

Figure 17: Summary of lipid productivity and μ_{max} values for cultivation under low (LN) and high (HN) concentrations of nitrate. The R-module was used for the calculation of μ_{max} with a minimum of 4 measuring points and a R^2-Threshold of 0.97.

3.1.3.4. Discussion

From the probes sampled during the field trip a huge number could be enriched under selective laboratory conditions and in different nutrient concentrations and media. Thus, it could be assured for the parameter salinity and temperature range, that the strains obtained in the further screening tolerate these conditions. Only the requirement for unicellular growth could not be fulfilled after the selective enrichment as filamentous growth states re-appeared during the screening, thus leading to the elimination of the corresponding strain from the process. This can be explained by the co-isolation of resting stages in the environmental samples which switch back to the filamentous form in favorable conditions [189]. Due to the similar size of spores and cysts to microalgae these filamentous species can only be filtered out effectively in the further course of a screening.

As selection criteria Q_{Fl} was postulated as primary and Q_{Abs} as the secondary criteria. For the screening with *Picochlorum* sp. and *D. salina KU11* as reference strains the Z'-Factor showed a good test quality with values of 0.527-0.636 for the primary criteria. The threshold for the further propagation was set to 30 % at that stage of the screening, resulting in 43 hits. In high-throughput screenings commonly 3 SDs away from the mean or 3 MADs from the median are used as the cut-off value [190]. Before applying this to a screening approach, the size of the library and the existing hardware for the further handling of the selected strains have to be considered. When 3 SDs above the mean would have been applied as a cut-off value, 13 strains were propagated to the secondary screening. However, this number inherits a risk of selecting false-positives which can reduce the outcome of the screening significantly if too many appear and the test quality is inferior. The false-positives in the case of this study were the filamentous strains which were excluded from the process, reducing the potential screening library to 63 % of the initial number of strains. The appearance of filamentous strains in this study, however, is not connected to the test quality, which was proved to be valid. With 3 MADs above the median as cut-off threshold 114 strains would have been propagated. This number of

strains could not adequately be handled in all subsequent purification, optimization and characterization steps with the existing hardware. Due to these considerations, it was deviated from the common cut-off threshold to enable a selective, yet feasible further screening.

The selected nine strains were subjected to two different purification methods namely FACS and antibiotic treatment. FACS could maintain the relative abundance of the desired population in four cultures. The abundance of the other five cultures was decreased below 1 %. The calculated cell concentrations showed that five out of nine cultures proliferated after sorting. Thus, a cell viability for this screening of 55.55 % could be obtained. This ratio lies above of other studies, where the strains showed a survival rate of 5-30 % [191, 192]. However, these were single-cell sortings which are more prone to failure due to sorting of artefacts like cell debris, inorganic particles, misplacement of sorted cells or sorting damage as Sensen et. al already stated in their work [191]. A non-growing sorted culture could also be caused by a then absent obligate symbiotic partner which was removed from the culture by the sorting procedure. An increasing cell viability with increasing sort events was shown by Sieracki et. al, who achieved an increase of cell viability from 28.92 ± 35.54 % for single-cell sorting to 100 % for sorting of 125 cells [193]. Therefore, as no clonal strains were searched for in this study but only pure strains, the sort number could be set to 100,000. This increased the probability of propagating cells in the sorted culture and therefore, the viability rate in this study was higher than the reported ones.

The culture which were not sorted showed with the exception of 6D6 and 7A1 a decrease in their abundance. In flow cytometry, no direct determination of cells can be conducted unless specific fluorophores or antibodies for the desired cells are applied. Therefore, this decrease could be assigned to two scenarios. In the first one, the desired, non-sorted population was already in the death phase of microbial growth and therefore artefacts of

dead cells decreased the abundance of the desired population. In the second, existing contaminants outgrew the microalgal population and therefore the abundance decreased. In four of the sorted cultures, the cell concentration could be maintained and the cell concentration increased after cell sorting. A slight increase over the initial value for the abundance could be achieved for 11D6 and 12A1. Strain 1D6 showed a very similar abundance before and after sorting. An explanation for this could be a co-sorting of contaminants from the initial culture, which in turn proliferate to a similar ratio compared to the initial culture. Thus, the contaminant and the algae co-exist in an optimum cell ratio which was again reached after 19 d. A general misplacement of the sorted cells outside of the sorting container can be can be ruled out, as five of the cultures showed an increase in cell concentration after the sorting and were therefore placed correctly. The FACS procedure could thus not enrich 1D6 in its culture. This was also the case for 3B2, 6D6, 7A1, 8B2 and 13B2. Where sorting did not lead to an enrichment either. In these cases, however, the strains were probably susceptible to the physical influences during sorting and did therefore not proliferate at all after the procedure.
Flow cytometry proved here not to be adequate for the purification of especially rare populations from a mixed culture. More frequent measurements after sorting could elucidate the development of the desired population versus the development of artefacts and contaminants.

The antibiotic treatment led only in three cultures to bacteria-free cultures. Due to the uncertainties in the discrimination between artefacts and cells of FACS and the inability to enrich and purify rare strains, these three cultures were propagated to the next screening round.

For the evaluation of FA productivity nitrogen replete and deficit conditions were imposed on the strains. At the end of the cultivation all strains except 3B2 showed a total consumption of nitrate, given the uncertainties of the nitrate assay. Although the

absence of nitrogen is considered as the major trigger for lipid accumulation in microalgae, strain 3B2 was the only strain that showed a significant increase in lipid content during the stationary phase [57]. This increase amounted to 57,7 % increase of lipid content for the HN culture and 38,6 % for the LN culture. As these elevated values could be measured in both cultures and given the nitrogen replete conditions at the end of cultivation, a limitation other than nitrogen must have caused the increase in the lipid content. Strain 1D6 showed a limitation to nitrogen which only translated for the HN culture into an increase in lipid content. Similarly, to 3B2 the lipid productivity of this strain was higher for the HN than for LN culture. This shows that an existing limitation not necessarily involves a production increase of lipids. 17A1 showed in general a low final CDW, with no exponential growth phase for the LN culture. This could appear as a false positive screening result, as a not growing strain should be eliminated at this stage of the screening. Due to the nature of the screening parameter, Q_{FL} and Q_{Abs}, which assess the fastest increase of the value and not the maximum CDW, fast growers are preferred, whereas strains with a high final CDW are penalized. Therefore, a strain such as 17A1, with a high growth rate and a very low lipid productivity can appear in the final screening phase. The low final CDW could be caused by general low nutrient concentration of the media. An increase thereof would then increase the performance of this strain further. Also for *N. salina* the nitrogen limitation measured in the media did not translate into an elevated lipid content. For this strain, for instance, lipid content values after nitrogen limitation of up to 35 % g/g were reported [194]. The values measured here are below the values for the nitrogen replete cultures obtained in the study by Griffiths et. al. Also, high light conditions could not increase the FA content further, but led to a decrease. In summary, 3B2 could be identified as most favorable strain extracted from this screening as it shows under the conditions and for the experiments applied the highest lipid productivity in a high salinity media. Nevertheless, its lipid productivity is significantly lower compared to other strains cultivated in a shaking flask batch cultivation. For

instance, in the work of Rodolfi et. al a lipid productivity range from 17.4 to 61.0 mg/L/d could be measured for 30 fresh water and marine algae [74].

3.1.4. Phylogenetic characterization of identified best candidates

From the 18S-region of the isolated best three strains could successfully be amplified and subjected to sequencing. Based on a NCBI blast sequence search all of the isolates could be assigned with an identity of 99 % to the genus *Dunaliella*. A summary of the findings is shown in Table 10. The strains were transferred to the culture collection of the Professorship of Industrial Biocatalysis and labeled according to internal institute's nomenclature. The three sequences were aligned in the software MEGA 7 with the MUSCLE tool and then best model for building a phylogenetic tree was determined in the same software. The gamma distributed Hasegawa-Kishino-Yano model was selected and subsequently used for the calculation of the tree shown in Figure 18.

Table 10: Summary of BLAST search of the amplified 18S-region of the isolated strains. Culture collection of the Professorship of Industrial Biocatalysis, Technical University of Munich (IBC-CC).

Isolated strain	Sequence length /bp	Closest BLAST search hit	Identity/%	NCBI Accession-No.	IBC-CC number
1D6	701	Uncultured Dunaliella isolate LT37	99	KC486848.1	IBA065
3B2	756	*Dunaliella* sp. SPMO 201-8	99	DQ324014.1	IBA075
17A1	502	*Dunaliella primolecta* strain SAG 183.80	99	KR607494.1	IBA132

The phylogenetic tree shows a close proximity of the strains among each other. Strains 1D6 and 17A1 showed a closer distance between each other compared to 3B2. This strain was also the furthers apart from the reference strain of the *Dunaliella* genus, *D. salina*. Considering the sampling site, strain 3B2 stemmed from Salt Creek (No. 9) and the strains 1D6 and 17A1 from Lake Eliza (No. 6). These sites showed an initial salinity of 49.79 ppt and 24.55 ppt respectively.

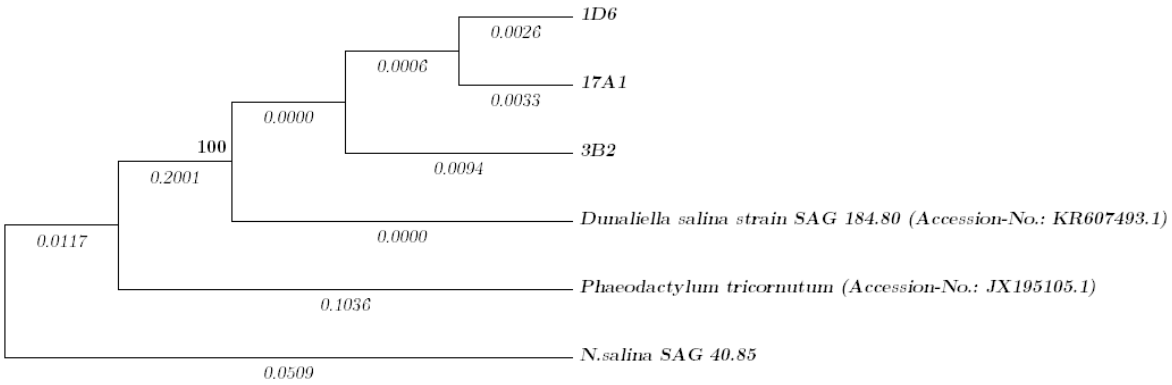

Figure 18: Molecular Phylogenetic analysis by Maximum Likelihood method of the isolated strains by comparison of 18S-rDNA sequences. *N. salina* and *P. tricornutum* were added as outgroups whereas the tree was rooted to the former strain. *D. salina* was added as reference strain from the genus. For *P. tricornutum* and *D. salina* accession-No. is given. The evolutionary history was inferred by using the Maximum Likelihood method based on the Hasegawa-Kishino-Yano model [1]. The tree with the highest log likelihood (-3895.0813) is shown. The percentage of trees in which the associated taxa clustered together is shown above the branches. Initial tree(s) for the heuristic search were obtained automatically by applying Neighbor-Join and BioNJ algorithms to a matrix of pairwise distances estimated using the Maximum Composite Likelihood (MCL) approach, and then selecting the topology with superior log likelihood value. A discrete Gamma distribution was used to model evolutionary rate differences among sites (3 categories (+G, parameter = 0.3601)). The branch lengths are given in numbers which are displayed on the branches. The bold value shows the reliability of the calculated branch. Cut-off values was set to 70 %. The analysis involved 6 nucleotide sequences. Codon positions included were 1st+2nd+3rd+Noncoding. There were a total of 2121 positions in the final dataset. Evolutionary analyses were conducted in MEGA7 [2].

3.1.4.1. Discussion

The selected strains could be characterized as representatives from the genus *Dunaliella* sp. with a high percentage of identity. This is in line with the resolution capacity of the 18S-rRNA gene [195]. Below that taxonomic category 18S-rDNA sequences are unable to show distinct differences between strains. The *Dunaliella* genus contains 22 members which show in general a broad tolerance towards varying salt concentrations [196, 197]. This is in line with the selection criteria applied in this study. Strain 1D6 and 17A1 were sampled from the same site and were also slightly closer related compared to 3B2 which stemmed from another site. These differences in branch length although are small and, given the amplicon lengths of 502-756 bp, could therefore also be caused random substitutions. Therefore, no distinction in two different ecotypes could be deviated from these findings [198]. The lipid content for three *Dunaliella* species ranges from 15-23 %

CDW for nutrient replete cultures which was above the values in this study [75, 114]. Contrary to what Sheehan et. al, the *Dunalliela* strains of this study did not decrease their lipid content during a nitrogen limitation [82].

3.1.5. Conclusion and Outlook

In many publications the calculation of the growth rate is either not exactly described or the data points taken into account for the calculation are not outlined clearly [199, 200]. In this study, a "R"-based analysis tool of the growth rate for the reproducible and facilitated calculation of μ could be established. By only selecting μ_{max} values above an adjustable threshold of the R^2-values between the ln-transformed CDW values and the time, it ensures that only the data points from the exponential growth rate are included into the calculation of the growth rate. This feature is independent of the number of measuring points during the cultivation. The module was tested on different data sets and subsequently used for the calculation of μ throughout this study. It contributed thus to the uniformity and ease of the analysis of multiple growth curves within one screening approach.

In many screenings targeting towards increased lipid productivity, Nile Red (NR) was used to indirectly show an increase in lipid content by an increase of NR fluorescence [65, 174, 175]. It could be shown that NR is not suitable for a lipid screening with algae strain from various phylogenetic groups, as these representatives possess different cell wall structures, sizes and intracellular compartments which alter the NR fluorescence response. Therefore, other techniques, which do not require strain-specific calibration and process optimization should be used. Direct Transesterification already proved previously to be applicable to a wide range of algae strains with no difference to the standard Folch-method throughout all the algal classes [201]. Furthermore, in this study it could be shown that the lowest quantifiable mass of fatty acids proved to be 40.20 mg. This amount makes the procedure amenable to analysis of biomass cultivated in microplate

volumes. In the search for high lipid producing algae strains, the throughput and validity of the detection of such strains could thus be significantly increased.

As genetically engineered algae strains are currently still in their infancy, the main source for new biomass producer for biofuel applications are environmental habitats. In this study it was shown for such a screening from environmental samples, that by carefully choosing the respective sampling sites, a significant number of strains could be enriched. In this case, 45 samples from eleven water bodies were distributed in different media and trace component concentrations, resulting in 360 samples, and cultivated under selective laboratory conditions. With an integrated selection process during this enrichment, the proliferating strains in the primary screening possessed the desired properties like tolerance to broad temperature ranges and a high salinity. Only the requirement for unicellular growth could not be guaranteed for all samples, as resting stages of multicellular algae species could not be excluded from the environmental samples due to their similar sizes. Their multicellularity became apparent in the subsequent screening round and they were therefore excluded as they are not suitable for large scale cultivations. However, by applying this selection-enrichment process the probability of false-positives is reduced.

For the detection of the strains showing a high growth rate, a combination of fluorescence and absorbance measurements in the mixed cultures during the first enrichment allowed for a readily selection for strains with a high growth rate in microplates. This parameter is used for the first selection of potential production strains particularly in small volumes. From them, fifteen strains were propagated, whereas only three of them did not show any filamentous growth and were susceptible to antibiotic purification. The strains could be identified as reprensentatives of the *Dunaliella* genus. Then, the lipid productivity of these three strains was evaluated and proved to be lower compared to the reference strain *Nannochloropsis salina*. This strain is however well-studied and further optimization of the three *Dunaliella* strains regarding pH-optimum, media composition and light

intensity could approximate the values of the strains. Especially in the latter parameter lies a tremendous potential for improvement of the strain performance. Wen et. al, for instance, could increase the lipid productivity of a *Chlorella pyrenoidosa* strain from 96.28 to 144.93 mg/(L · d) by continuous culturing in a nitrate chemostat [202]. Optimization like these represent however the last step of optimization approach, as they are not applicable to large-scale bioprospecting screens.

3.2. Development and assessment of microalgae screening platforms

In the first part of this chapter a miniaturized screening system is introduced, which consists mainly of purchasable components and which is operated manually. The core of this system is a microplate lid from the company *enzyscreen,* Heemstede, Netherlands. The implemented lid is supposed to provide a good gas transfer and a low evaporation for the cultures. Solely minor accessories were additionally designed and constructed in order to obtain a complete and working cultivation system. The overall performance and suitability for screening procedures was evaluated.

The second part outlines the design and development of a novel screening module containing an internal gas distribution system which was realized by Additive Manufacturing. The system is therefore denominated as *am*MTP throughout the study. The internal structure allowed for the automatization of the monitoring of the cultivation under constant gas supply in a laboratory robot set-up. Likewise, the screening performance was documented and compared to the manually operated system.

3.2.1. Design, validation and assessment of manually operated system (*es*MTP)

3.2.1.1. Selection of microplate

The choice of microplate considerably determines the whole process of screening. Whereas the outer dimensions of microplates are standardized, many different well and cover designs exist. For this study, 24-well-plates were chosen as standard based on several reasons: (i) Due to the low surface tension of the liquid which enables exceeding the critical shaking frequencies at lower rpm values, a good gas transfer can be obtained even with common laboratory shakers [203]. (ii) With 24 samples treated at the same time, still a good statistical base is given for media optimization and strain selection.

(iii) Furthermore, the amount of media volume used in those plates is sufficient for cultivations up to three weeks which are common in microalgae biotechnology.

As evaporation is interlocked with the gas transfer rates, also the choice of the MTP cover is essential for the overall process as it determines CO_2 availability for the cells during the process. Another important parameter is the availability of light. Clear microplates have the advantage of providing light homogenously to all wells, however, only the same light intensity can be applied at the same time.

Based on a literature research considering the before-mentioned requirements, the 24-well Costar® plates by the company Corning, Corning, NY, USA, were selected as standard plates. Furthermore, they fit to the lids by the company *enzyscreen.* This multi-layer membrane system has already been widely used, however only for heterotrophic cultivations and showed during these studies a good gas transfer combined with tolerable evaporation rates *[204–207]*. In favor of these lids was also the fact that they can be autoclaved. A drawback however is the metal lid which requires removal for measuring the absorbance in the wells. The metal lid was hereby replaced by a sterile transparent lid under the laminar flow hood (see Figure 21).

3.2.1.2. Design, construction and validation of *es*MTP set-ups

A mounting device for the manually operated microplates was designed in order to enable the cultivation of microalgae on a shaking platform which was placed in the CO_2-enriched cultivation chamber. The preliminary determined requirements for the mounting device were: (i) robust operation at maximum rpm of 350, (ii) homogenous light distribution from beneath to the microplates, (iii) avoidance of a heat buildup below the microplate, (iv) spatial dimensions so that three devices can be attached to the designated shaking platform, and (v) the possibility to cultivate several types of microplates and lids.

Based on this, three mounting devices were constructed in the course of this work, each one containing a *Lumitronix* LED panel which illuminates the plates from below (see Figure 19). A diffusive plate was inserted between LEDs and microplate in order to

distribute the light homogenously (see (6), Figure 19). On top of the plate, an aluminum frame was placed constructed by the in-house workshop (see (1), Figure 19). Microplates of different heights can be inserted into this frame. Four small threads attached to the crosslink of the frame act as vices in order to fix the lid tightly to the plates during rotation. As the microplates are sitting on a small stand, air and thus heat transfer to the ambient atmosphere is ensured (see (7), Figure 19).

The mounting devices were then attached to the shaking platform of a shaker via the ground plate and placed into a cultivation chamber (see (4), Figure 19). The rest of the manual screening set-up doesn't consist of components designed in the course of this work and can therefore be found in the Material and Methods section (see section 2.2.1).

After the construction of the device several quality control tests on the homogeneity of the cultivation were run. First of all, the incident PPFD on all three mounting devices was measured and compared throughout the three plates. For the variability within a LED cassette a mean variability of 4.92 % could be measured and 4.04 % for the variability between the three cassettes. As all of the data were normally distributed ($p_{1\text{-}3}$: 0.189-0.297), an analysis of variances (ANOVA) could be conducted and it was shown that there was no significant difference in the mean values of the three groups ($p = 0.842$).

Furthermore, the performance of the whole screening set-up was tested by cultivating the same batch of *Picochlorum* sp. in all three set-ups under the same conditions (see Figure 20).

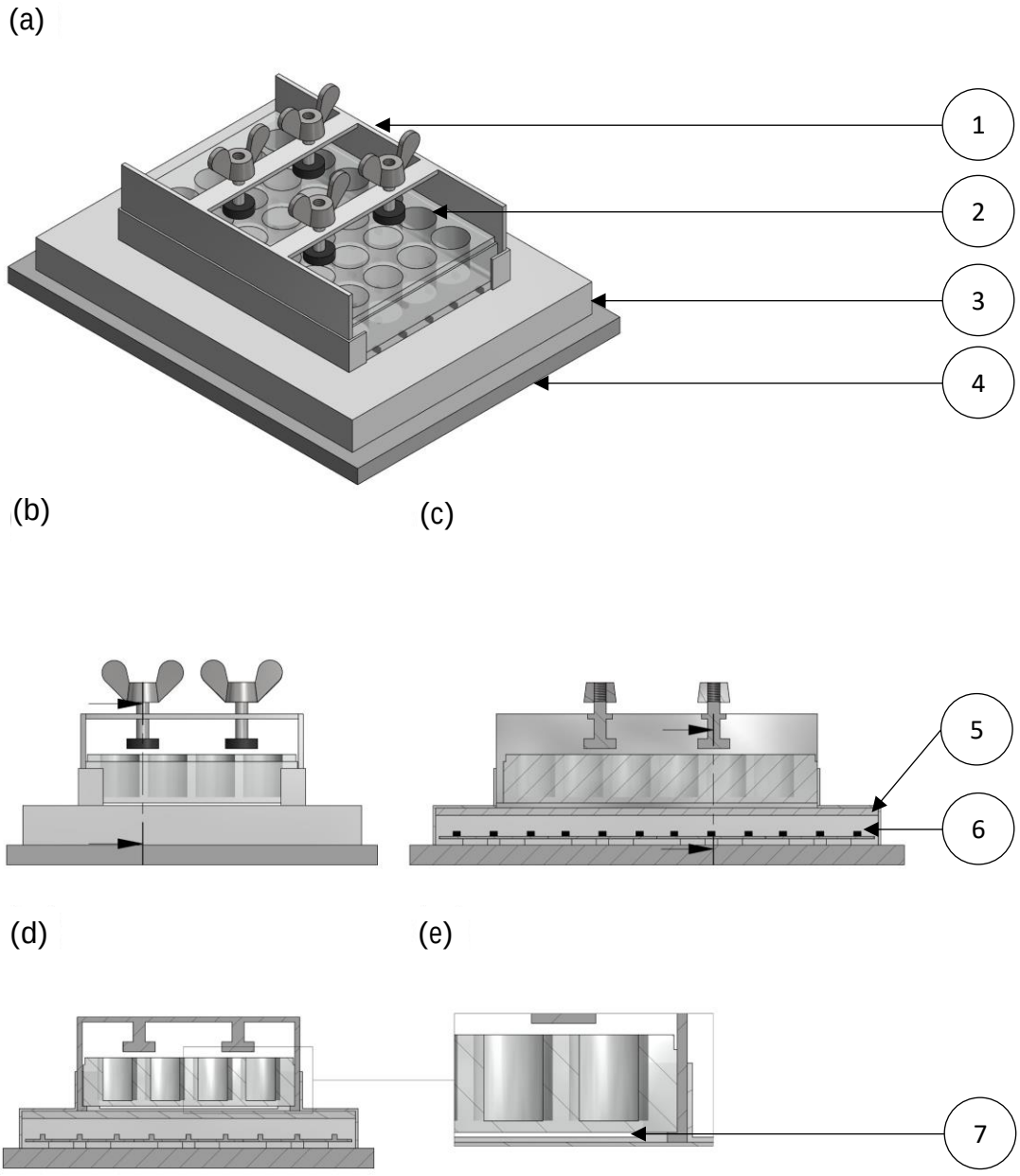

Figure 19: Illustration of the mounting device with a schematic microplate. (a) Overview, (b) Front view, (c) sectional view of (b) at marked line in (b), (d) Sectional view at the marked line in (c), (e) excerpt detail view of (d). (a): Aluminum frame with wing nuts (1), schematic microplate (2), MTP PVC frame (3), HDPE ground plate (4). (c): diffusive acrylic plate (5), LED panel (6). (e): Gap between microplate and the acrylic plate (7).

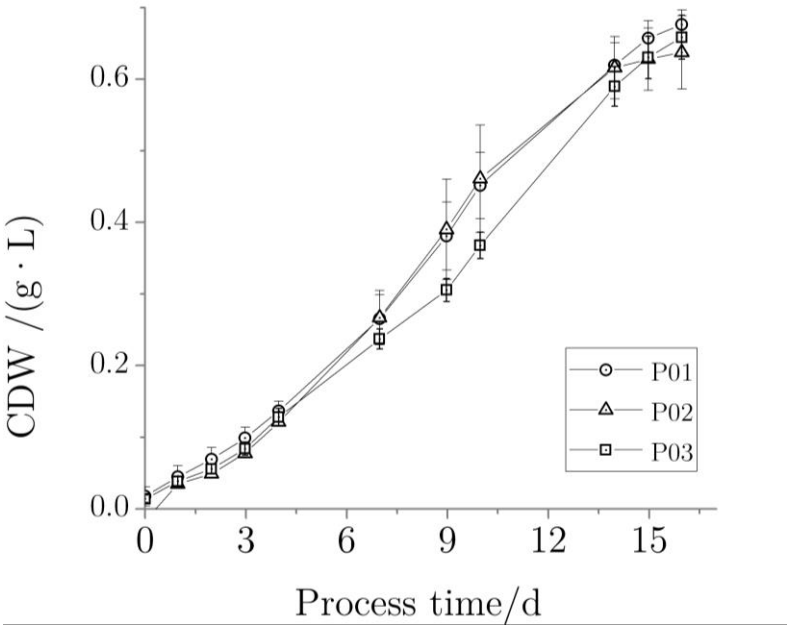

Figure 20: Homogeneity test of cultivations in three equal *es*MTPs with *Picochlorum* sp. Corner wells were excluded from analysis due to diverging evaporation properties. *Enzyscreen* lids were used for the sealing of the plates. T= 26°C, CO_2-air mixture 1/99 % (v/v) in incubator, PPFD 14 µmol/(s · m²). N=20 per plate.

The development of the CDW concentration showed a parallel growth within all three plates except for plate 3 in the time between 6.97 d and 9.97 d. The mean maximum CDW was 0.657 ± 0.02 g/L and the mean biomass productivity was 40.85 ± 0.46 mg/(L · d).

In order to evaluate further if this deviation infers with the homogeneity of the system, several descriptive statistical parameters were calculated (see Table 11). For the intraplate variabilities values of between 8.05 and 13.11 % were calculated whereas the interpolate variability amounted to 11.06 %. Two ANOVAs proved no sign of a significant difference (i) between the plates and (ii) the inner and outer wells of all plates as the p-values were higher than the chosen significance value (α=0.05).

Table 11: Descriptive statistics on the test of homogenous growth in the constructed LED cassettes. Intra- and interplate variabilities were calculated as described earlier. Parameter on which the calculation is based is given in brackets. The overall mean value represents the mean of all values from every measuring point (n=10) except from day 0. For intra- and interplate variability the CDW concentration values were used. For the determination of the growth rate the R-tool was used with a R^2-threshold of 0.9999 and 4 measuring points. Normality was tested as described above by conducting the Shapiro-Wilk-test (S-W-test). The mean growth rate between the plates and between the inner and outer wells of all plates were compared by ANOVA.

	P01	P02	P03
Mean intraplate variability (CDW)	13.11 %	10.50 %	8.05 %
Overall mean interplate variability (CDW)		11.06 %	
p-value S-W-test ($\mu/(d^{-1})$)	0.581	0.472	0.879
p-value ANOVA ($\mu/(d^{-1})$, Plates)		0.116	
p-value S-W-test ($\mu/(d^{-1})$, Inner – outer wells)	0.32 / 0.39	0.89 / 0.06	0.58 / 0.80
p-value ANOVA ($\mu/(d^{-1})$, Inner – outer wells)	0.08203	0.8511	0.88171

3.2.1.3. Comparison of *es*MTP to other systems

After showing the homogeneity of the system, the performance of other MTPs and lids were analyzed in comparison to the *es*MTP system. A summary of the plate and covers used is given in Table 12. A major drawback of the *es*MTP is the manual removal of the lid for absorbance measurements. Due to this problem, system P02 was specifically designed by *enzsyscreen* for this study and a comparison between standard and modified system is shown in (see Figure 21). With a polycarbonate lid instead of the metal one and an additional hole over every well for measuring the absorbance, the altered design is supposed to make the removal of the lid obsolete. The gas transfer is provided in both systems by the diffusion through the microfiber filter and the ePTFE layer.

The microplates by Porvair Sciences are opaque. The system P03 was sealed with a clear tape, which is supposed to be gas permeable.

Table 12: Summary of applied microplates and covers.

Plate No.	Plate brand	Plate type	Cover brand	Type
P01	Corning® Costar®	Clear 24-well, not treated	Enzyscreen	CR1524a
P02	Corning® Costar®	Clear 24-well, not treated	Enzyscreen	Custom-made lid. Like CR1524, but with a plastic lid instead of metal.
P03	Porvair Sciences	Krystal 24-well, not treated	Thermo Scientific™	Nunc® sealing tape

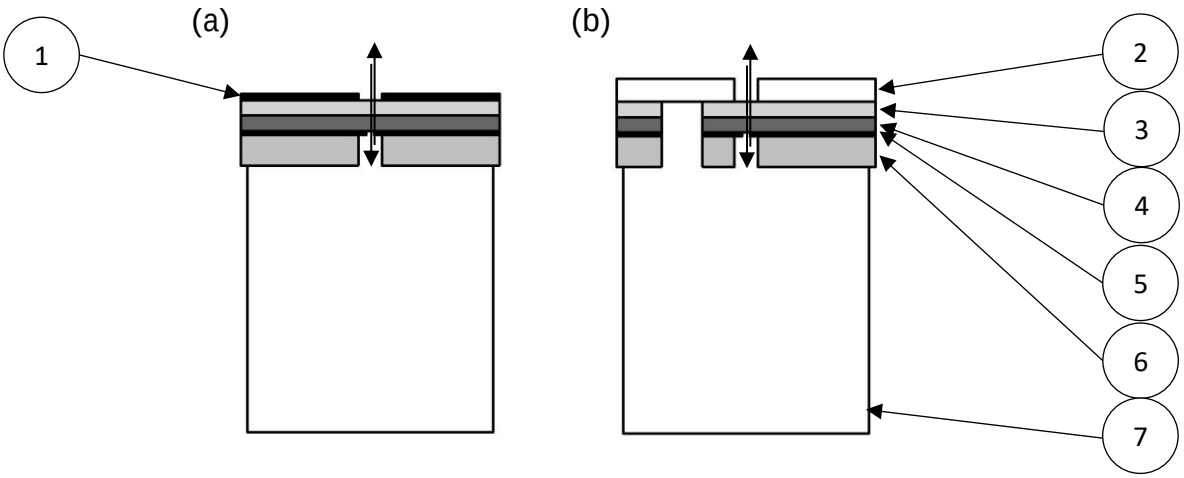

Figure 21: Cross section views of cover designs tested. The same components where used in both systems for the construction except for (1) which was replaced by (2). (a) Conventional *enzyscreen* cover: Stainless steel lid (1). (b) Modified cover: transparent PC lid (2), microfiber filter (3), ePTFE (0.3 µm) laminated between two polyester/polyamide fabrics (4), stainless steel foil with pinholes (5), soft silicone (6), well (7). Component description and illustration are adapted from enzyscreen.com.

In order to test the performances all set-ups were inoculated with *Picochlorum* sp. in its standard medium and growth, overall well homogeneity and evaporation rates were evaluated. A summary of the measured parameters and their values is listed in Table 13. The system P01 showed the lowest evaporation rate combined with the lowest intraplate variability and a μ_{max} and CDW concentration value slightly lower than system P03.

Table 13: Summary of the microplate evaluation assay with *Picochlorum* sp. for different plate and lid systems. P01-03 refer to the systems outlined in Table 12. Growth rates were measured with the R-module, a R^2-threshold value of 0.97 and a minimum of four of measuring points. For the mean intraplate variability, the mean from all time points during the cultivation were considered. Cultivation duration: 14 d, T=26 °C, PPFD=14 µmol/(s · m²), 1 mL/Well. N=20 for each plate, 1 plate per type.

	P01	P02	P03	
Mean μ_{max}	0.425 ± 0.036	(R^2 < 0.97)	0.488 ± 0.106	d^{-1}
Max. CDW conc.	0.549 ± 0.023	0.104 ± 0.017	0.574 ± 0.163	g/L
Mean interplate variability	8.32	16.86	25.02	%
Evaporation rate	8.01	1.55	19.41	µL/(Well · d)

Although the evaporation in System P02 was the lowest for all systems tested, no growth rate could be calculated with the R-module and the maximum CDW concentration only reached 18.94 % of system P01. Due to these attributes, it was selected as the reference system for the manual screening set-up.

3.2.1.4. Performance test of *es*MTP system

The reference system was then used to perform a comparative study to the *am*MTP system whose development is outlined in the succeeding sections of this work (see 3.2.2). The study consisted of a cultivation of *Picochlorum* sp. under the same process settings in both systems. The development of the CDW concentration in the *es*MTP system is shown in Figure 22. A summary for the obtained growth values is given in Table 14. The cultivations show intraplate variances between 5.93 and 41.61 %. The latter value was caused by a single well in plate 1. For plate 2 and 3 CDW productivities showed similar values, whereas μ_{max} differed at a 21 %. The evaporation rates range for the three plates between 10.79 and 15.40 µL/(well · d).

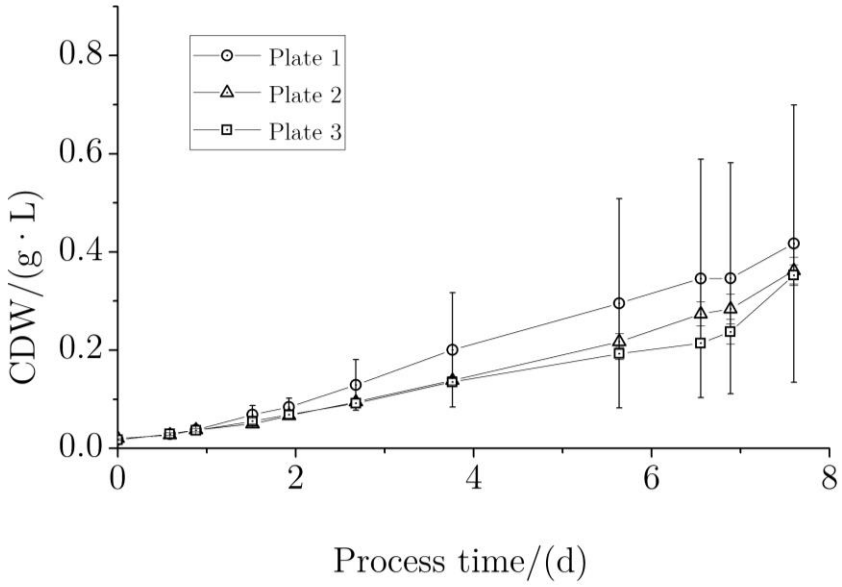

Figure 22: Performance test of the *es*MTP system with *Picochlorum* sp.. Shaking frequency 350 rpm, PPFD= 57,80 ± 2.91 µmol/(s · m²), T= 26 °C, gas mixture in headspace= 1 % CO_2, 99 % compressed air (v/v), N = 3 for each plate.

Table 14: Summarized growth performance and evaporation for *Picochlorum* sp. in the *es*MTP system. Mean μ_{max} was calculated based on the R-module with a R^2-threshold of 0.97 and a minimum of 4 measuring points.

	Plate 1	Plate 2	Plate 3	
Intraplate variability	41.61 ± 26.18	5.93 ± 2.52	7.96 ± 2.50	%
Mean μ_{max}	0.740 ± 0.046	0.524 ± 0.015	0.635 ± 0.104	d^{-1}
Max. CDW conc.	0.417 ± 0.282	0.362 ± 0.028	0.353 ± 0.020	g/L
CDW productivity	52.53 ± 37.18	45.26 ± 3.62	44.06 ± 2.69	mg/(L · d)
Evaporation rate	15.40	10.79	12.31	µL/(Well · d)

3.2.1.5. Discussion

The system by the company *enzyscreen* was to the best knowledge of the author for the first time incorporated in and evaluated for the cultivation of phototrophic unicellular microorganism. The developed mounting device proved to be robust during cultivation and is scalable on respective shaking platforms for larger screenings. The clamp provided a high contact pressure of the membrane to the plate which is essential in reducing the evaporation of the cultures. Compared to the values given by the company for

heterotrophic cultivations the evaporation were twice as high in the cultivation of this study [208]. This is most probably due to the increased amount of energy brought into the media by the LED from underneath the plates. As further optimization step, an optimized heat transfer away from the microplate should be targeted. An inherent problem of illuminating the plates from below is the increased temperature of the bottom of the plate compared to the membrane or a transparent lid. Evaporated water is more likely to condense on the membrane or lid compared to an illumination from the top, thus leading to altered scattering behavior of the transmitted light during measuring step. Another potential optimization would be the automatization of the system, yet a sophisticated laboratory robot system would be necessary in order to open the clamp and position the plate in a microplate reader. Another possibility would be a general re-design of the clamp system in order to make it automatable.

In order to obtain a uniform PPFD throughout the whole plate optimal distance of the microplate bottom from the LEDs, taking into consideration the angle of radiation of the LEDs and the opaqueness of the plate was determined iteratively. Although a transparent plate was used, only a variability for the illumination below 5 % were obtained with the applied distance. Values below 20 % of coefficient of variance (%CV) were considered acceptable for plate uniformity [209]. The application of a custom-made LED-panel, where each LED is positioned right below one well, ideally with a lens attached, could decrease the variability further as the light from one LED mainly illuminates the well above it. Still, a fraction of light would scatter or reflect to the other wells. The wells in the center of the plate would again receive a higher PPFD. A solution to this inhomogeneity would be the selection of an opaque microplate. In course of this study, no such plate fitting to the *enzyscreen* membrane was purchasable.

A validation cultivation in the designed set-up proved a tolerable maximum intraplate and interplate variability for the three plates. The CDW values from each measuring proved to be between 8.05 % and 13.11 % and thus within the above-mentioned

acceptance criteria for the validation of the assay. This uniformity of growth could be confirmed by an ANOVA for the calculated μ_{max} values in the three plates. The maximum CDW of 0.657 g/L (see Figure 20) corresponds in this set-up with the 0.5 mL of sample volume and *Picochlorum* sp. to an OD of 0.288 and 304.5 mg of biomass which can be harvested from one well. This amount would be in the range of the quantification limit of DT and therefore a one-point determination of the lipid content of the cells from one would be possible. Assuming a second well is harvested from a replicate cultivation at an OD of 0.5, which represents the end of the linear range of the correlation between cell concentration and absorbance, 529 mg of biomass could theoretically be harvested. With this sampling regime, a determination of lipid productivity could be conducted in microplate batch cultivations. This small window of possible data points admittedly poses a drawback but would nevertheless give a more valid indicator of the lipid productivity than an one-point determination and could above all be applied to a small-scale culture.

Compared to other microplate system and covers, the *es*MTP system showed favorable properties regarding growth performance and homogeneity. Plate P03 with the applied tape did not show any growth, probably to the reduced gas transfer. Also, due to elevated temperature at the bottom of the plate condensation occurred at the tape. System P03 could in principal be automated and maintain the advantages of the *enzyscreen* membrane. However, the highest evaporation and variability was measured for this system. Both could be related to a planar adjustment of the membrane to the plate. The lowered hardness of the polycarbonate led to small gaps between the membrane and the microplate. Therefore, the outer wells were more prone to evaporation and thus an altered cultivation development.

The performance test of the *es*MTP system showed a higher biomass productivity in all plates compared to the homogeneity test in the same system. This can be related to the altered PPFD value for this experiment, which was increased from 14 to 57 µmol/(s · m^2)

in order to obtain a comparison to the *am*MTP system. The PPFD setting within the ClimateSimulator software for the *am*MTP system would have been in the far low end of the PPFD range possibly provided by the LED panel. In order to guarantee a consistent and sufficient illumination of the cultures the PPFD of both systems was set equally to approximately 57 µmol/(s · m²). This elevated PPFD led to a higher biomass productivity and a higher mean μ_{max}, but also increased the evaporation rate, due to the increased amount of energy brought into the system. The large deviations in plate 1 are caused by a single cultivation showing a threefold higher final biomass concentration. That culture was positioned in well A01 and as the corner wells A06 and D06 showed aberrant evaporation behavior in the preliminary experiments and were therefore excluded from all further assays, this could also have happened in this case, leading to an altered cultivation development.

3.2.2. Design, validation and assessment of novel automated microplate system (*am*MTP)

3.2.2.1. Design consideration of plate corpus and production via Additive Manufacturing

In this chapter, the development and characterization of a novel microplate system will be described, which is supposed to circumvent (i) the drawback of manual OD measurements with the *es*MTP system. Additionally, several other requirements had to be taken into consideration in the development of the plate and its periphery:

The device should (ii) exhibit the standard outer microplate dimensions proposed by the Society for Laboratory Automation and Screening (SLAS) [210] in order to be capable of being integrated into standard laboratory robot and analyzing systems, (iii) furthermore have the same well dimensions for a direct comparison to the *es*MTP system, and (iv) be autoclavable including all of its accessory. Moreover, (v) a constant supply of a sterile CO_2/air-mixture should be provided to the interior of the plate during cultivation, (vi)

the temperature of one plate should be controlled for reproductive screenings and (vii) the light intensity should be adjustable for each well individually.

Due to these requirements, some necessities in the design and construction of the plate arouse: As (ii) could readily be fulfilled, (v) required some space of a standard microplate to be used for the gas connection parts. Therefore, room for actual wells within the plate was reduced and due to (iii) the overall number of wells had to be lowered from 24 to 12. After a prolonged literature research, requirement (v) couldn't be achieved in a practical manner with commonly offered parts from gas connection suppliers without reducing the number of wells further. Therefore, it was concluded to integrate an internal gas distribution system in the corpus of the plate, in order to minimize the use of commercially available connecting parts and to save the biggest space possible for the arrangement of wells. Given the small dimensions of the plate, the internal structure had to be placed into the edge regions of the plate as the center of the plate was reserved for the wells. These edge regions had a thickness of 5 mm. This value was restricted as the overall height of the plate including its upper and lower sealing was limited to 23 mm as this was the maximum height of the access of the microplate reader. So, for the implementation of the gas distribution within these edge regions it was necessary to construct a channel of 3 mm of diameter which is branched to four channels with a diameter of 1.35 mm each. The branching was considered necessary in order to provide a homogenous gas distribution to all of the three lines of wells. The gas distribution with the aforementioned restrictions could technically only be realized by Additive Manufacturing (AM). As with this technology also metal as material can be used, using AM for the construction of the plate both allowed fulfillment of (v) and (iv). The final design based on the above-mentioned requirements and subsequent considerations is shown in Figure 23. Throughout the rest of the study the additively manufactured system was denominated as *am*MTP.

The manufacturing of the component was appointed to the company Airbus APWORKS GmbH (Taufkirchen, Germany) where AlSi10Mg was used for the production process.

This aluminum-based alloy shows good resistance to corrosion and a low density of 2.67 cm^3/g which is favorable for the handling by laboratory systems [211]. A thermal conductivity of 130-190 $W/(m \cdot K)$ assures a rapid heat transfer provided by the temperature regulation system. The material also allowed for wall thicknesses down to 1.0 mm with allows for very fine structures like the twelve well holders in the middle of the plate [211].

In order to minimize the overall weight of the corpus, the spaces between the contacting wells were not filled with material (see (1) in Figure 23). Another measure for weight reduction were the hollow structures lateral of the in-gas connection and those at the side of plate (see (4,10,11) in Figure 23). The latter structures possess a dome shaped upper ceiling, as AM cannot process 90°-angle in the vertical direction [212]. In summary, the weight of the printed component amounted to 171 g.

In order to fulfill (v) on each side of the corpus space was reserved for the gas connection system (see (12) in Figure 23). As sterility was part of this requirement only 13 mm disc filter were spatially appropriate. The outer diameter of the purchased filter was thus the limiting criteria for the minimum height and width of the edge regions. On the top and bottom side of the plate a channel was incorporated for placing a sealing component (see (2 & 3) in Figure 23). Also on both sides six M3 threads were added by the in-house workshop (see (9) in Figure 23).

The main feature of the plate, the internal gas distribution, can be seen in Figure 24. Due to the afore-mentioned space requirements both for the gas connection system and maximum height of the plate, the position and diameter of the internal gas distribution system was set. A reduction of the internal diameter from 3 to 1.35 mm should minimize flow rate differences in the four terminal channels. The gas inlet was mirrored for the design of the gas outlet.

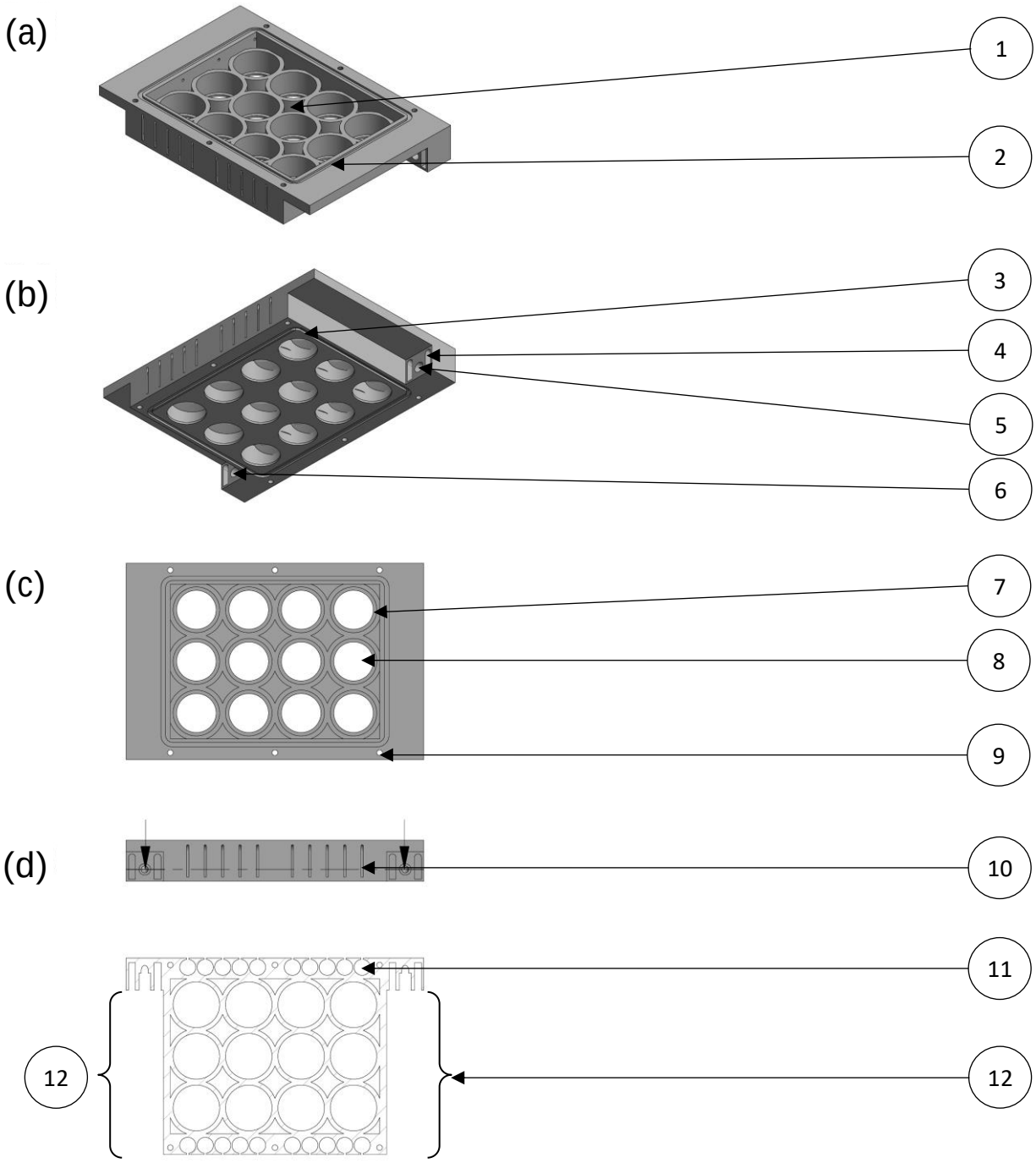

Figure 23: Illustration of the corpus of the *am*MTP. (a): (1) Space between wells, (2) upper sealing channel, (b): (3) lower sealing channel, (4) hollow structure, (5) off-gas drilling, (6) in-gas drilling screw thread, (c): (7) Glass insert stand Opening, (8) glass insert holder, (9) M3 thread, (d): (10) hollow structures, (11) hollow structures, (12) space for gas connection system and filter.

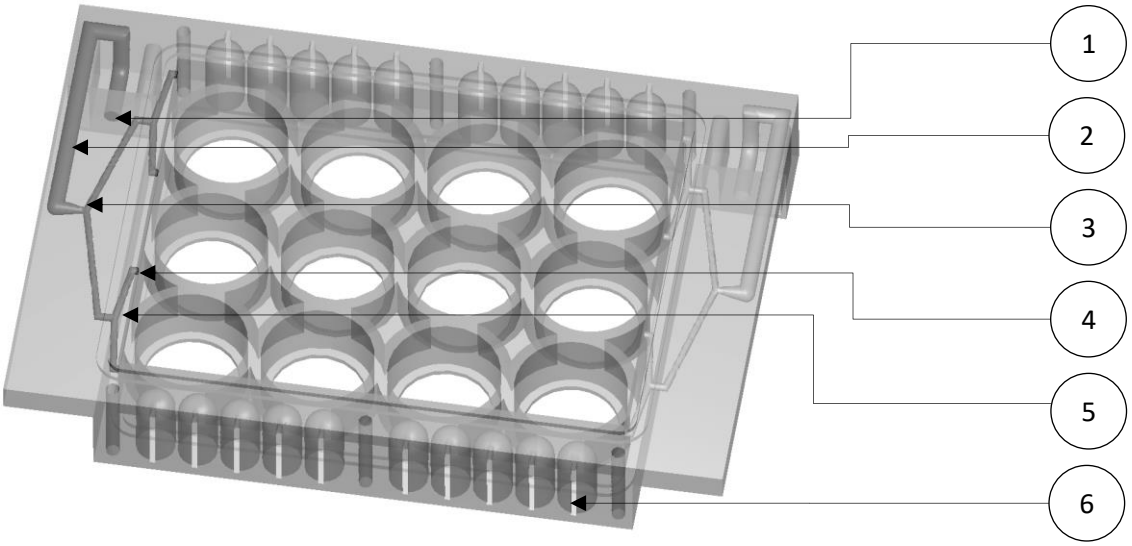

Figure 24: Transparent illustration of the *am*MTP corpus. The channel for the gas inlet to the interior of the plate is marked dark grey. (1) In-gas hole, (2) main channel (diameter=3 mm), (3) first branching to secondary channel (diameter=1.35 mm), (4) outlet hole, (5) second branching, (6) hollow structures.

3.2.2.2. Considerations on the selection of *am*MTP accessory and evaluation of chosen components

In the following section, the considerations are outlined leading to the choice of the final *am*MTP accessory. Also, validation tests on the previously postulated requirements of the systems were conducted. The final system, as it was used in the subsequent experiments, is shown in Figure 26.

Wells

Trimmed borofloat glass tubes were used as building blocks in order to fulfill requirement (iv). As a bottom plate, round cover slips from microscopic applications were used as these components show a small thickness and high transmission. They were attached to the trimmed glass tubes with a thermostable glue. The glass wells needed to be fixed tightly within the well holder of the plates but not permanently as thorough cleaning and repairing should still be possible. For these reasons, silicone stripes of 0.5 mm

thickness were cut out and wrapped around the inserts before placing them in the holders. OD_{750nm} measurements of the *am*MTP systems with inserted empty wells showed a significantly high %CV of 8.83 % to 21.87 %. For this reason, it was concluded to subtract the OD_{750nm} value of the empty well individually from every OD_{750nm} data point measured.

Plate sealing

No internal structures were intended for the lid and the lower plate of the *am*MTP, therefore the component could be manufactured in the in-house workshop of the Chemistry Department of the Technical University of Munich. Requirement (i) demanded an uninterrupted light path for automatized OD measurements, therefore borofloat glass plates were glued in the designated cavities. Glass plate were preferred over plastic plates due to (iv). The opening above each well in the lid and bottom plate were constructed in order to minimize the effect of scattered light in neighboring wells which could infer with requirement (vii). Also, the stability of the components was increased by this measure.

For sealing the plate, a silicone round cord was initially placed in the upper and lower sealing channel. Experiments on water-tightness although showed a significant loss of water. Furthermore, a flat silicone seal with a hardness of approximately 60° Shore A did not prevent water from entering the interior. A softer component was searched for and gastight ethylene propylene diene monomer (EPDM) foam rubber proved to retain the water in the filled *am*MTP corpus. It could also be proved that in the closed plate the injected air passed through the plate and left it – with a significantly lower flow rate – through the other opening. In order to resolve the decrease in the outgoing gas flow rate, air tightness tests were conducted. Submerged in water, bubbles arose mainly from the glued gaps between lid and glass plate, with several applied layers of silicone not avoiding it. As another major source of gas loss, the gap between the EPDM sealing and the lid on the short side of the plate could be detected. Due to the necessary tight fixing of the screws to the plate the lid was curved considerably. This resulted in a lowered

contact pressure of the sealing and therefore air could escape. The exact amount of air leaving the *am*MTP was tested with the CO_2-flushed system placed in a gastight plastic box. In the linear range of the degassing process, the loss of gas from the internal headspace was 0,44 mL/h at a total volume of 73.76 cm^3.

As the EPDM sealing itself proofed to be gas-tight and the loss of gas could be compensated readily which the applied gas flow, thus avoiding a decrease in CO_2-concentration in the plate, the component was used in the further course of this study. As EPDM is not autoclavable, requirement (iv) could not be fulfilled solely for this component. Instead, it was concluded to UV-sterilize the item.

Gas connection system

The intended system should connect the external gas supply with the internal, printed gas distribution system (see Figure 24) which leads the CO_2/air-mixture into the inner part of the plate. Due to requirement (i) no manual connection system like Luer or pneumatic push fittings could be considered. Therefore it was concluded to use a magnetic gas connection which is already published for microfluidic applications [213]. As a next step, the position of the interface between the external gas supply and the gas connection system of the plate had to be determined. Placed at the bottom of the plate, the connection would have required less accessory and therefore less space, as the gas was transferred by a 90° elbow fitting to the internal gas distribution system. However, attaching such an elbow fitting requires screwing it to the filter (see 3.2.1.2) which is due to the given spatial dimensions not possible. For this reason, it was determined to place the interface at the side of the plate. With a distance bush and a steel washer (see 11 & 12, Figure 26) the interface could be positioned at the edge of the plate. A short overhang provided a better fixation of the connection system to the external gas supply when place backed by the robot arm after OD measurements (see Figure 27). For the gas outlet on the other side of the plate only a MLL/M5-connector and the filter were used.

The fluidics of the gas transfer into the plate were simulated prior to the production of the plate. Here the gas flow rate was in all four terminal channels similar, resulting in an equal gas supply from each channel (see (a) in Figure 25). The homogeneity was checked for in the water filled *am*MTP corpus after sealing the bottom part with the EPDM sealing as described in section 3.2.2.2.. From the generated bubble in the top right corner of the interior of the plate in (b) in Figure 25 it is obvious that the gas transfer with the magnetic connector and the designed internal structure could be realized. Nevertheless, compared to the simulation the gas did not exit in equal amounts from the holes into the interior of the plates. The main portion of gas enters from the hole on the far right.

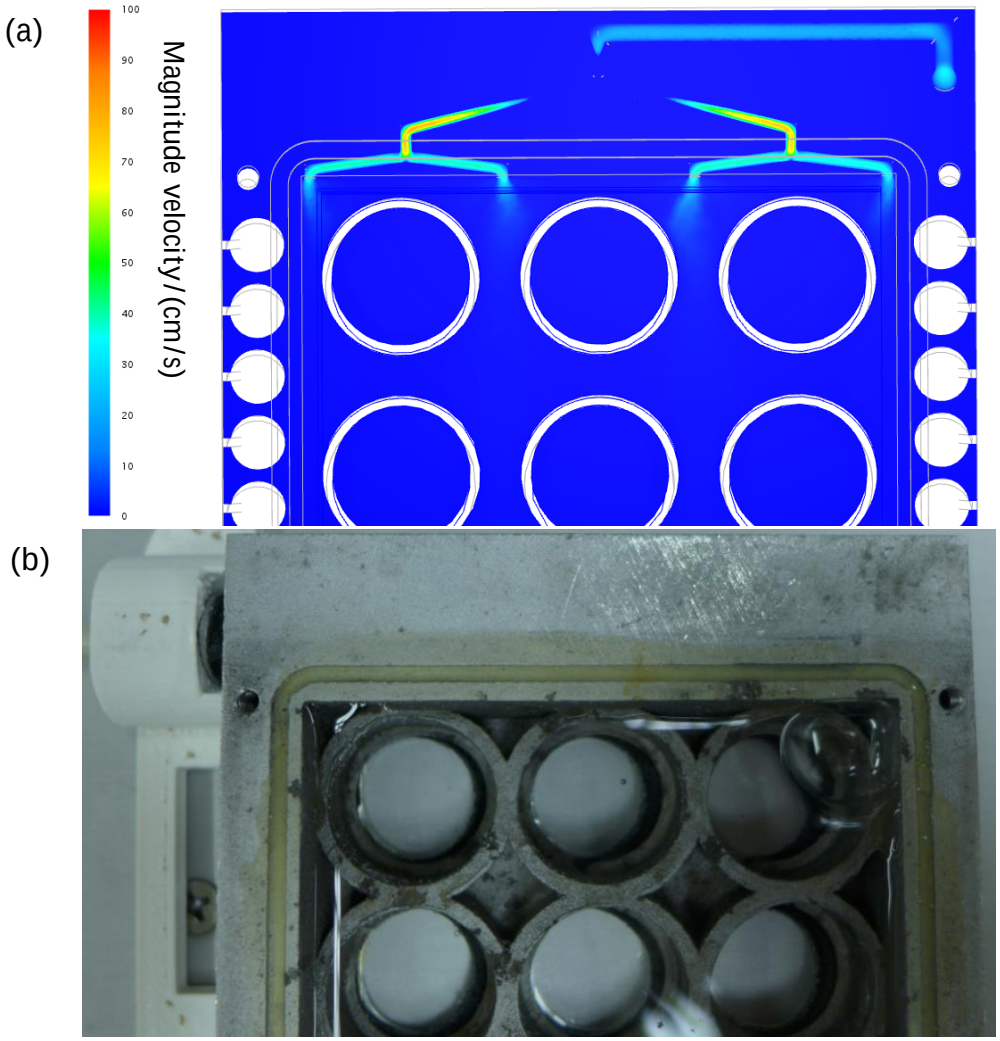

Figure 25: Simulated and actual gassing of *am*MTP. A simulation of incoming gas with a flow rate of 4 L/h is shown in (a). As entry point of gas, the drilling hole of the *am*MTP corpus was chosen (see (6), Figure 23). The layer shown is a horizontal plane through the center of all holes facing the interior of the plate. In (b) the same flow volume rate was applied with the magnetic connector and the gas connection system (not visible).

As the gas transfer via magnetic connectors proved to be applicable and the alteration of the internal gas distribution was not feasible, no further optimization in the structure of the internal gas distribution system was implemented and the system was used as it is shown in Figure 26.

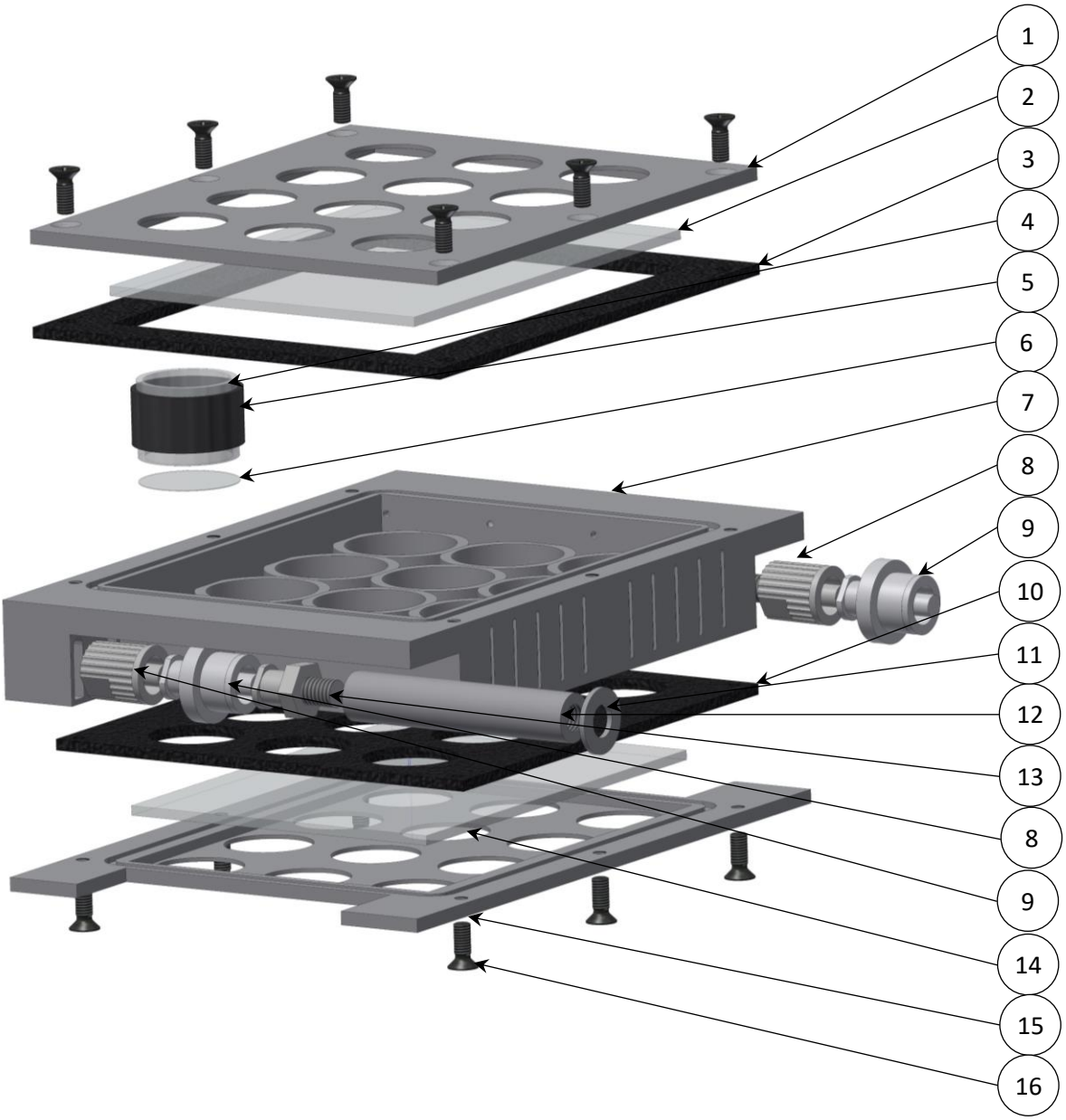

Figure 26: Exploded view of *am*MTP corpus and its accessory. (1) Lid, (2) top glass plate, (3) top sealing, (4) glass insert, (5) sealing, (6) cover glass, (7) *am*MTP corpus, (8) Male Luer Lock/M5-connector, (9) Male Luer Lock/Female Luer Lock filter capsule (10) bottom sealing, (11) steel washer, (12) distance bush, (13) Female Luer Lock/M5-connector, (14) bottom glass plate, (15) bottom plate, (16) screws.

3.2.2.3. Discussion

It could be shown that the design considerations of the plate corpus led to a microplate system which is suitable for the automated OD measurement under CO_2-enriched atmosphere. The requirements initially stated, could be fulfilled except for the total autoclavability of the system. As the autoclavable sealing methods led to increased loss of gas from the interior volume, an EPDM foam had to be used as sealing material. This material has an upper temperature tolerance of 120 °C according to the supplier and was deformed irretrievably after autoclaving. It was therefore UV-sterilized before the inoculation of the plate. As the whole *am*MTP system had to be assembled after autoclaving this measure did not extend the set-up time significantly. The application of the foam could nevertheless not stop the loss of gas but only minimize it. Gas leakage could be observed between the glass plate and the lid and the foam and the lid at the short side of the plate in the middle of the two screws. The point pressure of the screws in the corner led to a bent lid between the screws, so that the contact pressure there was reduced and the gas could escape. The bent lid assumingly led to small cracks in the glue between lid and glass plate which enabled the gas to leak from the plate. Re-applying silicone after the cultivations could not prevent this leakage permanently. A possible solution to the loss of gas would therefore lid and a bottom plate manufactured from a harder yet equally light material where bending does not occur. Also, the application of more screws for the fixation of the lid could have a positive effect or a sealing system where not a flat seal but a system with nut and spring is implemented.

After testing the *am*MTP some possible optimizations in the design became obvious: The incorporated sealing channel was obsolete as the plane sealing with an EPDM mat proved to be more effective. The wall thickness of the glass vial holders could be selected smaller as AlSi10Mg showed enough hardness. Likewise, the outer walls of the corpus could be manufactured thinner, except for the positions of the threads. Both measures would result in a higher interior space of the plate. The additional space can be used for e.g. the incorporation of smaller wells around the existing wells, which could be filled with water

or media during the cultivation. This principle for humidification of plate and thus the reduction of evaporation is already applied for conventional plates [65, 149]. The increased space in the interior not only reduces the weight of the plate significantly but also allows for a re-design of the gas distribution system. As the parallel gassing through four channels into the interior of the plate proved in this study to be not feasible, a single channel would be sufficient. This would further increase the space which in turn could be used for a smaller and more stable external gas connection system. For instance, an electromagnet could be used for the controlled attachment of the plate to the gas tube. Thus, the gas loss was lower and less gas needs to be applied. In spite of the possible optimizations, the *am*MTP system shows already the potential of Additive Manufacturing for the miniaturization of screening systems and thus the opportunities in increasing in throughput of the identification of new microalgal strains for biotechnological applications.

3.2.3. Proof-of-principle of automated cultivation monitoring

3.2.3.1. Development of prototype *am*MTP set-up

After the completion of the *am*MTP and its accessory the component was integrated in a set-up which enables the gassing of the plate during cultivation (see Figure 27). The *am*MTP was placed into a frame (see (4), Figure 27) which was fixed to the shaking platform and which holds the plate in the exact position while shaking. A clear PC plate (see (2), Figure 27) with the LED matrix (see (5), Figure 27) attached to it was placed over the microplate, held in position by four printed PLA corner components (see (3), Figure 27). The size of the LED matrix was chosen in such a way that every well receives the light from the same number of LEDs although the LEDs were not positioned right above the center of each well. A clear *Corning* microplate (see (1), Figure 27) was attached on top of the PC plate as a gripping point for the laboratory robot arm for the removal of the LED cassette within the measuring process. The frame in which the

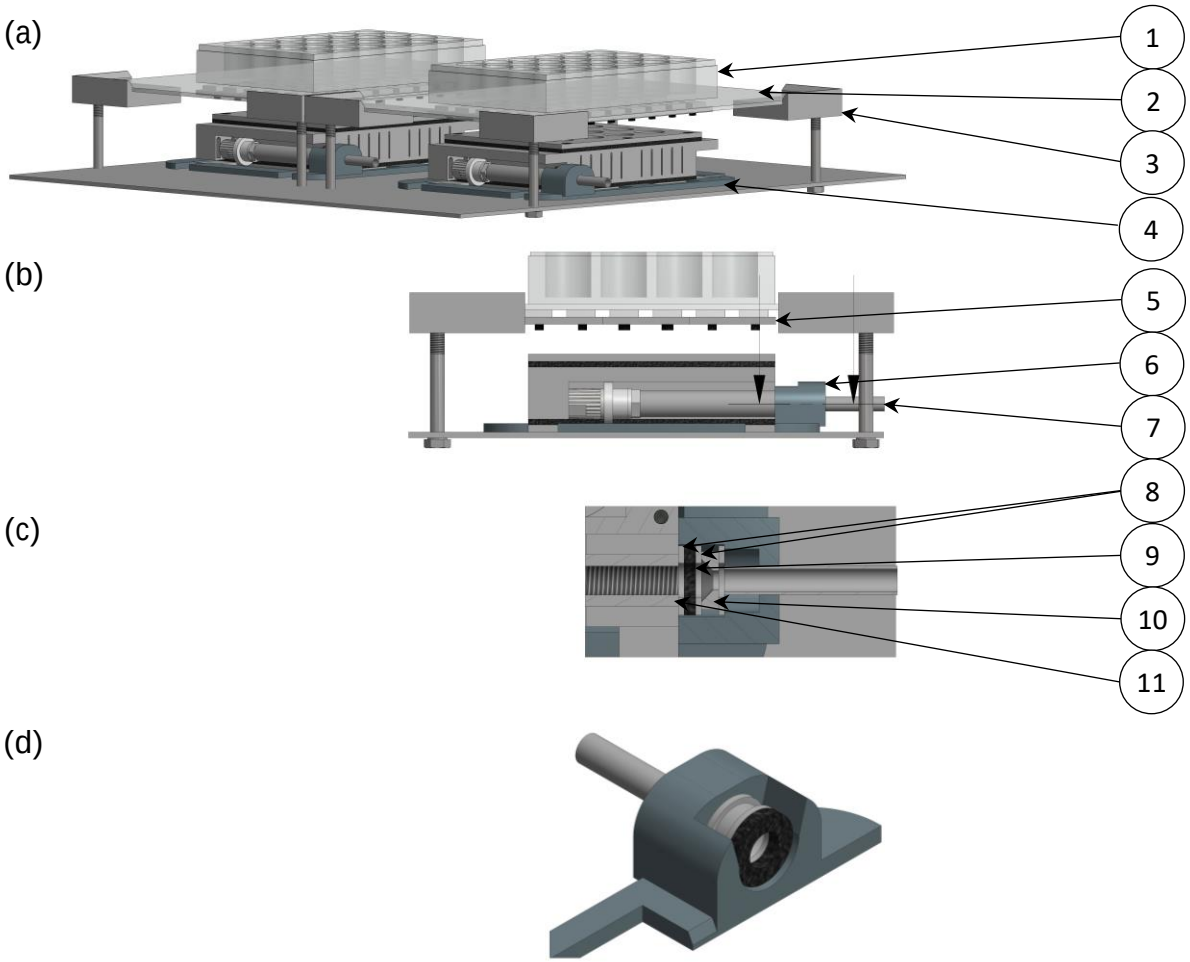

Figure 27: Illustration of prototype set-up for automated cultivation monitoring. Isometric rear view of complete set-up (a): Microplate (1), clear acrylic plate (2), PLA printed acrylic plate positioning component (3), *am*MTP frame (4). Rear view of one plate set-up (b): LED cassette (5), gas connection unit (6), tube for external gas supply (7). Sectional view of plane marked in (b) with dotted line (c): Steel washer (8), EPDM sealing ring (9), neodymium magnet (10), distance bush (11). Isometric view of gas connection unit (d).

*am*MTP was placed possessed a gas connection unit (see (6), Figure 27) which transfer the gas from the external supply (see (7), Figure 27) to the inner distribution system of the *am*MTP (see (11), Figure 27).

The connection between the external supply and the distance bush consisted of a magnet (see (10), Figure 27) attached to the tube and an EPDM ring (see (9), Figure 27) for sealing purposes. The EPDM ring was essential for the effective gas transfer from the external gas supply to the internal distribution system. Without it, the connection between the magnet and the steel washer proved to be not gastight. Furthermore, a direct contact between those two components resulted in such a strong magnetic

connection that the robotic arm was not able to remove the *am*MTP in a horizontal manner from the gas connection system. This led to a tilted plate which then eventually slipped out of the arm in the subsequent moving steps. The far left steel washer (see (8), Figure 27) was attached to the *am*MTP, whereas the rest of the set-up (see (8-10), Figure 27) was glued to the external tubing (see (7), Figure 27).

The far let steel washer extends with 1 mm over the outer dimensions of the plate. After measuring the plate is placed in the frame by the robotic arm. Due to the design of the gas connection unit that steel washer is forced into the right position and with it the whole gas connection system. This mechanical locking ensures the correct position of the connection and thus the proper transfer of gas from the external supply to the internal gas distribution system of the *am*MTP.

3.2.3.2. Automated measuring process

The prototype *am*MTP set-up was mounted on the shaking platform and integrated in the periphery (see Figure 28). The gas was provided by a gas mixing station and was humified passively by passing through a bottle filled with DI water (see (9) Figure 28).

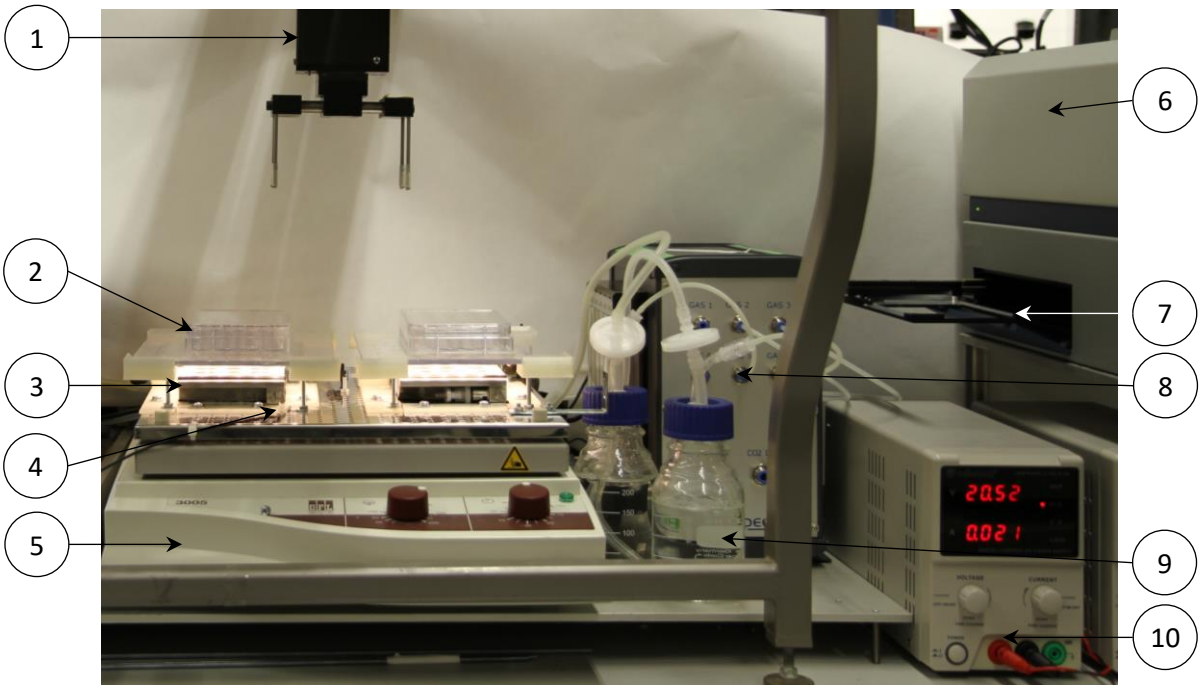

Figure 28: Laboratory set-up automated growth monitoring. Robot arm (1), MTP plate for gripping plate (2), *am*MTP (3), temperature sensor (4), shaker (5), microplate reader (6), MTP gripper (7), gas mixing station (8), passive humidification (9), power supply (10).

For an OD measurement, the gripper stopped the shaking platform by interrupting the power supply to the device. The used shaker didn't have a fix parking position at which the platform stands still. Thus, diverging parking positions led to diverging positions of the *am*MTP relative to the fix laboratory robot and incorrect gripping would occur. Therefore, a security mechanism was built in to assure a fix parking position of the shaking platform. It was realized by attaching a spring to the corner of the shaking platform, strong enough to pull the entire platform to the right rear corner of its orbit. Occasionally though, the platform halted exactly opposite of the fixation point of the spring. From this vertex, the spring did not execute any force on the platform and it stayed therefore at this position. This resulted again in false positions of the platform and, as there was no crosstalk between the shaker and the robot software to correct for this, the gripper would grab at a false position.

In order to circumvent the halt of the platform at the vertex position a security step was included. For this reason, a metal angle was attached to the platform. With the platform manually brought to the vertex position, the gripper was programmed to grip the metal angle, resulting in a weak movement of the shaking platform. This however proved to be sufficient to remove the platform from the vertex position and to bring it to the usual parking position determined by the spring. In case the platform already had been in the parking position the gripping during the security step missed the angle. Once the platform stood still, the gripper lifted the LED cassette by gripping the microplate (see (2) Figure 28) and stacked it on the other microplate. Then the gripper removed the microplate from its frame, placed it on the MTP gripper of the microplate reader (see (7) Figure 28) and the OD measurement protocol was run. After the measurement, the *am*MTP was replaced in the frame, likewise the LED cassette on its holders. Then, the same procedure was conducted for the second *am*MTP. Once that plate including its LED cassette were back on the original place the power supply of the shaker was switched on again by the gripper. After an interval of 3 h the procedure started over.

3.2.3.3. Proof-of-concept cultivation

After establishing the measuring process, a proof-of-concept cultivation was conducted in order to validate the whole system and especially the gassing of the interior of the *am*MTP. This was executed by providing one plate with ambient air and the other with of a mixture of 1 % CO_2 and 99 % compressed air (v/v), both at a gas flow rate of 4 L/h. Both gas streams were passively humified by passing through a DI water bottle. Temperature could not be regulated for the system at this point of the study and therefore the room temperature is shown (see Figure 29). The mean temperature during the experiment was 25.10 ± 1.55 °C. The glass vials of well C02 in plate 1 and A01 and B01 of plate 2 broke during the process and were therefore excluded from the analysis. The same was done for C01 and C02 in plate 2 as they did not show any growth during the whole cultivation. For the remaining wells, it could be shown that in the plate which

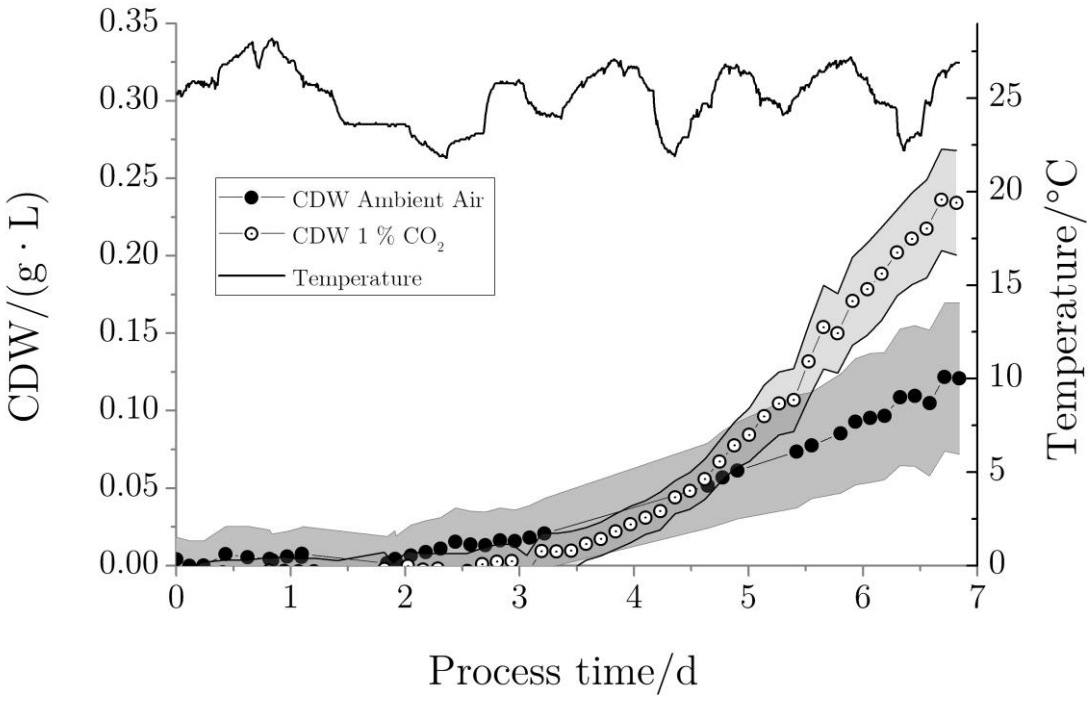

Figure 29: Development of *Picochlorum* sp. growth under ambient and CO_2-enriched conditions. Gas flow rate 4 h/L, shaking frequency 350 rpm, PPFD: 57.54 ± 7.7 µmol/(s · m²), measuring interval: 3 h. Standard deviations are displayed in grey bands for better visualization.

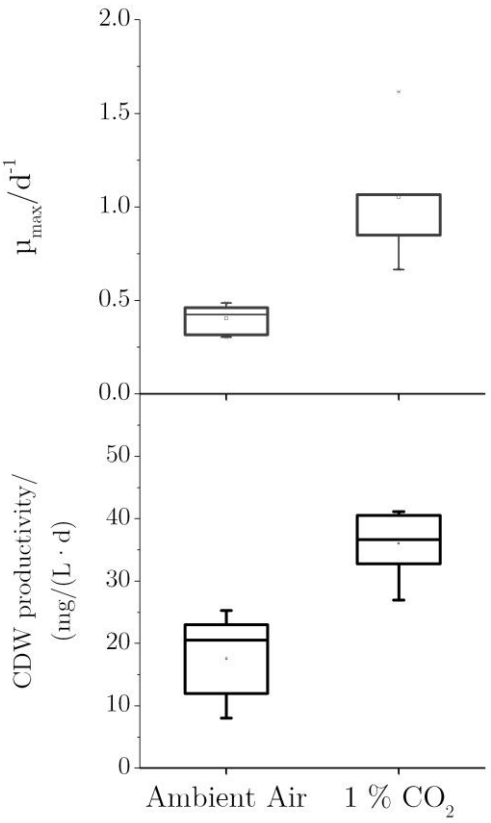

Figure 30: Mean μ_{max} and CDW productivity for the gassed microplates. Calculation was conducted with the R-module, using a R^2-threshold of 0.97 and a minimum of 4 measuring points. Values below the threshold were excluded from μ_{max} calculation. Broken wells and wells which didn't show growth were excluded from CDW productivity analysis. μ_{max}: N (ambient air) = 5, n (1 % CO_2) = 4. CDW productivity: N (ambient air) = 10, n (1 % CO_2) = 8.

was gassed with 1 % CO_2 a significantly higher maximum CDW concentration could be obtained. Whereas the cultivation under ambient air showed a lag-phase of approximately two days, the cultivation under the enriched CO_2-atmosphere reached after 3 days the exponential growth phase. The calculated μ_{max} and CDW productivity values were 160 %, respectively 105 % higher, for the cultivation with increased CO_2 concentration (see Figure 30). The end of the cultivation was reached after 6.8 d due to a false positioning of the plates by the robotic arm. In Table 15 the growth performance of the strain in both plates is summarized. Evaporation is higher in the *am*MTP gassed with 1 % CO_2 compared to the plate gassed with ambient air with a total volume reduction at the end of the cultivation of 48.85 µL and 109.56 µL respectively.

Table 15: Summary of calculated values for microplates gassed with ambient air and 1 % CO2. μ_{max} was calculated as described above, biomass productivity was measured based on the CDW at the end of the cultivation and evaporation was measured as the loss of *am*MTP weight over time.

	Ambient Air	1 % CO_2	
Mean μ_{max}	0.403 ± 0.076	1.052 ± 0.357	d^{-1}
Max. CDW conc.	0.121± 0.049	0.234± 0.034	g/L
CDW productivity	17.55 ± 6.33	36.02 ± 4.96	mg/(L · d)
Evaporation	7.14	16.07	µL/(well · d)

3.2.3.4. Discussion

The *am*MTP proved to be applicable for an automated cultivation within the prototype set-up. The biggest obstacle in the measuring process was hereby the performance of the laboratory robot arm in gripping and positioning of the plates. Several cultivations were aborted due to false placement of the plates by the robot arm. This led to false gripping of the arm in the next movement and a tilted plate which eventually would drop, spilling the cultures. In repeated movement of plates from one position to another, no general trend towards a false positioning could be observed, rather than being spontaneous phenomena. As no crosstalk between the shaker, the reader and the laboratory robot regarding the position of a plate existed, a misplacement inevitably led to an abortion of the experiment. Another major drawback was that the plate reader occasionally did not measure one plate even given the fact that the other plate indeed was transferred to the reader and analyzed in the same measuring cycle. This was for instance the case from 4.9 – 5.4 d during the proof-of-concept cultivation (see Figure 29). This occurred from the first cultivations on and an increase in the time interval between the measurements did not seem to solve this problem.

The proof-of-principle cultivation showed the advantage of the cultivation of microalgae under a CO_2-enriched atmosphere. A higher μ_{max} and a higher CDW productivity could be obtained. The maximum biomass which can harvested at an OD of 0.5 is in this set-up 216.29 mg from one well. As the lag-phase is large in relation to the whole cultivation, the duration of cultivation could be shortened by using a pre-culture also from

microplates under a CO_2-enriched atmosphere, in order to minimize adaption effects. This would also reduce total evaporation for the process as the screening could be ended sooner. Thus, the increase in nutrient and salt concentration in the media would be smaller. With a minimized lag-phase, 11 cultivations under CO_2-replete conditions could be conducted in the course of four days.

3.2.4. Implementation of a temperature regulating screening environment

In the first prototype of the automated set-up, the temperature could not be regulated and for this reason the validation of the set-up was conducted at room temperature which fluctuated considerably over the course of the experiment (see section 3.2.3.3). In order to establish stable conditions for further experiments a cultivation chamber was designed and manufactured via Rapid Prototyping. The *am*MTP were placed in the center of the cultivation chamber with the same gas connection system used in section 3.2.3.1 (see Figure 31). The outlet of an air oven was connected to both chambers via a Y-fitting and the off-gas from the two chambers was again directed in one EPDM tube to the inlet of the air oven (see (2) Figure 31). Thus, a circular air stream could be established. The sensor for the regulation of the temperature was inserted into one of the chambers via a small hole. LED panels were placed above the *am*MTP in such way that each LED was positioned centrally above one well (see (c), Figure 31). A lens was placed over each LED in order to focus the emitted light to a single well. In order to minimize the loss of tempered air from the chamber, a layer of EPDM sealing was glued to the parking position of the LED panel (see (1), Figure 31). The air oven, the LED panel and the control software for these two components were designed and constructed, respectively programmed, by the in-house Electronic Department. Further details regarding those components are therefore outlined in the Material and Methods section. The measuring process was not altered from the descriptions in section 3.2.3.2.

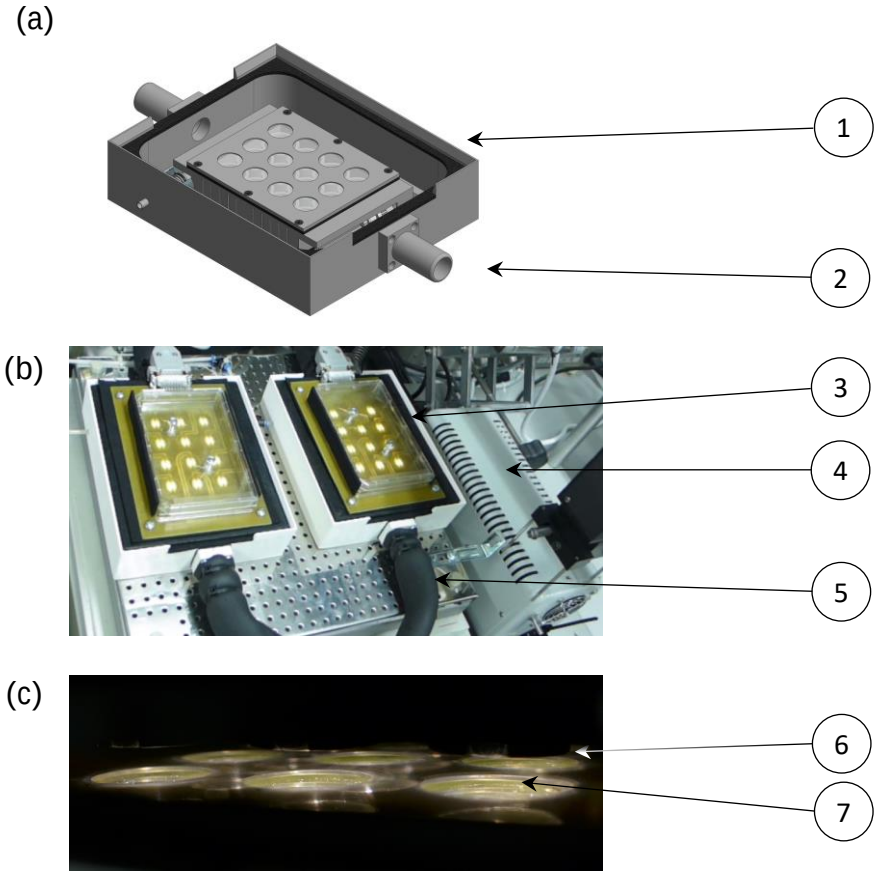

Figure 31: Isometric illustration of *am*MTP placed inside the cultivation chamber (a): EPDM sealing (1), gas inlet (2). Photo of robot set-up (b): LED panel (3), air oven (4), air tube (5). Illumination of wells by single LEDs (c): lens (6), well (7).

3.2.4.1. Temperature tests

Temperature homogeneity between two cultivation chambers

For the validation of the temperature homogeneity between the two chambers different set points were applied for 24 h by the *ClimateSimulator* software and the response of the temperature value in both boxes was recorded by two different temperature probes. The probe in box 2 was the measuring element of *ClimateSimulator* which in turn controlled the air oven. The probe in box 1 was an external probe. During the first day, the temperature could be regulated mostly to the set value. After changing the setpoint to 30 °C the temperature dropped in both boxes but reached the setpoint within 3.19 h in box 1 and 1.65 h in box 2 respectively. The temperature change from 30 °C and 22 °C could be reached within 3.31 h in box 1 and 5.00 h in box 2.

The diagram in Figure 32 shows that the mean absolute deviation from the setpoint did not exceed 1 K. The summarized temperature values in and outside of the cultivation chamber are shown in Figure 33. It can be seen, that the values in the box only minorly differed from the setpoint compared to the room temperature values outside the box. The mean value for the room temperature was 25.35 ± 0.98 °C and the mean for the chamber 25.86 ± 0.42 °C.

Homogenous light distribution

In order to compare the lightning conditions for both systems, the incident illumination at the surface of the algae suspension was measured by means of a created stencil of the well arrangement of the *am*MTP. A closer description of the measuring process is giving in section 2.2.2.1. The intraplate variability of the light intensity was evaluated by setting a pre-determined current for every LED in order to obtain the same PPFD value for each LED. For the intraplate variability, a value of 3.26 % for the LED panel used for *am*MTP 1 could be measured and 4.46 % for the LED panel used for *am*MTP 2 respectively. The interplate variability was 3.08 %.

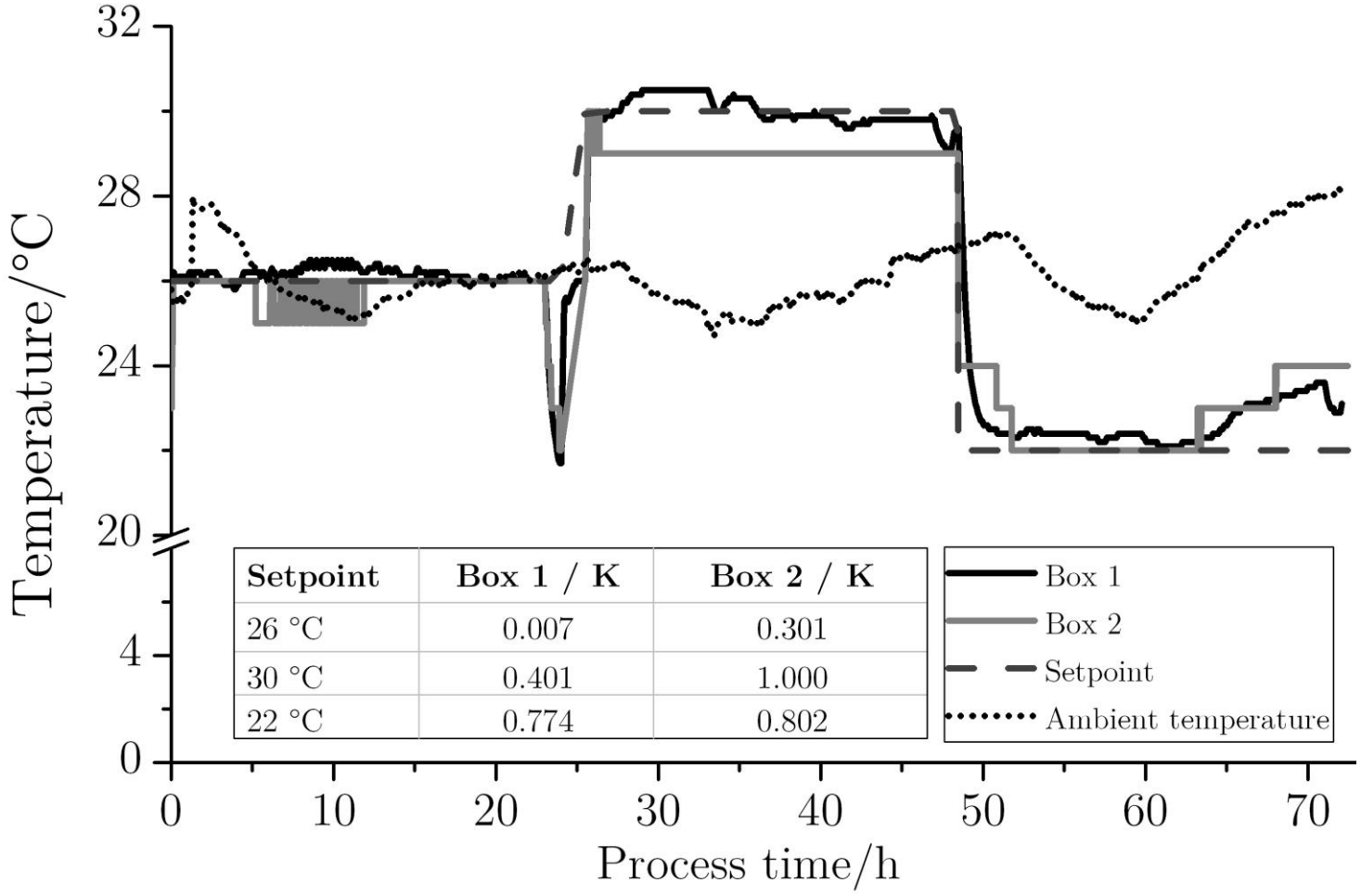

Setpoint	Box 1 / K	Box 2 / K
26 °C	0.007	0.301
30 °C	0.401	1.000
22 °C	0.774	0.802

Figure 32: Temperature development within the two cultivation chambers at 22, 26 and 30°C. Temperature set points were held for 24 h, surplus time stems from set-up time between two set points. Sensor for temperature regulated was located in box 2. The diagram lists the mean absolute deviation from the setpoint for the temperature values in both boxes.

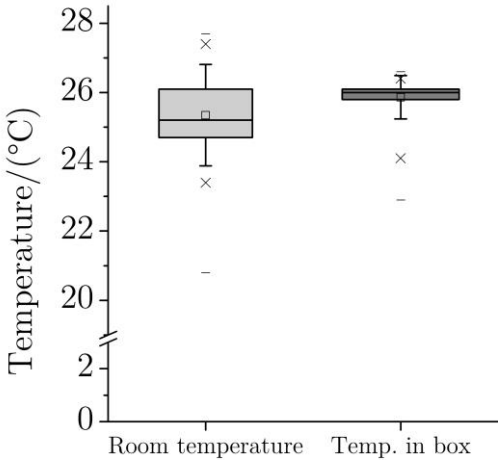

Figure 33: Summarized temperature values for box 2 and room temperature during the cultivation of amMTP in section 3.2.5. Plots are based on calculations of 7482 data pairs of set temperature and measured temperature.

3.2.4.2. Discussion

By the design and the construction of the temperature controllable cultivation chamber a more stable screening process could be achieved. With a maximum mean absolute deviation of 1 K from a given set point from 22 °C to 30 °C it provides valid temperature control for the process. The strongest deviations from the set-point occurred at a change of the setpoint when the regulation control cycle of the software showed strong fluctuations. These deviances, although, could be minimize by optimization of the control parameters. This temperature range tested here is for most outdoor applications of microalgae suitable, as a temperature control is thought to be economically not feasible. Beside the temperature also the PPFD could be controlled more thoroughly. By the application of the *ClimateSimulator* software also light kinetic studies are implementable.

3.2.5. Homogeneity test of *am*MTP under constant temperature conditions

An essential element of a screening system is the ability to provide robust experiments throughout different units of the system. In order to evaluate this for the *am*MTP system a parallel cultivation from the same batch of *Picochlorum* sp. was conducted in order to obtain the intraplate variability similar to the *es*MTP system in section 3.2.1.4. The

development of the CDW concentration throughout the cultivation is shown in Figure 34. It can be seen that both plates show a similar growth on average with large standard deviations. The mean of the CDW concentrations from both plates differs for three timepoints significantly from each other. Regarding the obtained growth rates also

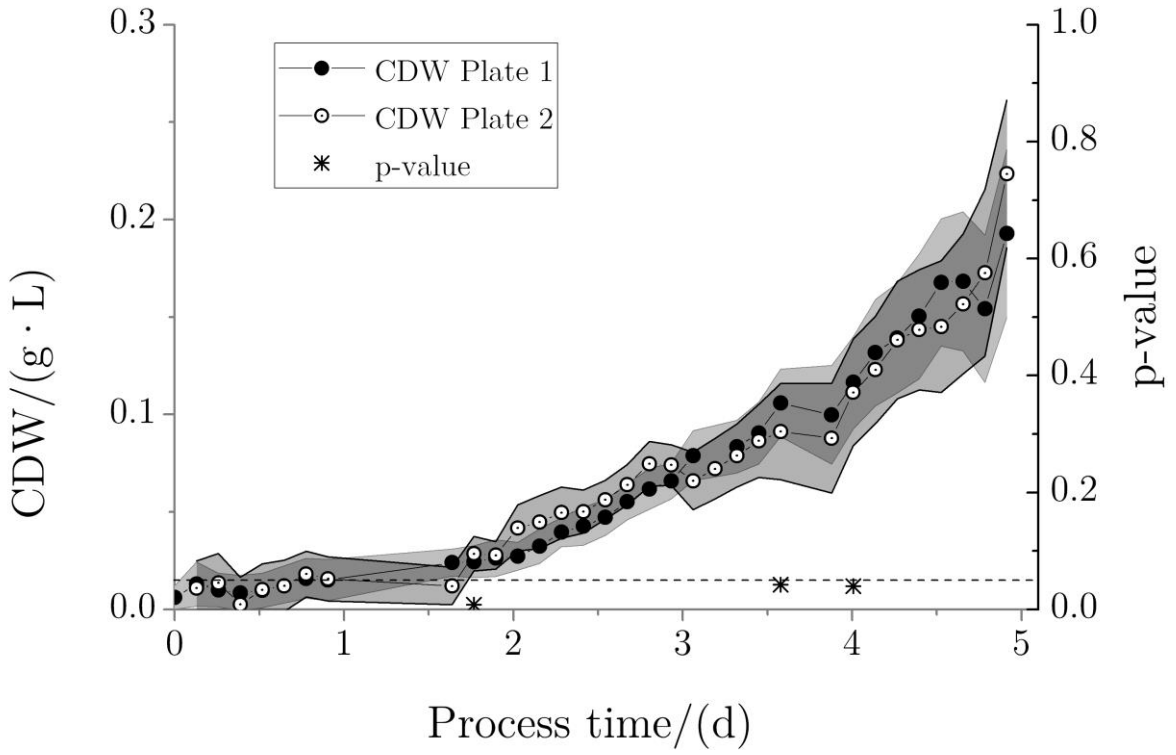

Figure 34: Cultivation of *Picochlorum* sp. in two parallel *am*MTPs under controlled temperature and light conditions. The horizontal line marks the significance level of the applied t-test (α=0.05) with the CDW concentration of the plates as groups Calculation was conducted with the R-module, using a R^2-threshold of 0.97 and a minimum of 4 measuring points. Values below the threshold were excluded from μ_{max} calculation. Asterisks indicate significant deviation between the CDW concentration of the two plates. Shaking frequency=350 rpm, T=26°C, PPFD=57.80 ± 2.57 µmol/(s · m^2), 1 mL/well. N=11 for both plates. Well A01 was filled with media. Grey bands represent standard deviations from mean.

significant standard deviations were measured. Nevertheless, the mean within both plates amounts to 1.038 and 1.012 d^{-1} (see Table 16). The cultivation was stopped after 5 d as the gripper of the robot arm dropped plate 2 and a further comparison of both cultivations was impossible.

Table 16: Summary of the growth performance of *Picochlorum* sp. in both *am*MTPs. N for μ_{max} determination was 8 and 5 for plate 1 and plate 2 respectively due to calculations from the R-module. For calculation of maximum CDW concentration and CDW productivity N=11. Plate 2 slipped from the robot arm and could therefore not be included in the evaporation measurement. N for evaporation values of plate 1 is 12.

	Plate 1	Plate 2	
Overall mean intraplate variability (CDW)	22.02	29.71	%
Overall mean interplate variability (CDW)	19.64		%
p-value Shapiro-Wilk-Test ($\mu/(d^{-1})$)	$2.617 \cdot 10^{-4}$	0.111	
p-value ANOVA ($\mu/(d^{-1})$, Plates)	0.948		
p-value ANOVA ($\mu/(d^{-1})$, Inner – outer wells)	0.613		
Mean μ_{max}	1.038 ± 0.800	1.012 ± 0.269	d^{-1}
Max. CDW concentration	0.193 ± 0.043	0.223 ± 0.038	g/L
CDW productivity	38.01 ± 0.008	40.9 ± 0.012	mg/(L · d)
Evaporation rate	6.56 ± 13.05	Not available	µL/(Well · d)

An assessment of the growth performance was conducted cultivating *Picochlorum* sp. under the same conditions in both systems. For the *es*MTP, the results of the cultivation are shown in section 3.2.1.4 and for the *am*MTP in section 3.2.5 and a summary of the relevant growth values is given in Figure 35. In this summary, the μ_{max} values for both systems differ compared to their performance tests in the afore-mentioned sections. The reason for this is an adjusted calculation which considers the differing time intervals of OD measurements with both systems in the initial calculation (see 3.2.1.4). The plates of the *es*MTP system were measured once or twice a day, resulting in 11 measuring points during a cultivation of 7.6 d. The R-module used a pre-set minimum of four measuring points for the calculation of μ_{max}. For the performance test, the calculation of the R-module showed that 6.33 ± 0.87 measuring points were used to calculate μ_{max} which corresponds to a mean exponential growth phase for the cultures of 4.37 ± 0.60 d.

The *am*MTP system was sampled every 3 h which resulted in 34 measuring points during a cultivation of 5.05 d. For the calculation of μ_{max}, the R-module used 7.82 ± 5.78 measuring points, corresponding to a mean exponential growth phase of 1.16 ± 0.86 d and thus a 5.45-fold shorter duration compared to the *es*MTP system. These differing durations can lead to a false conclusion when systems are compared based on those

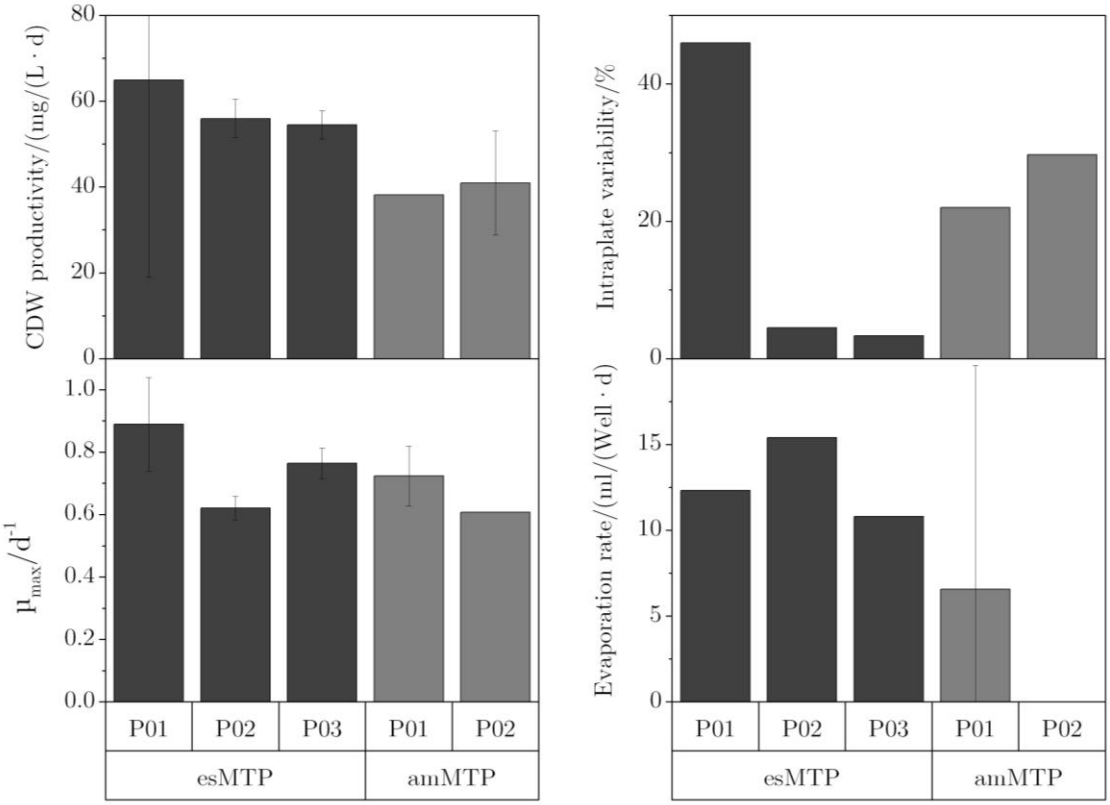

Figure 35: Growth performance of *Picochlorum* sp. in *es*MTP and *am*MTP system. μ_{max} values were calculated with the R-module, whereas for the *es*MTP system four measuring points and for the *am*MTP system 19 points were used with an R^2-threshold of 0.9999. All of the calculated values showing a R^2 value below 0.97 were excluded.

values. In order to harmonize the exponential growth phase durations first the growth rates for the *es*MTPs were calculated with a minimum of four measuring points which resulted in an exponential growth phase of 2.76 d. As R^2-threshold, a value of 0.9999 was chosen in order to force the algorithm to calculate values from a similar exponential growth phase. Then, for the *am*MTP system the amount of measuring points was calculated which would lead to an exponential growth phase of 2.76 d. This resulted in the application of 19 measuring points for the calculation of μ_{max} from an exponential

growth phase duration of 2.81 d. With this adaptation of the calculation of μ_{max} both systems are assessed based on the same duration for the exponential growth phases and the values can be compared directly.

It can be seen that after the adaptation the growth rates of the *es*MTP system were slightly higher compared to the initial calculation and the values *am*MTP. That resulted in an overall mean μ_{max} of 0.758 ± 0.79 d^{-1} for the *es*MTP system and 0.704 ± 0.098 d^{-1} respectively for the *am*MTP system. The overall mean CDW productivity amounted to 58.43 ± 5.66 mg/L/d in the *es*MTP and 39.53 ± 1.91 mg//(L · d) in the *am*MTP system respectively. The evaporation rate of 12.83 ± 2.35 µL/(Well · d) in the *es*MTP system is 95.61 % higher than in the *am*MTP system.

3.2.5.1. Discussion

The parallel cultivation of two *am*MTP systems under the same PPFD, temperature and CO_2-concentration showed a similar μ_{max}, maximum CDW and CDW productivity for both plates. The obtained values were also similar to the ones measured in the proof-of-concept cultivation. The analysis of uniform growth in both plates by a step-wise calculation of the student's t-test showed only three data points out of 32 at which the mean growth of the plates differed significantly. Furthermore, an ANOVA showed no significant effects between the means of μ_{max} in both plates, neither could a difference between the inner and outer wells be detected. However, the non-significant outcome of these tests is based partly on the large deviations which were measured for the development of the CDW values. The values exceed the afore-mentioned upper limit for the tolerable intraplate variability of 20 %. Reason for this could be an unequal distribution of gas in the headspace and thus to the vials. As the glass inserts were manually manufactured, slight differences in height could lead to different openings for single wells. This in turn could result in a varying accessibility to incoming gas which causes differences in growth. Machine-made glass inserts with an additionally reduced height, in order to avoid the opening of the glass insert as a bottleneck for gas transfer,

could decrease variability. The inhomogeneous evaporation throughout the plate could also have led to differences in growth. Although the value was lower compared to the proof-of-concept cultivation, large differences were measured with partly negative evaporation values, thus an increase in liquid in the well over the course of the cultivation. As this can only occur by condensation of humidified air at the well wall or spilling from other wells into the respective well. Both could not to be monitored during the cultivation and therefore the cause of the negative evaporation values remains unclear.

The comparison of both systems shows a comparable performance in regard to the growth parameters μ_{max} and CDW productivity. The intraplate variability is for the *es*MTP system significantly lower except for the plate 1, in which one cultivation showed an inexplicable high OD increase. Excluding this cultivation from the analysis, the variability in plate 1 is 5.54 % and thus in the range of the values from plate 2 and plate 3. The evaporation rates in the *am*MTP were significantly lower in the *am*MTP, however, only with the reservation of the unsecure origin of negative evaporation rate values.

In summary, the established *es*MTP system can be used for the screening of microalgae growth in the described set-up. Showing exponential growth in microplates up to a theoretical CDW concentration of 1.05 g/L, small intraplate variabilities and tolerable evaporation rates the set-up is applicable for primary screenings of fast biomass producers, media optimizations and also lipid content analyses.

The *am*MTP system showed comparable growth performances, however, under great deviances. Tackling those deviance would lead to a more valid screening process with considerably less manual handling required compared to the *es*MTP system. Also, light kinetic studies could be conducted with exact setting of the PPFD for each well. As the whole system is scalable, larger screening of potential candidates would be possible. These candidate strains need then a robust scale-up from the microplate system to shaking flask

and photobioreactor systems. This would be next step in the evaluating potential lipid producers for the large-scale cultivations.

3.2.6. Conclusion and outlook

In this study, a manual and an automatable microalgae screening system were designed, constructed and validated in a proof-of-concept approach. In the manual system the cultures grew up to a maximum CDW concentration of 0.657 ± 0.02 g/L, whereas a maximum of 13.11 % for the intraplate variability and 11.06 % for the variability between plates was obtained. Based on an ANOVA no significant differences between the growth rates of the different plates could be detected. Given these characteristics and a mean evaporation rate of 12.83 µL/(Well · d), the system allows for the parallel, homogenous screening of up to 66 strains. Furthermore, based on the miniaturization of the Direct Transesterification, the amount of biomass obtained from this system is in principal amenable to GC analysis. As it is constructed in a modular way, increasing the number of these cultivation units would further increase the throughput for growth evaluation screenings under CO_2-replete conditions.

After the validation of the manual screening system, an advanced system was designed and constructed. This system was designed in such a way, that it allows for the integration in a lab robot system, which enables a constant monitoring of the growth parameters like OD and fluorescence. Furthermore, a constant supply of a CO_2/air-mixture was provided to the interior of the plate constantly during the cultivation, thus avoiding a carbon source limitation. This was realized by an internal gas distribution within the corpus of the system, which was constructed by Additive Manufacturing. Due to the material used in this process, the system and its accessory could be except for one component autoclaved. The system was aligned to the conventional microplate dimensions in order to be applicable with standard laboratory equipment.

In this study it could be shown that the elevated CO_2-concentration provided by the internal gas distribution showed a 2.6-times higher growth rate and a 2.05-times higher

CDW productivity compared to a plate aerated by ambient air could. With this proof-of-concept cultivation it could be shown that shorter screenings under CO_2-replete conditions are feasible with the system established in this study. In order to further qualify the microplate system as a full screening set-up, also a temperature regulation system was designed, constructed and implemented. By a parallel regulation of the two microplates, the temperature fluctuations throughout a screening could be decreased and thus the screening validity and reproducibility increased.

Finally, two equal cultivations were compared in the two plates with 11 cultivations each, showing the homogeneity throughout the system. Although the standard deviations between the individual wells were higher (22.02 and 29.71 %) compared to the manual system, the overall CDW productivity and growth rate between all cultures differed only by 2,5 % and 7,6 % respectively. The measured evaporation was lower compared to the manual system. Given further modifications of the system which decrease the variations in growth further, this system could in principal both shorten the time for a screening and also increase its validity as more data points can be generated. With these data points a closer observation of the effect of different nutrient concentrations or CO_2-concentrations could be conducted. Furthermore, by applying different light intensities per well, also light kinetic studies can be conducted in those volumes.

3.3. Bacterial communities in open thin-layer cascade reactor system

3.3.1. Salinity and pH shifts in photobioreactors

In order to evaluate the applicability of sudden shifts in the chemical conditions during a pilot-scale cultivation, the strain *D. salina KU11* was subjected to these experiments on a laboratory scale first. Samples for metagenomic analysis were taken right before, in the middle and after the 3 h duration under altered cultivation conditions, after resetting the cultivation conditions and at the end of the cultivation. Two different shifts were implemented during the cultivation in the closed *Labfors* photobioreactors: A shift from the initial pH of 8 to 5 and back and a shift from a salinity 50 g/L to 150 g/L and back. Before the shift to a NaCl concentration of 150 g/L the culture reached OD_{750nm} of 8, but with a lower cell concentration of $2.09 \cdot 10^7$ cells/mL and a share of algae population of 62.25 % (see Figure 36). These values in increased after the shift to their pre-shift values.

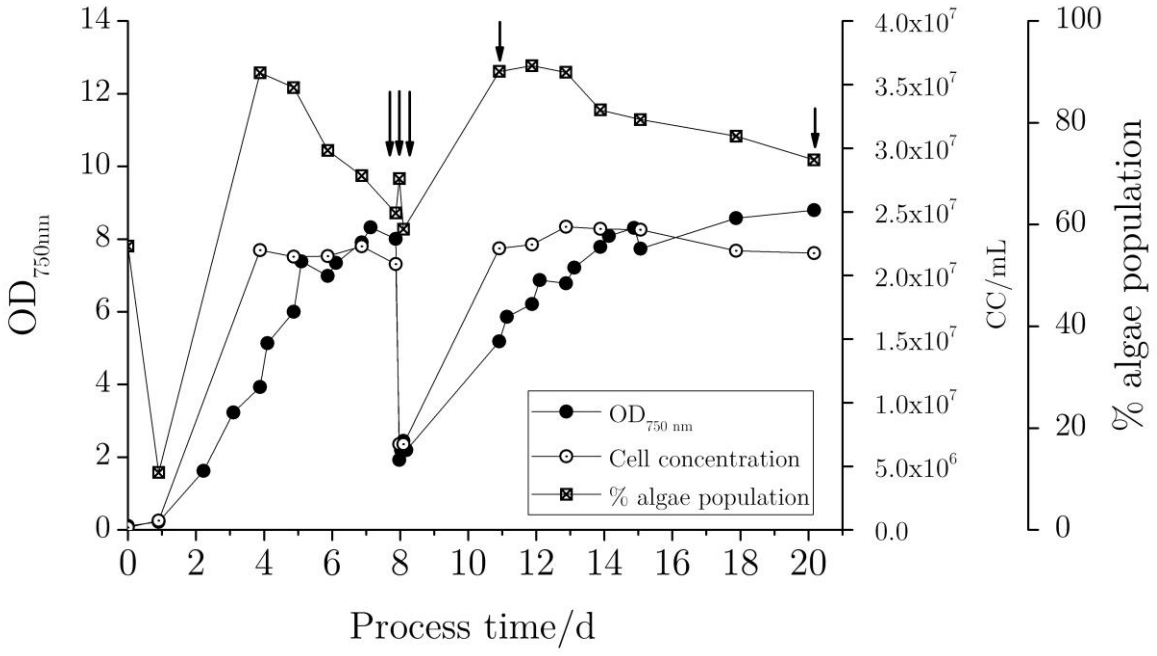

Figure 36: Shift of NaCl concentration for 3 h from 50 to 150 g/L and back during a cultivation of *D. salina KU11*. Arrows indicate sampling time of culture volume for metagenomic analysis. Cell concentration refers to the *D. salina KU11* cell count.

Figure 37 shows the growth development of *D. salina KU11* before and after the shift to pH 5. At the time of the shift, the culture reached an OD_{750nm} of 6.61, an algae population of 92.11 % of the total events and a cell concentration of $3.35 \cdot 10^7$ cells/mL. All of these values decreased after the implementation of the shift, whereas the decline reached a plateau after one day and at a CC of approximately $3 \cdot 10^7$ cells/mL and an algae population of 80 %. Only OD_{750nm} increased 6.79 after 6.8 d to 8.69 at the end of the cultivation.

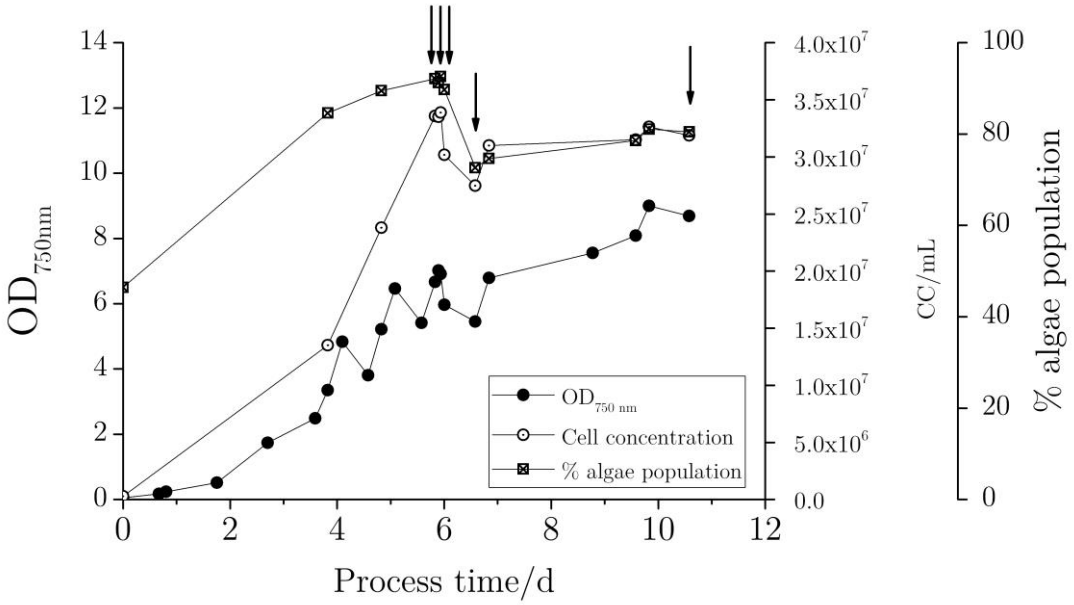

Figure 37: Shift pH for 3 h from 8 to 5 and back during a cultivation of *D. salina KU11*. Arrows indicate sampling time of culture volume for metagenomic analysis. Cell concentration refers to the *D. salina KU11* cell count.

3.3.2. Bacterial communities in photobioreactor experiments

The bacterial community was analyzed for both cultivations at five different time points during the cultivation (see arrows in Figure 36 and Figure 37). The increase to the higher salt concentration led to a similar trend in the change of the genera fractions (see Figure 38). Here, *Halamonas* increased in its overall abundance from 38.07 to 57.60 % and *Stappia* decreased from 56.01 to 36.92 %. At the end of the cultivation *Halamonas'*

abundance decreased below the pre-shift value. *Stappia*, however, increased to a maximum of 63.91 % at the end of the cultivation.

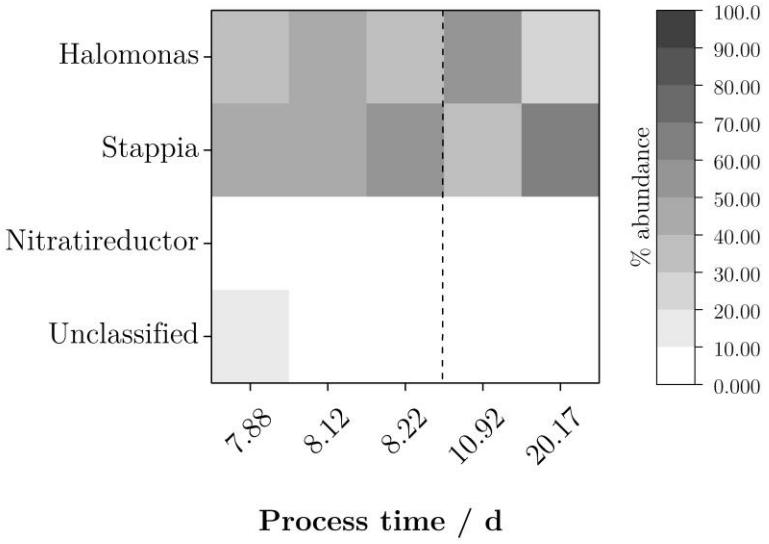

Figure 38: Relative abundances of reads assigned to bacterial microbiome on a genus-level in the salt-shift experiments for *D. salina KU11*. Reads that could not be assigned to specific genus were summarized as "unclassified". Taxonomic classification was based on sequence reads of hypervariable V3 and V4 region of the 16S rRNA regions. Dashed line marks time point of shift.

The relative abundances of the obtained reads in the pH-shift experiments is shown in Figure 39. It can be seen that three different genera could be detected in the course of the study. *Halomonas* and *Stappia* represent thereby with 65.28 – 72.05 % and 20.73 – 25.5 % the largest fractions before the shift. After the shift, the fraction of *Halomonas* increased to 81.93 % whereas *Stappia* decreased to 16.12 %. Both regained their initial abundance prior to the shift at the end of the cultivation.

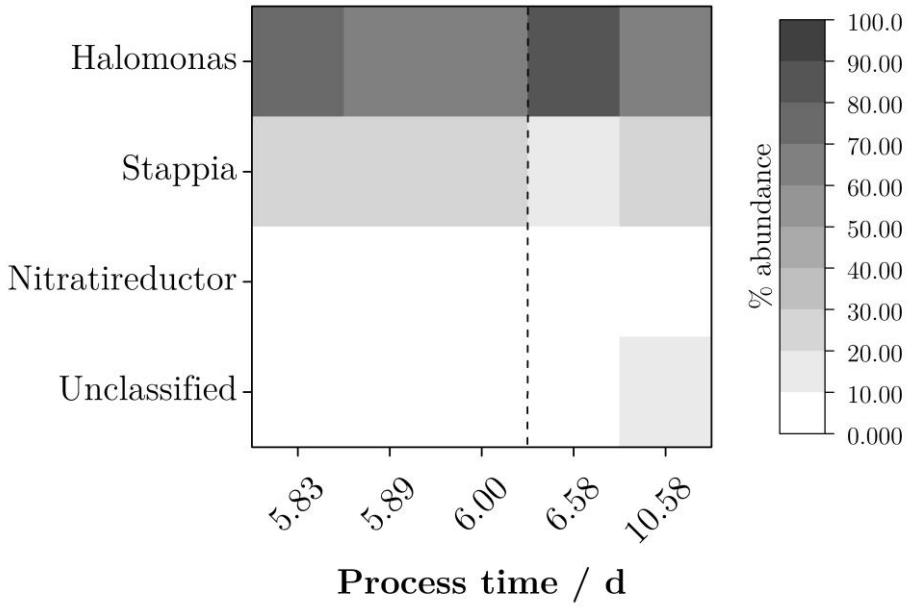

Figure 39: Relative abundances of reads assigned to bacterial microbiome on a genus-level in the pH-shift experiments for *D. salina KU11*. Reads that could not be assigned to specific genus were summarized as "unclassified". Taxonomic classification was based on sequence reads of hypervariable V3 and V4 region of the 16S rRNA regions. Dashed line marks time point of shift.

3.3.3. Salinity and pH shifts in open thin-layer cascade system

After proving the robustness of D. salina KU11 to harsh changes of the cultivation conditions, the open thin-layer cascade systems were inoculated with this strain. As the culture in the salt shift experiments recovered fully from the shifts, this biomass was used in order to inoculate both cascade systems. Then, the salt and pH shift were conducted in two parallel cultivations under the same set-up in two identical reactor systems. In the salt shift experiment the OD reached a maximum of 1.28 after 1.67 d and declined afterwards continuously until the end of the cultivation, reaching a plateau from day 9 of around 0.35 (see Figure 40). The CDW concentration showed strong fluctuations with only weak correlations to the OD values. The percentage of algae populations declined until the third day. After a slight increase to 77.13 % after 5.83 d it remained constant. A short decrease could be detected after shift, but the parameter regained a value of 28 % at the end of the cultivation. The analysis of cell concentrations by flow cytometry analysis showed a decrease in the total event concentration after day

3. From day 8 on, the cell concentration reached a plateau of approximately $5 \cdot 106$‘ events/mL. Only one day after the shift the event concentration decreased again but regained its initial value after one day. The population designated as D. salina KU11 was accompanied by a second population named “Pop. 2”, which reached its maximum

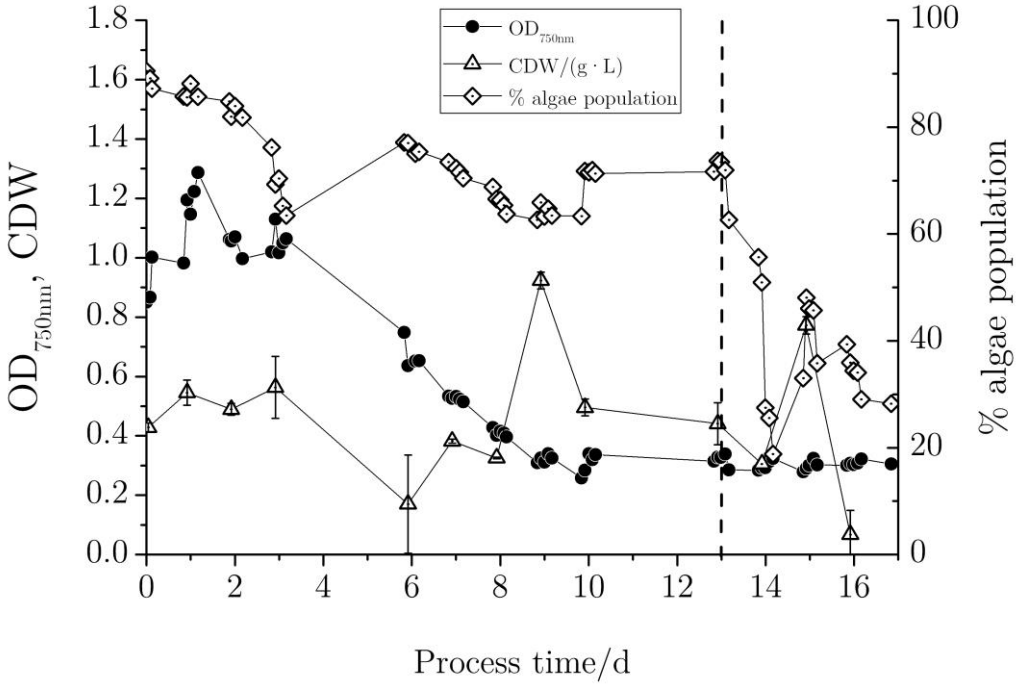

Figure 40: Development of growth parameter and population fraction of *D. salina KU11* population in salt shift cultivation for under simulated conditions of reference day. Dashed line marks the time point of shift. Error bars for OD values were omitted due to better visibility. Maximum RSD was 2 % from three OD measurements. Values for CDW concentration and algae population were calculated from two measurements.

fraction value of after 7 d (see Figure 41). In the pH shift experiments the OD reached a maximum of 1.61 also after 1.16 d (see Figure 42). Subsequently, the value of this parameter decreased and also beyond the time of the shift at day 13. The CDW concentration showed strong variations throughout the cultivation. The share of algae population showed only a slight variation until the shift, but decreased to 2.98 % after 13.84 d. Afterwards, this value increased to a value of 33.35 % at the final day. Concomitantly, the total event concentration decreased continuously from the third day until the end of the cultivation. Solely right after the shift experiment a short increase in the concentration could be detected. The designated *D. salina KU11* showed after the

shift a steep decline but regained in abundance until the end of the cultivation. The designated side population "Pop. 3" could gain its maximum share after 15 d. The emerging of the two side populations in the salt and pH shift experiments can be observed in Table 17 . Both plots at 14 d show an increase in unspecified events and a regain of the designated *D. salina KU11* population.

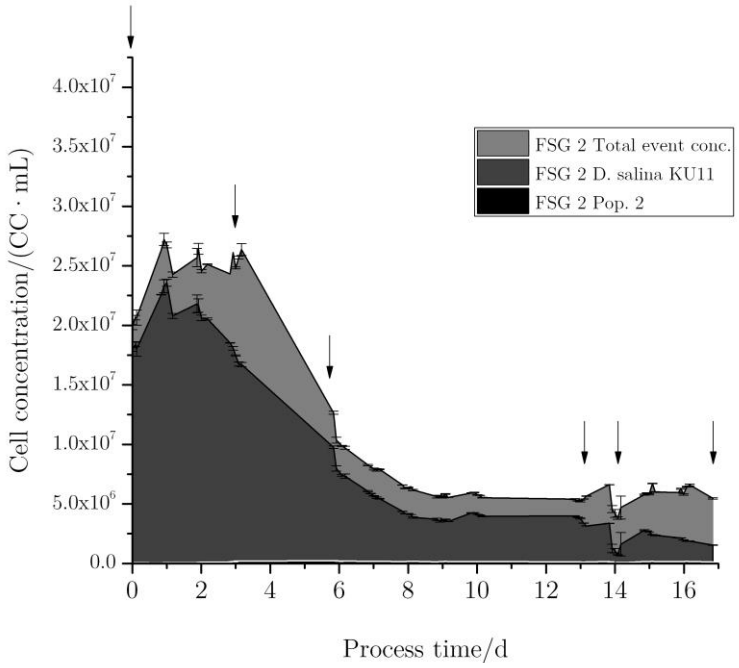

Figure 41: Development of the observed cell count concentrations of applied algae strain and side population in the course of the salt shift experiment. Arrows mark time points when samples were taken for flow cytometry (see Table 17).

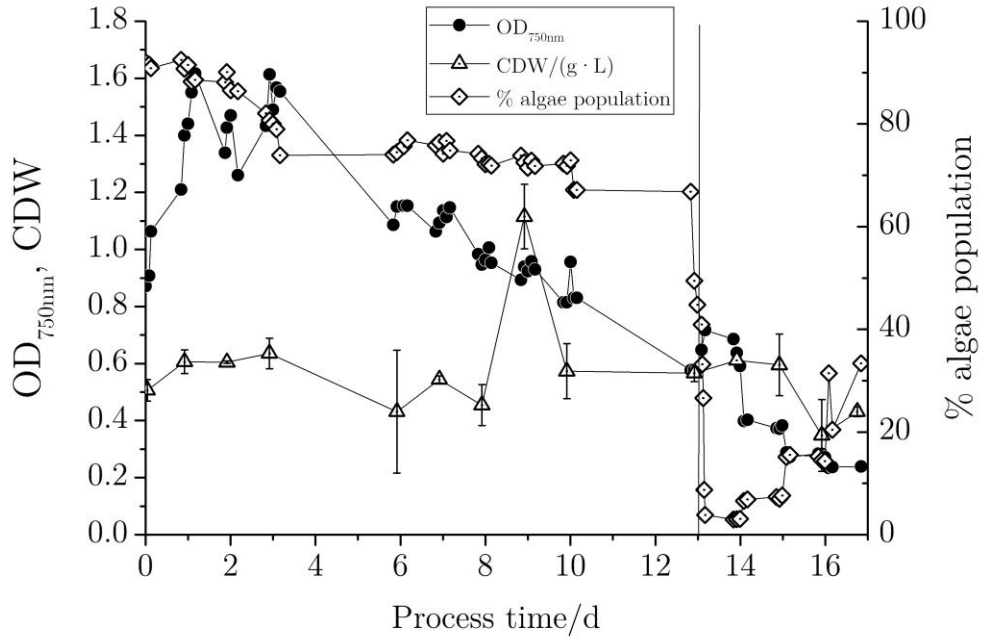

Figure 42: Development of growth parameter and population fraction of *D. salina KU11* in pH shift cultivation with simulated reference day. Dashed line marks the time point of shift. Error bars for OD values were omitted due to better visibility. Maximum RSD was 2.2 % from three measurements. Values for CDW concentration and algae population were calculated from two measurements.

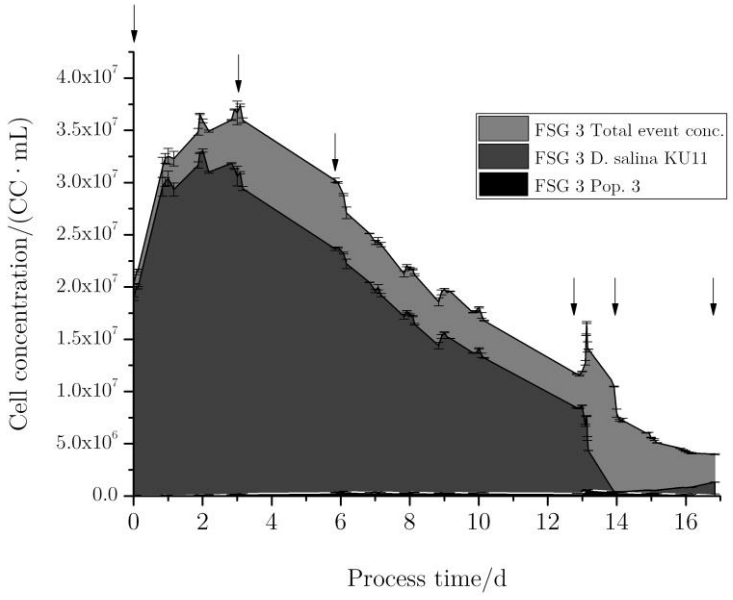

Figure 43: Development of the observed cell count concentrations of applied algae strain and side population in the course of the pH shift experiment. Arrows mark time points when samples were taken for flow cytometry (see Table 17).

Table 17: Flow cytometry plots of salt shift and pH shift experiments at selected time points during cultivation. For each sample 160,000 events were analyzed.

Process time	Salt shift	pH shift
0 d	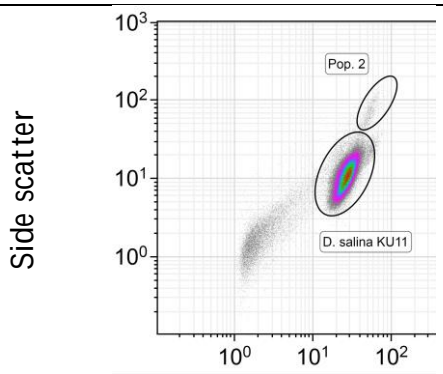	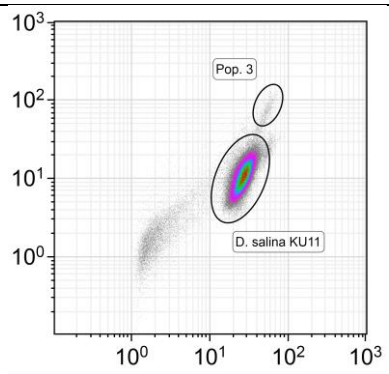
3.17 d	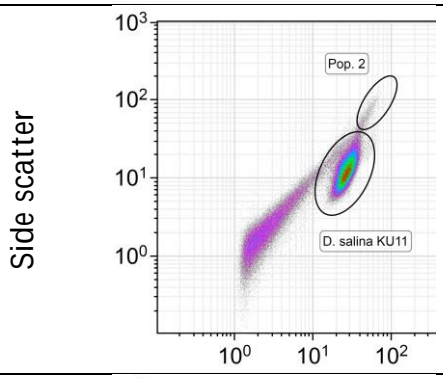	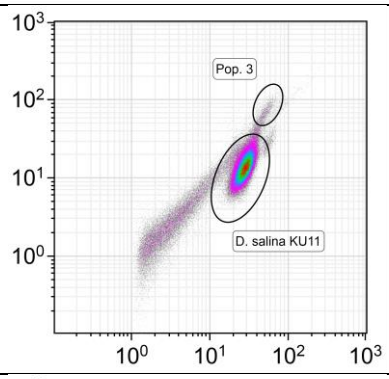
5.83 d	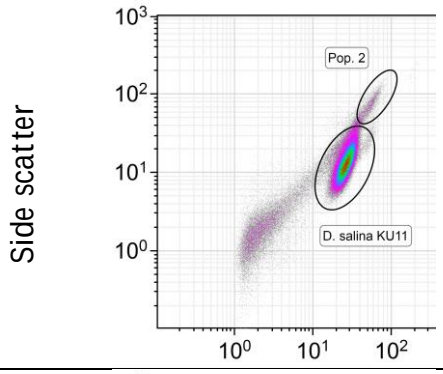	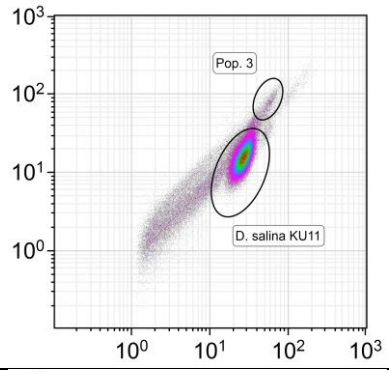
13 d	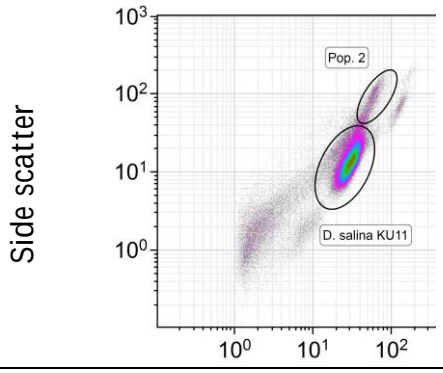	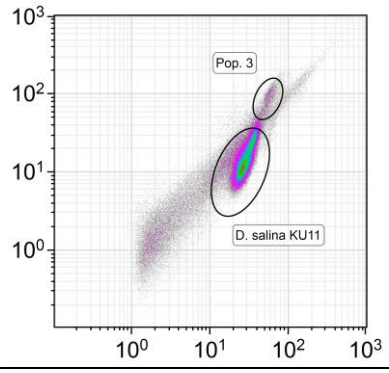

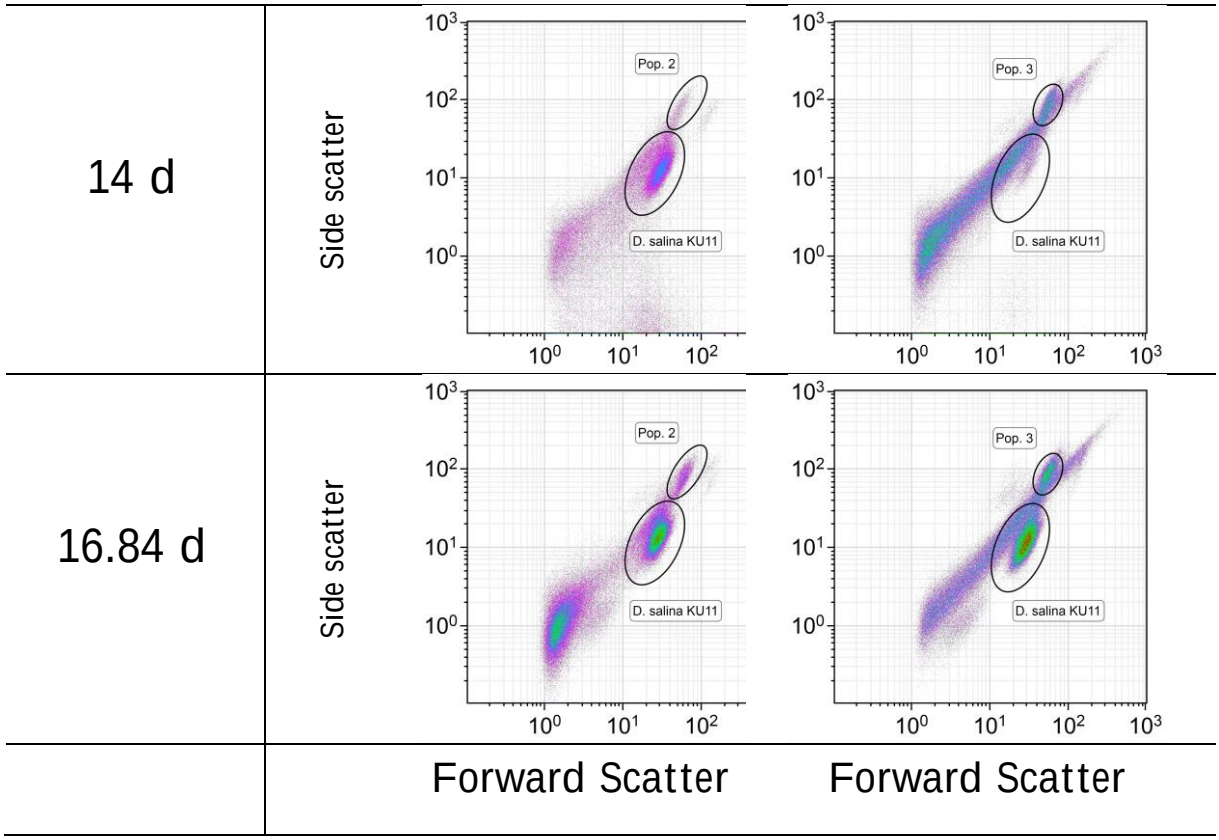

3.3.4. Bacterial communities in open thin-layer cascade system

Similar to the experiments in section 3.3.2, the bacterial community was analyzed in the open thin-layer cascade system by Next Generation Sequencing. Here, both shifts were conducted after 12.91 d of cultivation. The summarized analysis of the development of the different populations in the culture broth is shown in Figure 44. The most prominent groups detected were *Halomonas*, *Psychroflexus, Stappia* and *Salegentibacter*. Their fractions changed significantly after three days of cultivation, with *Stappia* reaching 55 % of all assigned reads and *Salegentibacter* vanishing from the culture. The fractions of *Halomonas* and *Psychroflexus* dropped to 7.6 and 9.3 %, respectively. At day nine and ten no DNA could be extracted from the sampled biomass and at day thirteen before the shift, only a large fraction of unclassified reads could be detected. After the shift, *Halomonas* and *Psychroflexus* represented the most dominant groups until the end of the cultivation.

Due to the usage of the same inoculum for both cultures and mixing between the two cascade systems, the initial fraction for the four most prominent groups *Halomonas*, *Psychroflexus, Stappia and Salegentibacter* were similar for both systems at the beginning of the cultivation (see Figure 45). *Halomonas* showed steady decrease in its fraction after two days until the shift at day 13. After the pH-shift it could shortly obtain a relative abundance of 62 % and remained then stable at around 27 % until the end of the cultivation. The *Psychroflexus* group decreased continuously after the first day and its

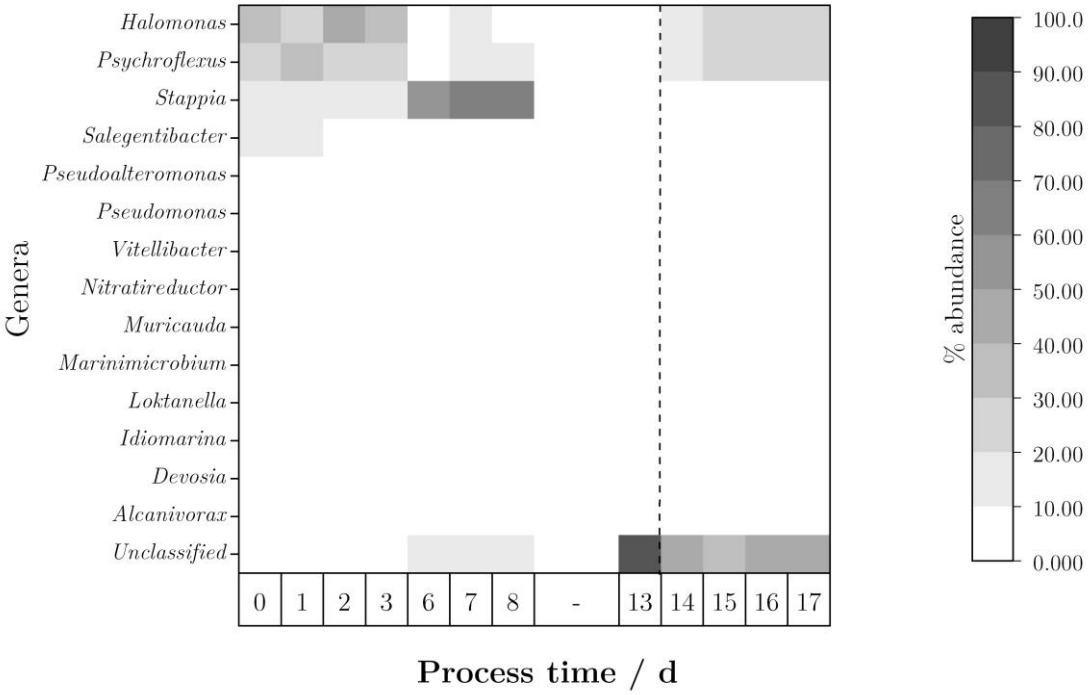

Figure 44: Relative abundances of reads assigned to bacterial microbiome on a genus-level in the salt-shift experiments of *D. salina KU11* in the cascade system. Reads that could not be assigned to specific genus were summarized as "unclassified". Taxonomic classification was based on sequence reads of hypervariable V3 and V4 region of the 16S rRNA regions. Dashed line marks time point of shift.

fraction stayed below 5 % of the assigned reads. *Salegentibacter* and *Stappia* did not show any changes in its fraction due to the pH-shift. Remarkably, at the end of the cultivation *Pseudoalteromonas* could reach a relative abundance of 28 %.

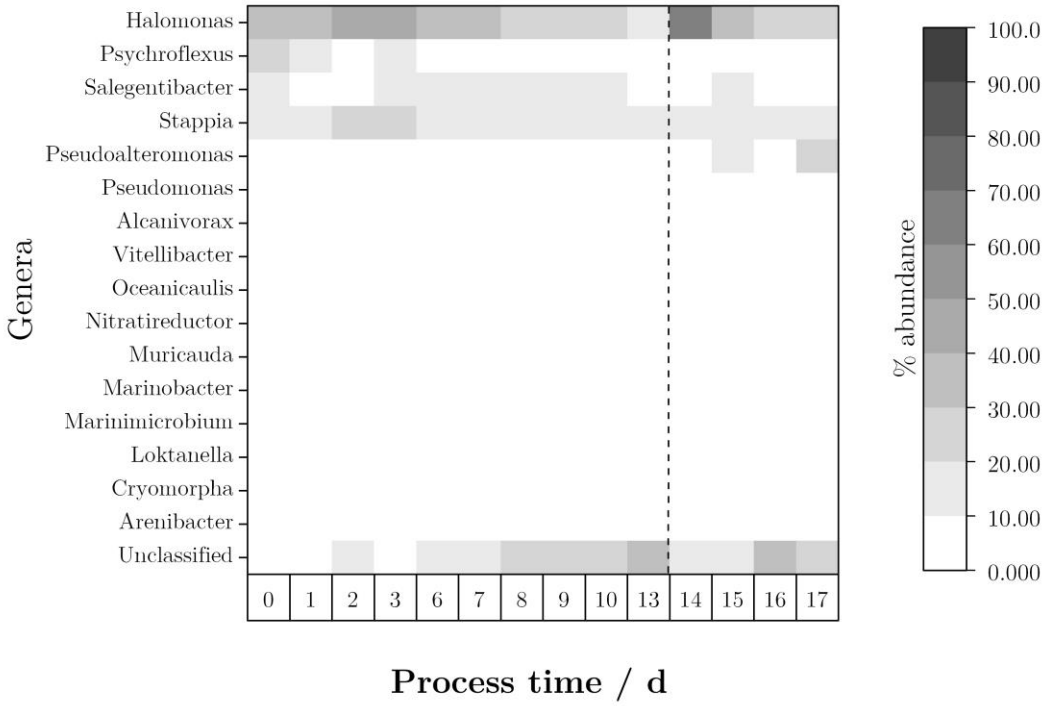

Figure 45: Relative abundances of reads assigned to bacterial microbiome on a genus-level in the pH-shift experiments for *D. salina KU11* in the cascade system. Reads that could not be assigned to specific genus were summarized as "unclassified". Taxonomic classification was based on sequence reads of hypervariable V3 and V4 region of the 16S rRNA regions. Dashed line marks time point of shift

3.3.5. Discussion

The salt shift in the PBRs proved to increase the algae population after a short decrease to a fraction higher than before the shift. This development, however, was only temporarily, as other populations grew faster than the algae and thus increased their fraction in the total community. Cell concentration and OD values increased right after the shift, which indicates that *D. salina KU11* can tolerate harsh salt shifts within few hours. Concomitantly with the decrease of the algae population, the *Halomonas* group decreased in its fraction. In contrast to that, *Stappia* increased its fraction in the cultivation before the shift. The shift favored the growth of *Halomonas* but at the end of the cultivation *Stappia* was the most abundant group. This shows that *Halomonas* is here related to the growth of *D. salina KU11*, whereas *Stappia* shows an opposing trend. It was already shown in the literature that representatives from *Halomonas* are often

associated with *D. salina* cultures in which they can lead to better growth under iron limiting conditions [214]. However, it also has been reported that *Halomonas* in co-cultivation with *D. salina* does not improve μ_{max} and biomass productivity over an axenic algae culture [215]. Furthermore, the effect of the *Stappia* population which contrasts in this study the algal growth, could not be confirmed by other authors. Park et. al e.g. found that *Stappia* had growth-promoting effect on a *Tetraselmis* species.

The shift to lower pH values led to a decrease in the algae population, potentially due to the death and lysis of already impaired cells. After the shift algae cell concentration and population fraction remained stable. As only the OD increases, a morphological change in the algal cells which results in a change of the attenuation coefficient could have driven this effect.
Regarding the bacterial population, also in this cultivation, the fraction of the *Halomonas* group could shortly be increased by the pH-shift and the *Stappia* fraction decreased. Approximately nine days after the shift the relations between those groups were re-established to the state prior to the shift. In case *Stappia* should indeed have a negative effect on algal growth, these shifts should be implemented after a shorter duration in order to maintain a constant, low *Stappia* population. However, this has to be balanced in relation to the growth of the algae population, which is also negatively affected.

The salt shift in the thin layer cascade system led to a decrease in the algae population with only small subsequent increase. The OD as an indirect measurement of the total cell concentration did not decrease due to the shift. A decreasing cell concentration with a constant OD could be explained by dead cells after the shift which are not detected anymore by the "algae population" gate during flow cytometry but still absorbs light at the applied wavelength. As the gate detects the algae cells by red fluorescence a change in fluorescence due to the harsh salt shift could also lead to this event. The steep decline in OD and total event concentration between day 3 and day 6 correlates with an increase

of the bacterial share of the *Stappia* group and a decrease of the *Halomonas* and *Psychroflexus* group. The potential explanation for this correlation aligns with the findings for the bacterial populations in the PBRs. Similar to the PBR experiments, the *Halomonas* group could be shortly increased in its relative abundance by the shift.

In the pH shift, the OD decreased continuously and the percentage of the algae population remained stable. Here, a decrease in contaminating populations is potentially the reason for this observation. After the shift, the algae population decreased significantly, showing an intensified effect compared to the PBR experiments. This is potentially related to the comparatively good growth in the PBRs compared to the thin-layer cascade system which maybe damaged the cells in the latter system stronger. However, the increase in the algae population was steeper compared to the salt shift, which shows the resilience of the strain and the applicability for further shift experiments. *Halomonas* was also in the pH shift experiments one of the major bacterial populations. Similar to the salt shift experiment, the *Halomonas* group gained a relative abundance after the shift.

3.3.6. Conclusion and outlook

In this part of this work a representative of the *Dunaliella* genus was subjected to shift experiments emulating process to purify contaminated open mass cultivations. In a laboratory set-up it could be shown that the strain is tolerant towards harsh, temporal shifts to a pH of 5 and a NaCl concentration of 150 g/L. The strain did not loose its viability and could – in the case of the salt shift – quickly regain its initial cell concentration and OD. Two main bacterial genera could be detected – *Halomonas* and *Stappia* – whose relative abundances were effected strongly by the shifts. Whereas the relative abundance of *Stappia* decreased after the salt shift and remained constant before and after the pH shift, the abundance of *Halomonas* increased after both shifts.

Based on these findings the experiments with the *Dunalialla* strain were repeated in open thin-layer cascade system under a realistic climate simulation in the AlgaeTec Centre. Here, for both cultivations no exponential growth could be obtained. After a short increase in OD after 3 d, the value for this parameter decreased continuously for both cultivations until the end of the experiment. However, after the implementation of the shifts after 13 d, the culture in the pH shift experiment could increase its relative abundance, showing the principal vitality of the cells. The culture within the pH shift experiments did not reconstitute its initial abundance. For both cultivations it could not be clarified what causes the constant decrease in OD and why the decline in cell concentration started after 3 d for both cultures. One smaller side population for each cultivation with a maximum relative abundance of 3.02 % in the salt shift experiment and 4.69 % in the pH shift experiment could be detected. However, no direct correlation to the decline could be established.

Also, by applying the shift, the relative abundance of the *Dunaliella* strain could not be increased above the value prior to the shift. This shows that the strain is potentially amenable to pond management strategies, however, further evaluation of the growth requirements and the bacterial communities have to be conducted. A possible approach could be the interaction with bacterial consortia from the *Halomonas* group. Interestingly, representatives of this system proved to be favorable for microalgae growth [214, 216]. Based on the findings in this study further pond management strategies can be evaluated in order to obtain a more consistent biomass yield from large scale cultivations.

List of figures

List of tables

Appendix

Appendix 1 Chemical composition and preparation of the applied media

Table 18: Chemical composition and preparation of the applied media in this work. PH was set before autoclaving. Marked components (*) were sterile filtered and added after autoclaving to the solution.

Compound	BG11	ASW	ASP-M	f/2	*Pico-chlorum* sp. medium	*Nanno-chloropsis salina* medium	Unit
Composition and concentration of nutrients							
Ammonium ferric citrate	0.006	---	---	---	---	---	g/L
$CaCl_2 \cdot 2\ H_2O$*	0.003	1.1	1.12	---	0.8	1.5	g/L
Citric Acid	0.006	---	---	---	---	---	g/L
$FeCl_3 \cdot 6\ H_2O$	---	---	0.00054	---	---	0.014	g/L
K_2HPO_4*	0.04	0.005	---	---	0.05	0.07	g/L
KCl	---	0.075	0.75	0.6	---	---	g/L
KNO_3	---	0.303	---	---	0.56	5.0	g/L
$MgCl_2 \cdot 7\ H_2O$	---	4.1	4.06	---	---	---	g/L
$MgSO_4 \cdot 7\ H_2O$	0.075	4.9	4.93	0.6	1.2	6.6	g/L
Na_2CO_3	0.02	---	---	---	---	---	g/L
$Na_2EDTA \cdot 2\ H_2O$	0.001	0.05	0.00074	---	---	0.021	g/L
$Na_2SiO_3 \cdot 9\ H_2O$	0.03	0.03	0.0568	0.03	---	---	g/L
NaH_2PO_4*	---	---	0.0138	0.005	---	---	g/L
$NaHCO_3$	---	---	---	---	---	---	g/L
$NaNO_3$	1.5	---	0.085	0.75	---	---	g/L
Tris Base	---	---	0.606	---	---	---	g/L
TrisHCl	---	0.156	---	---	---	---	g/L
Iron/EDTA-solution	---	---	---	1*	---	---	mL
Trace element solution	1*	1*	1*	1*	1*	1*	mL

Composition and concentration of trace element solution (1000-fold concentrated).							
$Co(NO_3)_2 \cdot 5\ H_2O$	0.0494	---	---	---	0.0007	---	g/L
$CoCl_2 \cdot 6\ H_2O$	---	---	0.071	0.01	0.0002	---	g/L
$CuCl_2 \cdot 2\ H_2O$	---	0.268	---	---	---	0.268	g/L
$CuSO_4 \cdot 5\ H_2O$	0.079	---	0.075	0.01	---	---	g/L
$FeCl_3 \cdot 6\ H_2O$	---	---	0.324	---	---	---	g/L
$FeSO_4 \cdot 7\ H_2O$	---	1.360	---	---	0.2	1.360	g/L
H_3BO_3	2.86	0.568	24.732	0.6	0.6	0.568	g/L
$MnCl_2 \cdot 2\ H_2O$	---	0.360	1.979	0.180	---	0.360	g/L
$MnCl_2 \cdot 4\ H_2O$	---	---	---	---	0.14	---	---
$MnSO_4 \cdot 4\ H_2O$	2.39	---	---	---	---	---	g/L
$Na_2EDTA \cdot 2\ H_2O$			14.026	---	3.0	---	g/L
$Na_2MoO_4 \cdot 2\ H_2O$	0.39	0.252	1.210	0.006	---	0.252	g/L
$ZnCl_2$	---	0.624	---	---	---	0.624	g/L
$ZnSO_4 \cdot 7\ H_2O$	0.222	---	10.064	0.222	0.033	---	g/L
Concentration of Iron/EDTA-solution							
$Na_2EDTA \cdot 2\ H_2O$	---	---	---	---	4.36	---	g/L
$FeCl_3 \cdot 6\ H_2O$	---	---	---	---	3.150	---	g/L

Appendix 2 Correlation coefficients for converting OD values to dry biomass concentration

Table 19: Correlation coefficients of OD values between used absorbance measurement devices obtained with *Picochlorum* sp.. The formula of a linear regression between OD values of the same sample in different devices or at different wavelengths is given. The light path correction between cuvettes in the Agilent Spectrophotometer (d_1= 10 mm) and the Perkin Elmer microplate reader wells (d_2=depending on the used volume) was taken into consideration. Values are transferred from one decive to another by applying the given factors, e.g. OD_{730nm} of Fluostar reader times 0.388 in order to get the Perkin Elmer OD_{730nm} values.

Device		Agilent	Perkin Elmer		FluoStar
		750 nm	*750 nm*	*730 nm*	*730nm*
Agilent	*750 nm*	X	$y = 0.474x \times \left(\frac{d_2}{d_1}\right)$	X	X
Perkin Elmer	*750 nm*	$y = 2.109x \times \left(\frac{d_1}{d_2}\right)$	X	$y = 1.003$	X
	730 nm	X	$y = 0.997$	X	$y = 2.579$
FluoStar	*730 nm*	X	X	$y = 0.388$	X

Table 20: Correlation coefficients for the calculation of CDW values from OD_{750nm} values.

Strain	CDW/OD coefficient
Picochlorum sp.	*0.2808*
Nannochloropsis salina	*0.197*
Dunaliella salina KU 11	*0.129*
IBA65	*0.397*
IBA75	*0.323*
IBA132	*0.255*

Appendix 3 Control sequence of light intensity, pH-regulation and temperature during cultivation in Labfors Photobioreactors

```
#0, Setup, 10
Light.sp=20
Temp.sp=25
pH.sp=8.00
Air_Flow.sp = 1.1

if (pH.v>pH.sp){CO2_Flow.sp=CO2_Flow.sp+2}
if(pH.v<=pH.sp){CO2_Flow.sp=0}

if SEQ_TIME >time(9:40) { SEQ = 2}

#1, Tag, 10
pH.sp=8.00
Air_Flow.sp = 1.1
Light.sp= -56.6984+157.5987*exp(-0.5*(((seq_time/60)-446.3572)/297.8790)^2)
Temp.sp=11.906+(0.0935*(seq_time/60))+((-1.6321*10^-
4)*(seq_time/60)^2)+((1.0975*10^-7)*(seq_time/60)^3)+((-3.0378*10^-
11)*(seq_time/60)^4)
if temp.sp<= 15 {temp.sp=15}
if (pH.v>pH.sp){CO2_Flow.sp=CO2_Flow.sp+2}
if(pH.v<=pH.sp){CO2_Flow.sp=0}

if SEQ_TIME >time(21:30) { SEQ = 2}

#2, Nacht, 30
pH.sp=8.00
Air_Flow.sp = 1.1
Light.sp=0
Temp.sp=15
if (pH.v>pH.sp){CO2_Flow.sp=CO2_Flow.sp+2}
if(pH.v<=pH.sp){CO2_Flow.sp=0}

if SEQ_TIME >time(2:30) { SEQ = 1}
```

Appendix 4 Sequencing results of isolated strains

>1D6

attagccatgcatgtctaagtataaactgcttatactgtgaaactgcgaatggctcattaaatcagttatagtttatttgatggt
acctttactcggataaccgtagtaattctagagctaatacgtgcgtaaatcccgacttctggaagggacgtatttattagataa
aaggccagccgggcttgcccgactcttggcgaatcatgataacttcacgaatcgcacggctttatgctggcgatgtttcattca
aatttctgccctatcaactttcgatggtaggatagaggcctaccatggtggtaacgggtgacggaggattagggttcgattccg
gagagggagcctgagaaacggctaccacatccaaggaaggcagcaggcgcgcaaattacccaatcccaacacggggaggta
gtgacaataaataacaataccgggcatttttgtctggtaattggaatgagtacaatctaaatcccttaacgagtatccattgga
gggcaagtctggtgccagcagccgcggtaattccagctccaatagcgtatatttaagttgttgcagttaaaaagctcgtagttg
gatttcgggtggggttgtagcggtcagcctttggttagtactgctatggcctacctttctgccgggggacgagctcctggggctt
aactgtcccgggactcggaatcggcgaggt

>3B2

agccatgcatgtctaagtataaactgcttatactgtgaaactgcgaatggctcattaaatcagttatagtttatttgatggtacc
tttactcggataaccgtagtaattctagagctaatacgtgcgtaaatcccgacttctggaagggacgtatttattagataaaag
gccagccgggcttgcccgactcttggcgaatcatgataacttcacgaatcgcacggcttcggccggcgatgtttcattcaaatt
tctgccctatcaactttcgatggtaggatagaggcctaccatggtggtaacgggtgacggaggattagggttcgattccggag
agggagcctgagaaacggctaccacatccaaggaaggcagcaggcgcgcaaattacccaatcccaacacggggaggtagtg
acaataaataacaataccgggcatttttgtctggtaattggaatgagtacaatctaaatcccttaacgagtatccattggaggg
caagtctggtgccagcagccgcggtaattccagctccaatagcgtatatttaagttgttgcagttaaaaagctcgtagttggat
ttcgggtgggttgtagcggtcagcctttggttagtactgctacggcctacctttctgccggggacgagctcctgggcttaactgt
ctgggactcggaatcggcgaggttactttgagtaaattaaagtgttcaaagcaagcatacgctctgaatacattagcatgaaa
tag

>17A1

Aggattagggttcgattccggagagggagcctgagaaacggctaccacatccaaggaaggcagcaggcgcgcaaattaccc
aatcccaacacggggaggtagtgacaataaataacaataccgggcatttttgtctggtaattggaatgagtacaatctaaatc

ccttaacgagtatccattggagggcaagtctggtgccagcagccgcggtaattccagctccaatagcgtatatttaagttgttg
cagttaaaaagctcgtagttggatttcgggtgggttgtagcggtcagcctttggttagtactgctacggcctacctttctgccgg
ggacgagctcctgggcttaactgtccgggactcggaatcggcgaggttactttgagtaaattagagtgttcaaagcaagccta
cgctctgaatacattagcatggaataacacgataggactctggcttatcttgttggtctgtaagaccggagtaatgattaaaag
ga

Appendix 5 Code of R-module

```
#Wells: name of unique wells
#twell:number of unique wells

######Loading Packages and Data######
#Packages
require(lattice)
require(dplyr)
require(growthrates)
require(tidyr)
require(rlang)
require(deSolve)
#Input data:
R2Des<-0.97        #Desirable R2
min_steps_all<-4    #Minimum h

#Load data from AFK format

AFK <-
read.csv2("G:/Documents/Promotion/Johannes/Promotion/Projekte/Algenflugkraft/M
ikrotiterplatte/Druckplatte/Laborrobotorkultivierung/170317_LabRobot06_Homogenit
```

```
ätstest/LB06_Auswertung_P1_R.csv", header=FALSE,na.strings=c("","NA"), dec=",",
blank.lines.skip = TRUE)

#####From AFK format to easylinear format#####
str(AFKT)
AFKT<-AFK #copy to new file
colnames(AFKT)<-AFK[1,]#names from first row
colnames(AFKT)
AFKT<-AFKT[-1,]#delete first row

AFKTG<-gather(Time,OD,3:(ncol(AFKT)),data = AFKT) #gather columns to long
format

afkdf<-cbind(c(1:nrow(AFKTG)),AFKTG)#add first column with indexcolumn
afkdf
colnames(afkdf)<-c("X","plate","well","time","value")#change names
colnames(afkdf)

#SUBSETTING
afkdf<-afkdf[afkdf$plate=="Platte01",]
afkdf<-afkdf[order(afkdf$well, afkdf$X,afkdf$time),]#Order Data
afkdf$X<-c(1:nrow(afkdf))#Reorder index
afkdf$time<-as.numeric(afkdf$time)#change time datatype to numeric
str(afkdf)


######Testing of data######
```

```
#Testing and Variables
afkdf
Well_no3<-table(afkdf$well)
Well_no3 # Check: how many measurement points for each well?
tot_steps<-max(Well_no3)#total steps as maximum
tot_steps
Wells<-as.data.frame(unique(afkdf$well)) #Names of unique wells
Wells
twell<-nrow(as.data.frame(unique(afkdf$well)))#number of unique wells
cat("Total of",twell,"wells with",tot_steps,"measurements each")
twell

#####Calculation of growth curves#####

#Determining minimum + maximum number of data points
#min steps is defined in line 26
max_steps_all<-(tot_steps) #max steps as total-1
max_steps_all
min_steps_all
T_all<-min_steps_all:max_steps_all #scope of testing: min to max number of data points
T_all
#Introduction of variables
df1<-as.data.frame(Wells)
df2<-as.data.frame(Wells)
afkdf
#Easylinear Loop
for (i in T_all) {
```

```
  S1<-as.data.frame(coef(all_easylinear(afkdf, value~time|plate + well, h=i, quota =
1)))
  S2<-S1$mumax
  print(S2)
  R2<-rsquared(all_easylinear(value~time|plate + well,afkdf, h=i, quota = 1))
  print(R2)
  df1[[(i-min_steps_all+1)]]<-as.numeric(S2)
  df2[[(i-min_steps_all+1)]]<-R2
}

df1
df2

colnames(df1)<-c((T_all))#df1: SLOPE. Change column name to number of
measurement points
colnames(df2)<-c(T_all)#DF2: R2. Change column name to number of measurement
points
df1
"testing easylinear-loop output"
if (ncol(df2)==ncol(df1)) {"Number of test points points ok"}else {"Number of test
points NOT ok"}
if (nrow(df2)==nrow(df1)) {"Number of wells ok"}else {"Number of wells NOT ok"}
df1
df2
#####Extraction of growth data#####

#df11-table of growth rates
#df22-table of rsq values
```

```
#dfh-table with numbers of steps
#dfindex-vector with index of correct value within each column (with rsq over RsqDes and Maximum h)
df11
df22
#Create table with h values
dfh<-as.data.frame(min_steps_all:max_steps_all)
for (i in 1:twell) {dfh[i]<-as.numeric(min_steps_all:max_steps_all)
i<-i+1}
colnames(dfh)[1]<-"V1" #change first (empty) column name

"testing h value table"
if (ncol(dfh)==twell) {"Number of test points points ok"}else {"Number of test points NOT ok"}
if (nrow(dfh)==1+max_steps_all-min_steps_all) {"Number of test points points ok"}else { "Number of test points NOT ok"}

#Transposing Data frames:
df11<-t(df1);colnames(df11)<-1:ncol(df11)
df22<-t(df2);colnames(df22)<-1:ncol(df11)
df11
df22
dfindex
#Replace all values under RsqDes with NA
dfSig2<-as.data.frame(df22)
dfSig2[dfSig2<R2Des]<-NA
dfSig2
#Creating index of values with highest index (numbers of MP)
```

```
dfindex<-suppressWarnings(apply(dfSig2, 2, function(x) max(which(!is.na(x)))))
dfindex[!is.finite(dfindex)] <- 1 #If all values under 0,97, then take the first value in vector

#Loop for extraction of data

#Extraction of r2 data based on index
dfrf<-NULL;i<-0;indcount<-0;dfsf<-NULL;dfhf<-NULL # introduction of variables
for (i in 1:twell) {
  va<-df11[dfindex[i],i]
  vb<-df22[dfindex[i],i]
  vc<-dfh[dfindex[i],i]
  dfsf[i]<-as.numeric(va)
  dfrf[i]<-as.numeric(vb)
  dfhf[i]<-as.numeric(vc)
  #indcount[i]<-dfindex[i]
}

#final table
dfF<-cbind(Wells,dfsf,dfrf,dfhf)
colnames(dfF)<-c("Well","Slope","R2","#Points")
dfF

#ENDE
```

References

[1] P. Spolaore, C. Joannis-Cassan, E. Duran, and A. Isambert, "Commercial applications of microalgae," *Journal of bioscience and bioengineering*, vol. 101, no. 2, pp. 87–96, 2006, doi: 10.1263/jbb.101.87.

[2] M. D. Guiry, "How many species of algae are there?," *Journal of phycology*, vol. 48, no. 5, pp. 1057–1063, 2012, doi: 10.1111/j.1529-8817.2012.01222.x.

[3] L. T. Carney and T. W. Lane, "Parasites in algae mass culture," *Frontiers in microbiology*, vol. 5, p. 278, 2014, doi: 10.3389/fmicb.2014.00278.

[4] United Nations, Department of Economic and Social Affairs, Population Division, "World Population Prospects: The 2017 Revision," New York, 2017,

[5] H.-W. Yen *et al.,* "Microalgae-based biorefinery--from biofuels to natural products," *Bioresource Technology*, vol. 135, pp. 166–174, 2013, doi: 10.1016/j.biortech.2012.10.099.

[6] Y. Chisti, "Biodiesel from microalgae," *Biotechnology advances*, vol. 25, no. 3, pp. 294–306, 2007, doi: 10.1016/j.biotechadv.2007.02.001.

[7] H. C. Bold and M. J. Wynne, *Introduction to the algae: Structure and reproduction,* 2nd ed. Englewood Cliffs, NJ: Prentice-Hall, 1985.

[8] P. J. Keeling, "Diversity and evolutionary history of plastids and their hosts," *American Journal of Botany*, vol. 91, no. 10, pp. 1481–1493, 2004, doi: 10.3732/ajb.91.10.1481.

[9] H. Kawai, T. Motomura, and K. Okuda, "Isolation and purification techniques for macroalgae," *Algal culturing techniques. Academic Press, London*, pp. 133–143, 2005, doi: 10.1016/B978-012088426-1/50010-X.

[10] P. J. Keeling, "The endosymbiotic origin, diversification and fate of plastids," *Philosophical transactions of the Royal Society of London. Series B, Biological sciences*, vol. 365, no. 1541, pp. 729–748, 2010, doi: 10.1098/rstb.2009.0103.

[11] R. A. Andersen, "Diversity of eukaryotic algae," *Biodivers Conserv*, vol. 1, no. 4, pp. 267–292, 1992, doi: 10.1007/BF00693765.

[12] T. A. Norton, M. Melkonian, and R. A. Andersen, "Algal biodiversity," *Phycologia*, vol. 35, no. 4, pp. 308–326, 1996, doi: 10.2216/i0031-8884-35-4-308.1.

[13] T. Hodkinson, Ed., *Reconstructing the Tree of Life*: CRC Press, 2006.

[14] P. G. Falkowski and J. A. Raven, *Aquatic Photosynthesis: (Second Edition),* 2nd ed. Princeton: Princeton University Press, 2013.

[15] A.H. Knoll and P.G. Falkowski, Eds., *Evolution of primary producers in the sea*. Amsterdam, Boston: Elsevier Academic Press, 2007.

[16] P. G. Falkowski, "The role of phytoplankton photosynthesis in global biogeochemical cycles," *Photosynth Res*, vol. 39, no. 3, pp. 235–258, 1994, doi: 10.1007/BF00014586.

[17] D. Remias, H. Wastian, C. Lütz, and T. Leya, "Insights into the biology and phylogeny of Chloromonas polyptera (Chlorophyta), an alga causing orange snow

in Maritime Antarctica," *Antarctic Science*, vol. 25, no. 05, pp. 648–656, 2013, doi: 10.1017/S0954102013000060.

[18] W. F. Vincent, D. R. Mueller, and S. Bonilla, "Ecosystems on ice: The microbial ecology of Markham Ice Shelf in the high Arctic," *Cryobiology*, vol. 48, no. 2, pp. 103–112, 2004, doi: 10.1016/j.cryobiol.2004.01.006.

[19] T. D. Brock, "Life at High Temperatures," *Science (New York, N.Y.)*, vol. 158, no. 3804, pp. 1012–1019, 1967, doi: 10.1126/science.158.3804.1012.

[20] I. Nancucheo and D. Barrie Johnson, "Acidophilic algae isolated from mine-impacted environments and their roles in sustaining heterotrophic acidophiles," *Frontiers in microbiology*, vol. 3, p. 325, 2012, doi: 10.3389/fmicb.2012.00325.

[21] J. Seckbach, "Survey of Algae in Extreme Environments," in *Cellular Origin, Life in Extreme Habitats and Astrobiology, The Algae World*, D. Sahoo and J. Seckbach, Eds., Dordrecht: Springer Netherlands, 2015, pp. 307–315,

[22] Z. Chi *et al.,* "Bicarbonate-based Integrated Carbon Capture and Algae Production System with alkalihalophilic cyanobacterium," *Bioresource Technology*, vol. 133, pp. 513–521, 2013, doi: 10.1016/j.biortech.2013.01.150.

[23] N. B. Costa, M. A. Kolman, and A. Giani, "Cyanobacteria diversity in alkaline saline lakes in the Brazilian Pantanal wetland: A polyphasic approach," *Journal of Plankton Research*, 2016, doi: 10.1093/plankt/fbw066.

[24] M. A. Borowitzka, L. J. Borowitzka, and D. Kessly, "Effects of salinity increase on carotenoid accumulation in the green alga Dunaliella salina," *J Appl Phycol*, vol. 2, no. 2, pp. 111–119, 1990, doi: 10.1007/BF00023372.

[25] A. Ben-Amotz and M. Avron, "The Role of Glycerol in the Osmotic Regulation of the Halophilic Alga Dunaliella parva," *Plant physiology*, vol. 51, no. 5, pp. 875–878, 1973, doi: 10.1104/pp.51.5.875.

[26] Y. Liang, N. Sarkany, and Y. Cui, "Biomass and lipid productivities of Chlorella vulgaris under autotrophic, heterotrophic and mixotrophic growth conditions," *Biotechnol Lett*, vol. 31, no. 7, pp. 1043–1049, 2009, doi: 10.1007/s10529-009-9975-7.

[27] E. Mohammad Basri and W. O. Wan Maznah, "Differential growth and biochemical composition of photoautotrophic and heterotrophic Isochrysis maritima: Evaluation for use as aquaculture feed," *J Appl Phycol*, vol. 29, no. 3, pp. 1159–1170, 2017, doi: 10.1007/s10811-017-1054-1.

[28] D. Morales-Sánchez, O. A. Martinez-Rodriguez, J. Kyndt, and A. Martinez, "Heterotrophic growth of microalgae: Metabolic aspects," *World J Microbiol Biotechnol*, vol. 31, no. 1, pp. 1–9, 2015, doi: 10.1007/s11274-014-1773-2.

[29] L. A. Zaslavskaia *et al.,* "Trophic conversion of an obligate photoautotrophic organism through metabolic engineering," *Science (New York, N.Y.)*, vol. 292, no. 5524, pp. 2073–2075, 2001, doi: 10.1126/science.160015.

[30] J. C. Ogbonna, H. Masui, and H. Tanaka, "Sequential heterotrophic/autotrophic cultivation – An efficient method of producing Chlorella biomass for health food

and animal feed," *J Appl Phycol*, vol. 9, no. 4, pp. 359–366, 1997, doi: 10.1023/A:1007981930676.

[31] C. Posten and C. Walter, *Microalgal Biotechnology: Potential and Production*: De Gruyter, 2013.

[32] K. J. McCree, "The measurement of photosynthetically active radiation," *Solar Energy*, vol. 15, no. 1, pp. 83–87, 1973, doi: 10.1016/0038-092X(73)90010-8.

[33] M. R. Tredici, "Photobiology of microalgae mass cultures: Understanding the tools for the next green revolution," *Biofuels*, vol. 1, no. 1, pp. 143–162, 2010, doi: 10.4155/bfs.09.10.

[34] R. J. Ritchie, "Modelling photosynthetic photon flux density and maximum potential gross photosynthesis," *Photosynthetica*, vol. 48, no. 4, pp. 596–609, 2010, doi: 10.1007/s11099-010-0077-5.

[35] C. Buschmann and K. Grumbach, *Physiologie der Photosynthese*. Berlin, Heidelberg: Springer, 1985.

[36] A. Chenu and G. D. Scholes, "Coherence in energy transfer and photosynthesis," *Annual review of physical chemistry*, vol. 66, pp. 69–96, 2015, doi: 10.1146/annurev-physchem-040214-121713.

[37] J. M. Berg, J. L. Tymoczko, L. Stryer, and G. J. Gatto, *Biochemie,* 7th ed. Berlin, Heidelberg: Springer Spektrum, 2014.

[38] J. Barber, "P680: What is it and where is it?," *Bioelectrochemistry*, vol. 55, no. 1-2, pp. 135–138, 2002, doi: 10.1016/S1567-5394(01)00141-4.

[39] G. Raszewski, B. A. Diner, E. Schlodder, and T. Renger, "Spectroscopic properties of reaction center pigments in photosystem II core complexes: Revision of the multimer model," *Biophysical journal*, vol. 95, no. 1, pp. 105–119, 2008, doi: 10.1529/biophysj.107.123935.

[40] A. Richmond and Q. Hu, Eds., *Handbook of microalgal culture: Applied phycology and biotechnology,* 2nd ed. Chichester, Hoboken, NJ: Wiley-Blackwell; Wiley, 2013.

[41] L. H. Skibsted, "Carotenoids in antioxidant networks. Colorants or radical scavengers," *Journal of agricultural and food chemistry*, vol. 60, no. 10, pp. 2409–2417, 2012, doi: 10.1021/jf2051416.

[42] M. Nymark *et al.,* "Molecular and photosynthetic responses to prolonged darkness and subsequent acclimation to re-illumination in the diatom Phaeodactylum tricornutum," *PLoS ONE*, vol. 8, no. 3, pp. e58722, 2013, doi: 10.1371/journal.pone.0058722.

[43] M. Mitra, H. Kirst, D. Dewez, and A. Melis, "Modulation of the light-harvesting chlorophyll antenna size in Chlamydomonas reinhardtii by TLA1 gene over-expression and RNA interference," *Philosophical transactions of the Royal Society of London. Series B, Biological sciences*, vol. 367, no. 1608, pp. 3430–3443, 2012, doi: 10.1098/rstb.2012.0229.

[44] B. KOK, B. Forbrush, and M. McGLOIN, "Cooperation of charges in photosynthetic O2 evolution–I. A linear four step mechanism," *Photochem*

Photobiol, vol. 11, no. 6, pp. 457–475, 1970, doi: 10.1111/j.1751-1097.1970.tb06017.x.

[45] H. W. Heldt and B. Piechulla, *Pflanzenbiochemie,* 5th ed. Berlin: Springer Spektrum, 2015.

[46] I. A. Guschina and J. L. Harwood, "Algal Lipids and Their Metabolism," in *Algae for Biofuels and Energy*, M. A. Borowitzka and N. R. Moheimani, Eds., Dordrecht: Springer Netherlands, 2013, pp. 17–36,

[47] Q. Hu *et al.,* "Microalgal triacylglycerols as feedstocks for biofuel production: Perspectives and advances," *The Plant journal : for cell and molecular biology*, vol. 54, no. 4, pp. 621–639, 2008, doi: 10.1111/j.1365-313X.2008.03492.x.

[48] J. Ohlrogge and J. Browse, "Lipid biosynthesis," *The Plant Cell*, vol. 7, no. 7, pp. 957–970, 1995, doi: 10.1105/tpc.7.7.957.

[49] B. Liu and C. Benning, "Lipid metabolism in microalgae distinguishes itself," *Current opinion in biotechnology*, vol. 24, no. 2, pp. 300–309, 2013, doi: 10.1016/j.copbio.2012.08.008.

[50] W. R. Riekhof, B. B. Sears, and C. Benning, "Annotation of genes involved in glycerolipid biosynthesis in Chlamydomonas reinhardtii: Discovery of the betaine lipid synthase BTA1Cr," *Eukaryotic cell*, vol. 4, no. 2, pp. 242–252, 2005, doi: 10.1128/EC.4.2.242-252.2005.

[51] K. M. Koo *et al.,* "The Mechanism of Starch Over-Accumulation in Chlamydomonas reinhardtii High-Starch Mutants Identified by Comparative Transcriptome Analysis," *Frontiers in microbiology*, vol. 8, p. 858, 2017, doi: 10.3389/fmicb.2017.00858.

[52] S. Bellou *et al.,* "Microalgal lipids biochemistry and biotechnological perspectives," *Biotechnology advances*, vol. 32, no. 8, pp. 1476–1493, 2014, doi: 10.1016/j.biotechadv.2014.10.003.

[53] R. Radakovits, R. E. Jinkerson, A. Darzins, and M. C. Posewitz, "Genetic engineering of algae for enhanced biofuel production," *Eukaryotic cell*, vol. 9, no. 4, pp. 486–501, 2010, doi: 10.1128/EC.00364-09.

[54] H. Goold, F. Beisson, G. Peltier, and Y. Li-Beisson, "Microalgal lipid droplets: Composition, diversity, biogenesis and functions," *Plant Cell Reports*, vol. 34, no. 4, pp. 545–555, 2015, doi: 10.1007/s00299-014-1711-7.

[55] D. Zweytick, K. Athenstaedt, and G. Daum, "Intracellular lipid particles of eukaryotic cells," *Biochimica et Biophysica Acta (BBA) - Reviews on Biomembranes*, vol. 1469, no. 2, pp. 101–120, 2000, doi: 10.1016/S0005-2736(00)00294-7.

[56] E. M. Fakhry and D. M. El Maghraby, "Lipid accumulation in response to nitrogen limitation and variation of temperature in Nannochloropsis salina," *Botanical studies*, vol. 56, no. 1, p. 6, 2015, doi: 10.1186/s40529-015-0085-7.

[57] G. Breuer, P. P. Lamers, D. E. Martens, R. B. Draaisma, and R. H. Wijffels, "The impact of nitrogen starvation on the dynamics of triacylglycerol

accumulation in nine microalgae strains," *Bioresource Technology*, vol. 124, pp. 217–226, 2012, doi: 10.1016/j.biortech.2012.08.003.

[58] Y. X. Li, F. J. Zhao, and D. D. Yu, "Effect of nitrogen limitation on cell growth, lipid accumulation and gene expression in Chlorella sorokiniana," *Brazilian Archives of Biology and Technology*, vol. 58, pp. 462–467, 2015, doi: 10.1590/S1516-8913201500391.

[59] P. G. Roessler, "Changes in the activities of various lipid and carbohydrate biosynthetic enzymes in the diatom Cyclotella cryptica in response to silicon deficiency," *Archives of Biochemistry and Biophysics*, vol. 267, no. 2, pp. 521–528, 1988, doi: 10.1016/0003-9861(88)90059-8.

[60] M. Hildebrand, A. K. Davis, S. R. Smith, J. C. Traller, and R. Abbriano, "The place of diatoms in the biofuels industry," *Biofuels*, vol. 3, no. 2, pp. 221–240, 2014, doi: 10.4155/BFS.11.157.

[61] K. I. Reitan, J. R. Rainuzzo, and Y. Olsen, "Effect of nutrient limitation on fatty acid and lipid content of marine microalgae," *J. Phycol.*, vol. 30, no. 6, pp. 972–979, 1994, doi: 10.1111/j.0022-3646.1994.00972.x.

[62] I. Khozin-Goldberg and Z. Cohen, "The effect of phosphate starvation on the lipid and fatty acid composition of the fresh water eustigmatophyte Monodus subterraneus," *Phytochemistry*, vol. 67, no. 7, pp. 696–701, 2006, doi: 10.1016/j.phytochem.2006.01.010.

[63] M. Takagi, Karseno, and T. Yoshida, "Effect of salt concentration on intracellular accumulation of lipids and triacylglyceride in marine microalgae Dunaliella cells," *Journal of bioscience and bioengineering*, vol. 101, no. 3, pp. 223–226, 2006, doi: 10.1263/jbb.101.223.

[64] C. Yeesang and B. Cheirsilp, "Effect of nitrogen, salt, and iron content in the growth medium and light intensity on lipid production by microalgae isolated from freshwater sources in Thailand," *Bioresource Technology*, vol. 102, no. 3, pp. 3034–3040, 2011, doi: 10.1016/j.biortech.2010.10.013.

[65] A. K. Franz, M. A. Danielewicz, D. M. Wong, L. A. Anderson, and J. R. Boothe, "Phenotypic screening with oleaginous microalgae reveals modulators of lipid productivity," *ACS chemical biology*, vol. 8, no. 5, pp. 1053–1062, 2013, doi: 10.1021/cb300573r.

[66] S. Aaronson, "Effect of incubation temperature on the macromolecular and lipid content of the phytoflagellate *Ochromonas danica*," *J. Phycol.*, vol. 9, no. 1, pp. 111–113, 1973, doi: 10.1111/j.0022-3646.1973.00111.x.

[67] S. Boussiba, A. Vonshak, Z. Cohen, Y. Avissar, and A. Richmond, "Lipid and biomass production by the halotolerant microalga Nannochloropsis salina," *Biomass*, vol. 12, no. 1, pp. 37–47, 1987, doi: 10.1016/0144-4565(87)90006-0.

[68] S. V. Khotimchenko and I. M. Yakovleva, "Lipid composition of the red alga Tichocarpus crinitus exposed to different levels of photon irradiance," *Phytochemistry*, vol. 66, no. 1, pp. 73–79, 2005, doi: 10.1016/j.phytochem.2004.10.024.

[69] Q. He, H. Yang, L. Wu, and C. Hu, "Effect of light intensity on physiological changes, carbon allocation and neutral lipid accumulation in oleaginous microalgae," *Bioresource Technology*, vol. 191, pp. 219–228, 2015, doi: 10.1016/j.biortech.2015.05.021.

[70] R. Radakovits, P. M. Eduafo, and M. C. Posewitz, "Genetic engineering of fatty acid chain length in Phaeodactylum tricornutum," *Metabolic engineering*, vol. 13, no. 1, pp. 89–95, 2011, doi: 10.1016/j.ymben.2010.10.003.

[71] G. Breuer *et al.,* "Superior triacylglycerol (TAG) accumulation in starchless mutants of Scenedesmus obliquus: (II) evaluation of TAG yield and productivity in controlled photobioreactors," *Biotechnol Biofuels*, vol. 7, no. 1, p. 70, 2014, doi: 10.1186/1754-6834-7-70.

[72] Y. Li *et al.,* "Chlamydomonas starchless mutant defective in ADP-glucose pyrophosphorylase hyper-accumulates triacylglycerol," *Metabolic engineering*, vol. 12, no. 4, pp. 387–391, 2010, doi: 10.1016/j.ymben.2010.02.002.

[73] E. M. Trentacoste *et al.,* "Metabolic engineering of lipid catabolism increases microalgal lipid accumulation without compromising growth," *Proceedings of the National Academy of Sciences of the United States of America*, vol. 110, no. 49, pp. 19748–19753, 2013, doi: 10.1073/pnas.1309299110.

[74] L. Rodolfi *et al.,* "Microalgae for oil: strain selection, induction of lipid synthesis and outdoor mass cultivation in a low-cost photobioreactor," *Biotechnology and bioengineering*, vol. 102, no. 1, pp. 100–112, 2008, doi: 10.1002/bit.22033.

[75] M. J. Griffiths and S. T. L. Harrison, "Lipid productivity as a key characteristic for choosing algal species for biodiesel production," *J Appl Phycol*, vol. 21, no. 5, pp. 493–507, 2009, doi: 10.1007/s10811-008-9392-7.

[76] Y. XU and W. J. Boeing, "Modeling maximum lipid productivity of microalgae: Review and next step," *Renewable and Sustainable Energy Reviews*, vol. 32, pp. 29–39, 2014, doi: 10.1016/j.rser.2014.01.002.

[77] C.-H. Su *et al.,* "Factors affecting lipid accumulation by Nannochloropsis oculata in a two-stage cultivation process," *J Appl Phycol*, vol. 23, no. 5, pp. 903–908, 2011, doi: 10.1007/s10811-010-9609-4.

[78] G. Breuer, P. P. Lamers, D. E. Martens, R. B. Draaisma, and R. H. Wijffels, "Effect of light intensity, pH, and temperature on triacylglycerol (TAG) accumulation induced by nitrogen starvation in Scenedesmus obliquus," *Bioresource Technology*, vol. 143, pp. 1–9, 2013, doi: 10.1016/j.biortech.2013.05.105.

[79] A. Converti, A. A. Casazza, E. Y. Ortiz, P. Perego, and M. Del Borghi, "Effect of temperature and nitrogen concentration on the growth and lipid content of Nannochloropsis oculata and Chlorella vulgaris for biodiesel production," *Chemical Engineering and Processing: Process Intensification*, vol. 48, no. 6, pp. 1146–1151, 2009, doi: 10.1016/j.cep.2009.03.006.

[80] S.-Y. Chiu *et al.,* "Lipid accumulation and CO2 utilization of Nannochloropsis oculata in response to CO2 aeration," *Bioresource Technology*, vol. 100, no. 2, pp. 833–838, 2009, doi: 10.1016/j.biortech.2008.06.061.

[81] A. J. Klok, P. P. Lamers, D. E. Martens, R. B. Draaisma, and R. H. Wijffels, "Edible oils from microalgae: Insights in TAG accumulation," *Trends in Biotechnology*, vol. 32, no. 10, pp. 521–528, 2014, doi: 10.1016/j.tibtech.2014.07.004.

[82] J. Sheehan, T.G. Dunahay, J.R. Benemann, and P.G. Roessler, "Look back at the U. S. Department of Energy's Aquatic Species Program: Biodiesel from Algae; Close-Out Report," doi: 10.2172/15003040.

[83] T. J. Lundquist, I. C. Woertz, N. W.T. Quinn, and Benemann, JR, "A Realistic Technology and Engineering Assessment of Algae Biofuel Production. Energy Biosciences Institute," *University of California, Berkeley, California*, 2010, doi: [DOI fehlt!].

[84] Z. Dubinsky, Ed., *Mass Production of Microalgae at Optimal Photosynthetic Rates*: InTech, 2013.

[85] M. A. Borowitzka and N. R. Moheimani, "Open Pond Culture Systems," in *Algae for Biofuels and Energy*, M. A. Borowitzka and N. R. Moheimani, Eds., Dordrecht: Springer Netherlands, 2013, pp. 133–152,

[86] A. Richmond, "Biological Principles of Mass Cultivation of Photoautotrophic Microalgae," in *Handbook of Microalgal Culture*: John Wiley & Sons, Ltd, 2013, pp. 169–204,

[87] A. C. Apel *et al.,* "Open thin-layer cascade reactors for saline microalgae production evaluated in a physically simulated Mediterranean summer climate," *Algal Research*, vol. 25, pp. 381–390, 2017, doi: 10.1016/j.algal.2017.06.004.

[88] J. Doucha and K. Livansky, "Novel outdoor thin-layer high density micro-algal culture system: Productivity and operational parameters," *Archiv für Hydrobiogie*, vol. 106, p. 129, 1995, doi: [DOI fehlt!].

[89] A. C. Apel and D. Weuster-Botz, "Engineering solutions for open microalgae mass cultivation and realistic indoor simulation of outdoor environments," *Bioprocess and biosystems engineering*, vol. 38, no. 6, pp. 995–1008, 2015, doi: 10.1007/s00449-015-1363-1.

[90] E. Ganuza, C. E. Sellers, B. W. Bennett, E. M. Lyons, and L. T. Carney, "A Novel Treatment Protects Chlorella at Commercial Scale from the Predatory Bacterium Vampirovibrio chlorellavorus," *Frontiers in microbiology*, vol. 7, p. 848, 2016, doi: 10.3389/fmicb.2016.00848.

[91] L. T. Carney *et al.,* "Pond Crash Forensics: Presumptive identification of pond crash agents by next generation sequencing in replicate raceway mass cultures of Nannochloropsis salina," *Algal Research*, vol. 17, pp. 341–347, 2016, doi: 10.1016/j.algal.2016.05.011.

[92] M.A. Borowitzka and N.R. Moheimani, Eds., *Algae for Biofuels and Energy*. Dordrecht: Springer Netherlands, 2013.

[93] G. Shelef, "Microalgae Harvesting and Processing: A Literature Review; A Subcontract Report," vol. 1984, doi: [DOI fehlt!].

[94] N. Uduman, Y. Qi, M. K. Danquah, G. M. Forde, and A. Hoadley, "Dewatering of microalgal cultures: A major bottleneck to algae-based fuels," *J. Renewable Sustainable Energy*, vol. 2, no. 1, p. 12701, 2010, doi: 10.1063/1.3294480.

[95] L. Brennan and P. Owende, "Biofuels from microalgae—A review of technologies for production, processing, and extractions of biofuels and co-products," *Renewable and Sustainable Energy Reviews*, vol. 14, no. 2, pp. 557–577, 2010, doi: 10.1016/j.rser.2009.10.009.

[96] R. Divakaran and V. N. Sivasankara Pillai, "locculation of algae using chitosan," *J Appl Phycol*, vol. 14, no. 5, pp. 419–422, 2002, doi: 10.1023/A:1022137023257.

[97] E. Molina Grima, E.-H. Belarbi, F.G. Acién Fernández, A. Robles Medina, and Y. Chisti, "Recovery of microalgal biomass and metabolites: Process options and economics," *Biotechnology advances*, vol. 20, no. 7-8, pp. 491–515, 2003, doi: 10.1016/S0734-9750(02)00050-2.

[98] A. Papazi, P. Makridis, and P. Divanach, "Harvesting Chlorella minutissima using cell coagulants," *J Appl Phycol*, vol. 22, no. 3, pp. 349–355, 2010, doi: 10.1007/s10811-009-9465-2.

[99] T. Ndikubwimana *et al.,* "Flotation: A promising microalgae harvesting and dewatering technology for biofuels production," *Biotechnology journal*, vol. 11, no. 3, pp. 315–326, 2016, doi: 10.1002/biot.201500175.

[100] P. E. Wiley, K. J. Brenneman, and A. E. Jacobson, "Improved Algal Harvesting Using Suspended Air Flotation," *water environ res*, vol. 81, no. 7, pp. 702–708, 2009, doi: 10.2175/106143009X407474.

[101] F. H. Mohn, *Experiences and strategies in the recovery of biomass from mass cultures of microalgae*, 1980.

[102] A. I. Barros, A. L. Gonçalves, M. Simões, and J. C.M. Pires, "Harvesting techniques applied to microalgae: A review," *Renewable and Sustainable Energy Reviews*, vol. 41, pp. 1489–1500, 2015, doi: 10.1016/j.rser.2014.09.037.

[103] L. Christenson and R. Sims, "Production and harvesting of microalgae for wastewater treatment, biofuels, and bioproducts," *Biotechnology advances*, vol. 29, no. 6, pp. 686–702, 2011, doi: 10.1016/j.biotechadv.2011.05.015.

[104] S. L. Pahl *et al.,* "Harvesting, Thickening and Dewatering Microalgae Biomass," in *Algae for Biofuels and Energy*, M. A. Borowitzka and N. R. Moheimani, Eds., Dordrecht: Springer Netherlands, 2013, pp. 165–185,

[105] J. Prakash *et al.,* "Microalgal biomass drying by a simple solar device," *International Journal of Solar Energy*, vol. 18, no. 4, pp. 303–311, 2007, doi: 10.1080/01425919708914325.

[106] E. G. Bligh and W. J. Dyer, "A rapid method of total lipid extraction and purification," *Can. J. Physiol. Pharmacol.*, vol. 37, no. 8, pp. 911–917, 1959, doi: 10.1139/y59-099.

[107] H.-W. Yen, S.-C. Yang, C.-H. Chen, Jesisca, and J.-S. Chang, "Supercritical fluid extraction of valuable compounds from microalgal biomass," *Bioresource Technology*, vol. 184, pp. 291–296, 2015, doi: 10.1016/j.biortech.2014.10.030.

[108] J. Lorenzen *et al.,* "Extraction of microalgae derived lipids with supercritical carbon dioxide in an industrial relevant pilot plant," *Bioprocess and biosystems engineering*, vol. 40, no. 6, pp. 911–918, 2017, doi: 10.1007/s00449-017-1755-5.

[109] F. Sahena *et al.,* "Application of supercritical CO2 in lipid extraction – A review," *Journal of Food Engineering*, vol. 95, no. 2, pp. 240–253, 2009, doi: 10.1016/j.jfoodeng.2009.06.026.

[110] S. A. Scott *et al.,* "Biodiesel from algae: challenges and prospects," *Current opinion in biotechnology*, vol. 21, no. 3, pp. 277–286, 2010, doi: 10.1016/j.copbio.2010.03.005.

[111] M. J. Ibáñez González *et al.,* "Optimization of fatty acid extraction from Phaeodactylum tricornutum UTEX 640 biomass," *J Am Oil Chem Soc*, vol. 75, no. 12, pp. 1735–1740, 1998, doi: 10.1007/s11746-998-0325-z.

[112] E. H. Belarbi, E. Molina, and Y. Chisti, "A process for high yield and scaleable recovery of high purity eicosapentaenoic acid esters from microalgae and fish oil," *Enzyme and Microbial Technology*, vol. 26, no. 7, pp. 516–529, 2000, doi: 10.1016/S0141-0229(99)00191-X.

[113] J.-Y. Park, M. S. Park, Y.-C. Lee, and J.-W. Yang, "Advances in direct transesterification of algal oils from wet biomass," *Bioresource Technology*, vol. 184, pp. 267–275, 2015, doi: 10.1016/j.biortech.2014.10.089.

[114] M. J. Griffiths, R. P. van Hille, and S. T. L. Harrison, "Selection of direct transesterification as the preferred method for assay of fatty acid content of microalgae," *Lipids*, vol. 45, no. 11, pp. 1053–1060, 2010, doi: 10.1007/s11745-010-3468-2.

[115] J. E. Shepherd, C. D. Nuyt, J. J. Lee, and J. E. Woodrow, "Flash Point and Chemical Composition of Aviation Kerosene (jet A)," in 2000,

[116] The American Petroleum Institute, "Kerosene/jet fuel category assessment document," Sep. 2010,

[117] C. Zhao, T. Brück, and J. A. Lercher, "Catalytic deoxygenation of microalgae oil to green hydrocarbons," *Green Chem.*, vol. 15, no. 7, p. 1720, 2013, doi: 10.1039/c3gc40558c.

[118] M. W. Schreiber, D. Rodriguez-Niño, O. Y. Gutiérrez, and J. A. Lercher, "Hydrodeoxygenation of fatty acid esters catalyzed by Ni on nano-sized MFI type zeolites," *Catal. Sci. Technol.*, vol. 6, no. 22, pp. 7976–7984, 2016, doi: 10.1039/c6cy01598k.

[119] A. J. Ward, D. M. Lewis, and F. B. Green, "Anaerobic digestion of algae biomass: A review," *Algal Research*, vol. 5, pp. 204–214, 2014, doi: 10.1016/j.algal.2014.02.001.

[120] K. B. Cantrell, T. Ducey, K. S. Ro, and P. G. Hunt, "Livestock waste-to-bioenergy generation opportunities," *Bioresource Technology*, vol. 99, no. 17, pp. 7941–7953, 2008, doi: 10.1016/j.biortech.2008.02.061.

[121] T. van Harmelen and H. Oonk, "Microalgae biofixation processes: Applications and Potential Contributions to Greenhouse Gas Mitigation Options: Microalgae biofixation processes: Applications and Potential Contributions to Greenhouse Gas Mitigation Options," Apeldoorn, 2006,

[122] R. Davis, A. Aden, and P. T. Pienkos, "Techno-economic analysis of autotrophic microalgae for fuel production," *Applied Energy*, vol. 88, no. 10, pp. 3524–3531, 2011, doi: 10.1016/j.apenergy.2011.04.018.

[123] L. Lardon, A. Hélias, B. Sialve, J.-P. Steyer, and O. Bernard, "Life-Cycle Assessment of Biodiesel Production from Microalgae," *Environ. Sci. Technol.*, vol. 43, no. 17, pp. 6475–6481, 2009, doi: 10.1021/es900705j.

[124] Williams, Peter J. le B. and L. M. L. Laurens, "Microalgae as biodiesel & biomass feedstocks: Review & analysis of the biochemistry, energetics & economics," *Energy Environ. Sci.*, vol. 3, no. 5, p. 554, 2010, doi: 10.1039/B924978H.

[125] D. Klein-Marcuschamer *et al.,* "Technoeconomic analysis of renewable aviation fuel from microalgae, Pongamia pinnata and sugarcane," *Biofuels, Bioprod. Bioref.*, vol. 7, no. 4, pp. 416–428, 2013, doi: 10.1002/bbb.1404.

[126] D. R. Georgianna and S. P. Mayfield, "Exploiting diversity and synthetic biology for the production of algal biofuels," *Nature*, vol. 488, no. 7411, pp. 329–335, 2012, doi: 10.1038/nature11479.

[127] M. Hannon, J. Gimpel, M. Tran, B. Rasala, and S. Mayfield, "Biofuels from algae: Challenges and potential," *Biofuels*, vol. 1, no. 5, pp. 763–784, 2010, doi: [DOI fehlt!].

[128] L. Carney, R. McBride, V. Smith, and T. Lane, "Molecular Diagnostic Solutions in Algal Cultivation Systems," in *Microalgal Production for Biomass and High-Value Products*, S. Slocombe and J. Benemann, Eds.: CRC Press, 2016, pp. 183–204,

[129] L. T. Carney *et al.,* "Microbiome analysis of a microalgal mass culture growing in municipal wastewater in a prototype OMEGA photobioreactor," *Algal Research*, vol. 4, pp. 52–61, 2014, doi: 10.1016/j.algal.2013.11.006.

[130] E. Kazamia, A. S. Riseley, C. J. Howe, and A. G. Smith, "An Engineered Community Approach for Industrial Cultivation of Microalgae," *Industrial biotechnology (New Rochelle, N.Y.)*, vol. 10, no. 3, pp. 184–190, 2014, doi: 10.1089/ind.2013.0041.

[131] P. R. Mooij, G. R. Stouten, van Loosdrecht, Mark C M, and R. Kleerebezem, "Ecology-based selective environments as solution to contamination in microalgal cultivation," *Current opinion in biotechnology*, vol. 33, pp. 46–51, 2015, doi: 10.1016/j.copbio.2014.11.001.

[132] Y. Chisti, "Constraints to commercialization of algal fuels," *Journal of Biotechnology*, vol. 167, no. 3, pp. 201–214, 2013, doi: 10.1016/j.jbiotec.2013.07.020.

[133] T. L. da Silva, L. Gouveia, and A. Reis, "Integrated microbial processes for biofuels and high value-added products: the way to improve the cost effectiveness of biofuel production," *Applied microbiology and biotechnology*, vol. 98, no. 3, pp. 1043–1053, 2014, doi: 10.1007/s00253-013-5389-5.

[134] E. Stephens *et al.,* "Future prospects of microalgal biofuel production systems," *Trends in plant science*, vol. 15, no. 10, pp. 554–564, 2010, doi: 10.1016/j.tplants.2010.06.003.

[135] M. Vanthoor-Koopmans, R. H. Wijffels, M. J. Barbosa, and M. H. M. Eppink, "Biorefinery of microalgae for food and fuel," *Bioresource Technology*, vol. 135, pp. 142–149, 2013, doi: 10.1016/j.biortech.2012.10.135.

[136] G. Jakob, "Surveying a Diverse Pool of Microalgae as a Bioresource for Future Biotechnological Applications," *J Pet Environ Biotechnol*, vol. 04, no. 05, 2013, doi: 10.4172/2157-7463.1000153.

[137] D. Weuster-Botz, "Parallel reactor systems for bioprocess development," *Technology Transfer in Biotechnology*, pp. 125–143, 2005, doi: [DOI fehlt!].

[138] R. Bareither and D. Pollard, "A review of advanced small-scale parallel bioreactor technology for accelerated process development: Current state and future need," *Biotechnology progress*, vol. 27, no. 1, pp. 2–14, 2011, doi: 10.1002/btpr.522.

[139] J. I. Betts and F. Baganz, "Miniature bioreactors: current practices and future opportunities," *Microbial cell factories*, vol. 5, p. 21, 2006, doi: 10.1186/1475-2859-5-21.

[140] Q. Long *et al.,* "The development and application of high throughput cultivation technology in bioprocess development," *Journal of Biotechnology*, vol. 192 Pt B, pp. 323–338, 2014, doi: 10.1016/j.jbiotec.2014.03.028.

[141] C. Posten, "Design principles of photo-bioreactors for cultivation of microalgae," *Eng. Life Sci.*, vol. 9, no. 3, pp. 165–177, 2009, doi: 10.1002/elsc.200900003.

[142] V. Lob, T. Geisler, M. Brischwein, R. Uhl, and B. Wolf, "Automated live cell screening system based on a 24-well-microplate with integrated micro fluidics," *Medical & Biological Engineering & Computing*, vol. 45, no. 11, pp. 1023–1028, 2007, doi: 10.1007/s11517-007-0260-4.

[143] M. Takeuchi *et al.,* "Hydroxy fatty acid production by Pediococcus sp," *Eur. J. Lipid Sci. Technol.*, vol. 115, no. 4, pp. 386–393, 2013, doi: 10.1002/ejlt.201200414.

[144] T. Mutanda *et al.,* "Bioprospecting for hyper-lipid producing microalgal strains for sustainable biofuel production," *Bioresource Technology*, vol. 102, no. 1, pp. 57–70, 2011, doi: 10.1016/j.biortech.2010.06.077.

[145] C. Casal, M. Cuaresma, J. M. Vega, and C. Vilchez, "Enhanced productivity of a lutein-enriched novel acidophile microalga grown on urea," *Marine Drugs*, vol. 9, no. 1, pp. 29–42, 2010, doi: 10.3390/md9010029.

[146] Z. Cohen and C. Ratledge, *Single Cell Oils: Microbial and Algal Oils,* 2nd ed. s.l.: Elsevier Science, 2015.

[147] R. Altenburger, M. Schmitt-Jansen, and J. Riedl, "Bioassays with unicellular algae: deviations from exponential growth and its implications for toxicity test results," *Journal of environmental quality*, vol. 37, no. 1, pp. 16–21, 2008, doi: 10.2134/jeq2006.0556.

[148] W. Han, C. Li, X. Miao, and G. Yu, "A Novel Miniature Culture System to Screen CO2-Sequestering Microalgae," *Energies*, vol. 5, no. 12, pp. 4372–4389, 2012, doi: 10.3390/en5114372.

[149] A. Pacheco, I. Hernández-Mireles, C. García-Martínez, and M. M. Álvarez, "Microplates as a microreactor platform for microalgae research," *Biotechnol Progress*, vol. 29, no. 3, pp. 638–644, 2013, doi: 10.1002/btpr.1721.

[150] J. van Wagenen *et al.,* "Microplate-based method for high-throughput screening of microalgae growth potential," *Bioresource Technology*, vol. 169, pp. 566–572, 2014, doi: 10.1016/j.biortech.2014.06.096.

[151] K. A. Radzun *et al.,* "Automated nutrient screening system enables high-throughput optimisation of microalgae production conditions," *Biotechnol Biofuels*, vol. 8, no. 1, p. 31, 2015, doi: 10.1186/s13068-015-0238-7.

[152] U. M. Tillich *et al.,* "High-throughput cultivation and screening platform for unicellular phototrophs," *BMC Microbiol*, vol. 14, no. 1, p. 1960, 2014, doi: 10.1186/s12866-014-0239-x.

[153] H. Morschett *et al.,* "Design and validation of a parallelized micro-photobioreactor enabling phototrophic bioprocess development at elevated throughput," *Biotechnol. Bioeng.*, vol. 114, no. 1, pp. 122–131, 2017, doi: 10.1002/bit.26051.

[154] M. Glemser, *Enhancing microalgae cultivation: Lightning effects and mutation procedures*. PhD Thesis. Munich.

[155] B. Diez, C. Pedros-Alio, T. L. Marsh, and R. Massana, "Application of denaturing gradient gel electrophoresis (DGGE) to study the diversity of marine picoeukaryotic assemblages and comparison of DGGE with other molecular techniques," *Applied and Environmental Microbiology*, vol. 67, no. 7, pp. 2942–2951, 2001, doi: 10.1128/AEM.67.7.2942-2951.2001.

[156] Z. Zhang, S. Schwartz, L. Wagner, and W. Miller, "A greedy algorithm for aligning DNA sequences," *Journal of computational biology : a journal of computational molecular cell biology*, vol. 7, no. 1-2, pp. 203–214, 2000, doi: 10.1089/10665270050081478.

[157] R. C. Edgar, "MUSCLE: multiple sequence alignment with high accuracy and high throughput," *Nucleic acids research*, vol. 32, no. 5, pp. 1792–1797, 2004, doi: 10.1093/nar/gkh340.

[158] S. Kumar, G. Stecher, and K. Tamura, "MEGA7: Molecular Evolutionary Genetics Analysis Version 7.0 for Bigger Datasets," *Molecular Biology and Evolution*, vol. 33, no. 7, pp. 1870–1874, 2016, doi: 10.1093/molbev/msw054.

[159] M. Hasegawa, H. Kishino, and T.-a. Yano, "Dating of the human-ape splitting by a molecular clock of mitochondrial DNA," *J Mol Evol*, vol. 22, no. 2, pp. 160–174, 1985, doi: 10.1007/BF02101694.

[160] F. Bracharz, "Harvest of the oleaginous microalgae Scenedesmus obtusiusculus from optimized salt water culture by flocculation," 2017, doi: [DOI fehlt!].

[161] I. Maus *et al.,* "Biphasic Study to Characterize Agricultural Biogas Plants by High-Throughput 16S rRNA Gene Amplicon Sequencing and Microscopic Analysis," *Journal of microbiology and biotechnology*, vol. 27, no. 2, pp. 321–334, 2017, doi: 10.4014/jmb.1605.05083.

[162] S. Takahashi, J. Tomita, K. Nishioka, T. Hisada, and M. Nishijima, "Development of a prokaryotic universal primer for simultaneous analysis of Bacteria and Archaea using next-generation sequencing," *PLoS ONE*, vol. 9, no. 8, e105592, 2014, doi: 10.1371/journal.pone.0105592.

[163] D. Wibberg *et al.,* "Genome analysis of the sugar beet pathogen Rhizoctonia solani AG2-2IIIB revealed high numbers in secreted proteins and cell wall degrading enzymes," *BMC genomics*, vol. 17, p. 245, 2016, doi: 10.1186/s12864-016-2561-1.

[164] T. Magoč and S. L. Salzberg, "FLASH: Fast length adjustment of short reads to improve genome assemblies," *Bioinformatics (Oxford, England)*, vol. 27, no. 21, pp. 2957–2963, 2011, doi: 10.1093/bioinformatics/btr507.

[165] R. C. Edgar, "Search and clustering orders of magnitude faster than BLAST," *Bioinformatics (Oxford, England)*, vol. 26, no. 19, pp. 2460–2461, 2010, doi: 10.1093/bioinformatics/btq461.

[166] R. C. Edgar, "UPARSE: Highly accurate OTU sequences from microbial amplicon reads," *Nature methods*, vol. 10, no. 10, pp. 996–998, 2013, doi: 10.1038/nmeth.2604.

[167] Q. Wang, G. M. Garrity, J. M. Tiedje, and J. R. Cole, "Naive Bayesian classifier for rapid assignment of rRNA sequences into the new bacterial taxonomy," *Applied and Environmental Microbiology*, vol. 73, no. 16, pp. 5261–5267, 2007, doi: 10.1128/AEM.00062-07.

[168] S. Liebe *et al.,* "Taxonomic analysis of the microbial community in stored sugar beets using high-throughput sequencing of different marker genes," *FEMS microbiology ecology*, vol. 92, no. 2, 2016, doi: 10.1093/femsec/fiw004.

[169] S. Theuerl *et al.,* "Community shifts in a well-operating agricultural biogas plant: How process variations are handled by the microbiome," *Applied microbiology and biotechnology*, vol. 99, no. 18, pp. 7791–7803, 2015, doi: 10.1007/s00253-015-6627-9.

[170] J.-H. Zhang, "A Simple Statistical Parameter for Use in Evaluation and Validation of High Throughput Screening Assays," *Journal of Biomolecular Screening*, vol. 4, no. 2, pp. 67–73, 1999, doi: 10.1177/108705719900400206.

[171] T. Petzoldt, *Estimation of Growth Rates with Package growthrates.* [Online] Available: https://cran.r-project.org/web/packages/growthrates/vignettes/Introduction.pdf.

[172] E. Hounslow, J. Noirel, D. J. Gilmour, and P. C. Wright, "Lipid quantification techniques for screening oleaginous species of microalgae for biofuel production," *Eur. J. Lipid Sci. Technol.*, pp. n/a-n/a, 2016, doi: 10.1002/ejlt.201500469.

[173] L. R. Cavonius, N.-G. Carlsson, and I. Undeland, "Quantification of total fatty acids in microalgae: comparison of extraction and transesterification methods," *Analytical and bioanalytical chemistry*, vol. 406, no. 28, pp. 7313–7322, 2014, doi: 10.1007/s00216-014-8155-3.

[174] W. Chen, C. Zhang, L. Song, M. Sommerfeld, and Q. Hu, "A high throughput Nile red method for quantitative measurement of neutral lipids in microalgae," *Journal of Microbiological Methods*, vol. 77, no. 1, pp. 41–47, 2009, doi: 10.1016/j.mimet.2009.01.001.

[175] J. Rumin *et al.,* "The use of fluorescent Nile red and BODIPY for lipid measurement in microalgae," *Biotechnology for biofuels*, vol. 8, p. 42, 2015, doi: 10.1186/s13068-015-0220-4.

[176] P. de Deckker, "Australian salt lakes their history, chemistry, and biota a review," *Hydrobiologia*, pp. 231–244, 1983, doi: 10.1007/BF00025191.

[177] P. de Deckker and M. C. Geddes, "Seasonal fauna of ephemeral saline lakes near the Coorong lagoon, South Australia," *Mar. Freshwater Res.*, vol. 31, no. 5, pp. 677–699, 1980, doi: 10.1071/MF9800677.

[178] M. Schapira, M.-J. Buscot, T. Pollet, S. C. Leterme, and L. Seuront, "Distribution of picophytoplankton communities from brackish to hypersaline waters in a South Australian coastal lagoon," *Saline systems*, vol. 6, p. 2, 2010, doi: 10.1186/1746-1448-6-2.

[179] R. V. Burne and J. Ferguson, "Contrasting marginal sediments of a seasonally flooded saline lake—Lake Eliza, South Australia: significance for oil shale genesis," *BMR, J. Aust. Geol. Geophys.*, vol. 8, pp. 99–108, 1983, doi: [DOI fehlt!].

[180] I. A.E. Bayly and W. D. Williams, "Chemical and biological studies on some saline lakes of south-east Australia," *Mar. Freshwater Res.*, vol. 17, no. 2, p. 177, 1966, doi: 10.1071/MF9660177.

[181] W. D. Williams, "Lake Corangamite, Australia, a permanent saline lake: Conservation and management issues," *Lakes & Reservoirs: Research & Management*, vol. 1, no. 1, pp. 55–64, 1995, doi: 10.1111/j.1440-1770.1995.tb00006.x.

[182] U. T. Hammer, "A Comparative Study of Primary Production and Related Factors in Four Saline Lakes in Victoria, Australia," *Int. Revue ges. Hydrobiol. Hydrogr.*, vol. 66, no. 5, pp. 701–743, 1981, doi: 10.1002/iroh.19810660509.

[183] U.S. CLIVAR Office, "Report of the U:S: CLIVAR Salinity Science Working Group: U.S. CLIVAR Report 2007-1," Washington DC.

[184] S. Ribeiro *et al.*, "Phytoplankton growth after a century of dormancy illuminates past resilience to catastrophic darkness," *Nature communications*, vol. 2, p. 311, 2011, doi: 10.1038/ncomms1314.

[185] C. A. Maggs and M. E. Callow, "Algal Spores," doi: 10.1038/npg.els.0000311.

[186] C. Butterwick, S. I. Heaney, and J. F. Talling, "A comparison of eight methods for estimating the biomass and growth of planktonic algae," *British Phycological Journal*, vol. 17, no. 1, pp. 69–79, 2007, doi: 10.1080/00071618200650091.

[187] B. Skjelbred, B. Edvardsen, and T. Andersen, "A high-throughput method for measuring growth and loss rates in microalgal cultures," *J Appl Phycol*, vol. 24, no. 6, pp. 1589–1599, 2012, doi: 10.1007/s10811-012-9819-z.

[188] M. J. Griffiths, C. Garcin, R. P. van Hille, and S. T. L. Harrison, "Interference by pigment in the estimation of microalgal biomass concentration by optical density," *Journal of Microbiological Methods*, vol. 85, no. 2, pp. 119–123, 2011, doi: 10.1016/j.mimet.2011.02.005.

[189] N. LAZAROFF and W. VISHNIAC, "The effect of light on this developmental cycle of Nostoc muscorum, a filamentous blue-green alga," *Journal of general microbiology*, vol. 25, pp. 365–374, 1961, doi: 10.1099/00221287-25-3-365.

[190] Z. Wu, D. Liu, and Y. Sui, "Quantitative assessment of hit detection and confirmation in single and duplicate high-throughput screenings," *Journal of Biomolecular Screening*, vol. 13, no. 2, pp. 159–167, 2008, doi: 10.1177/1087057107312628.

[191] C. W. Sensen, K. Heimann, and M. Melkonian, "The production of clonal and axenic cultures of microalgae using fluorescence-activated cell sorting," *European Journal of Phycology*, vol. 28, no. 2, pp. 93–97, 1993, doi: 10.1080/09670269300650151.

[192] M. Terashima, E. S. Freeman, R. E. Jinkerson, and M. C. Jonikas, "A fluorescence-activated cell sorting-based strategy for rapid isolation of high-lipid Chlamydomonas mutants," *The Plant journal : for cell and molecular biology*, vol. 81, no. 1, pp. 147–159, 2015, doi: 10.1111/tpj.12682.

[193] M. Sieracki, N. Poulton, and N. Crosbie, "Automated Isolation," *Algal culturing techniques*, p. 101, 2005, doi: 10.1016/B978-012088426-1/50008-1.

[194] M. J. Griffiths, R. P. van Hille, and S. T. L. Harrison, "Lipid productivity, settling potential and fatty acid profile of 11 microalgal species grown under nitrogen replete and limited conditions," *J Appl Phycol*, vol. 24, no. 5, pp. 989–1001, 2012, doi: 10.1007/s10811-011-9723-y.

[195] A. W. Coleman, "ITS2 is a double-edged tool for eukaryote evolutionary comparisons," *Trends in Genetics*, vol. 19, no. 7, pp. 370–375, 2003, doi: 10.1016/S0168-9525(03)00118-5.

[196] M. A. Borowitzka and C. J. Siva, "The taxonomy of the genus Dunaliella (Chlorophyta, Dunaliellales) with emphasis on the marine and halophilic species," *J Appl Phycol*, vol. 19, no. 5, pp. 567–590, 2007, doi: 10.1007/s10811-007-9171-x.

[197] W. Lerche, "Untersuchungen über Entwicklung und Fortpflanzung in der Gattung Dunaliella," *Archiv für Protistenkunde*, no. 88, pp. 236–268, 1937, doi: [DOI fehlt!].

[198] M. J. Griffiths, R. P. van Hille, and S. T. L. Harrison, "The effect of degree and timing of nitrogen limitation on lipid productivity in Chlorella vulgaris," *Appl Microbiol Biotechnol*, vol. 98, no. 13, pp. 6147–6159, 2014, doi: 10.1007/s00253-014-5757-9.

[199] E. B. Sydney *et al.,* "Screening of microalgae with potential for biodiesel production and nutrient removal from treated domestic sewage," *Applied Energy*, vol. 88, no. 10, pp. 3291–3294, 2011, doi: 10.1016/j.apenergy.2010.11.024.

[200] N. Hanagata, T. Takeuchi, Y. Fukuju, D. J. Barnes, and I. Karube, "Tolerance of microalgae to high CO2 and high temperature," *Phytochemistry*, vol. 31, no. 10, pp. 3345–3348, 1992, doi: 10.1016/0031-9422(92)83682-O.

[201] S. P. Slocombe, Q. Zhang, K. D. Black, J. G. Day, and M. S. Stanley, "Comparison of screening methods for high-throughput determination of oil yields in micro-algal biofuel strains," *Journal of Applied Phycology*, vol. 25, no. 4, pp. 961–972, 2013, doi: 10.1007/s10811-012-9947-5.

[202] X. Wen, Y. Geng, and Y. Li, "Enhanced lipid production in Chlorella pyrenoidosa by continuous culture," *Bioresource Technology*, vol. 161, pp. 297–303, 2014, doi: 10.1016/j.biortech.2014.03.077.

[203] R. Hermann, M. Lehmann, and J. Buchs, "Characterization of gas-liquid mass transfer phenomena in microtiter plates," *Biotechnology and bioengineering*, vol. 81, no. 2, pp. 178–186, 2003, doi: 10.1002/bit.10456.

[204] W. A. Duetz and B. Witholt, "Effectiveness of orbital shaking for the aeration of suspended bacterial cultures in square-deepwell microtiter plates," *Biochemical Engineering Journal*, vol. 7, no. 2, pp. 113–115, 2001, doi: 10.1016/S1369-703X(00)00109-1.

[205] K. Chaturvedi, S. Y. Sun, T. O'Brien, Y. J. Liu, and J. W. Brooks, "Comparison of the behavior of CHO cells during cultivation in 24-square deep well microplates and conventional shake flask systems," *Biotechnology reports (Amsterdam, Netherlands)*, vol. 1-2, pp. 22–26, 2014, doi: 10.1016/j.btre.2014.04.001.

[206] H. G. Hansen *et al.,* "Versatile microscale screening platform for improving recombinant protein productivity in Chinese hamster ovary cells," *Scientific reports*, vol. 5, p. 18016, 2015, doi: 10.1038/srep18016.

[207] N. J. Silk *et al.,* "Fed-batch operation of an industrial cell culture process in shaken microwells," *Biotechnol Lett*, vol. 32, no. 1, pp. 73–78, 2010, doi: 10.1007/s10529-009-0124-0.

[208] W. A. Duetz. [Online] Available: http://www.enzyscreen.com/sandwich_covers_24_mtps.htm. Accessed on: Aug. 08 2017.

[209] P. W. Iversen *et al.,* "HTS Assay Validation," in *Assay Guidance Manual*, G. S. Sittampalam, N. P. Coussens, K. Brimacombe, A. Grossman, M. Arkin, D. Auld,

C. Austin, J. Baell, B. Bejcek, T. D.Y. Chung, J. L. Dahlin, V. Devanaryan, T. L. Foley, M. Glicksman, M. D. Hall, J. V. Hass, J. Inglese, P. W. Iversen, S. D. Kahl, S. C. Kales, M. Lal-Nag, Z. Li, J. McGee, O. McManus, T. Riss, O. J. Trask, J. R. Weidner, M. Xia, and X. Xu, Eds., Bethesda (MD), 2004.

[210] *ANSI/SLAS 1-2004: Microplates — Footprint Dimensions*, 2004.

[211] APworks, "Material Data Sheet -ScalMalloy," APworks, REV 0008. [Online] Available: http://www.apworks.de/wp-content/uploads/2015/07/20170626_SCALMALLOY_REV0010.pdf.

[212] M. Schmidt *et al.,* "Laser based additive manufacturing in industry and academia," *CIRP Annals - Manufacturing Technology*, 2017, doi: 10.1016/j.cirp.2017.05.011.

[213] J. Atencia *et al.,* "Magnetic connectors for microfluidic applications," *Lab Chip*, vol. 10, no. 2, p. 246, 2009, doi: 10.1039/b913331c.

[214] C. Baggesen, C. Gjermansen, and A. B. Brandt, "A Study of Microalgal Symbiotic Communities with the Aim to Increase Biomass and Biodiesel Production," 2014.

[215] M. Le Chevanton *et al.,* "Screening and selection of growth-promoting bacteria for Dunaliella cultures," *Algal Research*, vol. 2, no. 3, pp. 212–222, 2013, doi: 10.1016/j.algal.2013.05.003.

[216] M. T. Croft, A. D. Lawrence, E. Raux-Deery, M. J. Warren, and A. G. Smith, "Algae acquire vitamin B12 through a symbiotic relationship with bacteria," *Nature*, vol. 438, no. 7064, pp. 90–93, 2005, doi: 10.1038/nature04056.